Optimization of High Protein Formulations Using Wear and Mechanical Behaviors

A Thesis

Presented in Partial Fulfillment of the Requirements for the

Degree of Master of Science

with a

Major in Food Science

in the

College of Graduate Studies

University of Idaho

by

Kristen Sparkman

Major Professor: Helen Joyner, Ph.D.

Committee Members: Girish Ganjyal, Ph.D.; Brennan Smith, Ph.D.

Department Administrator: Barbara Rasco, Ph.D., J.D.

December 2018

AUTHORIZATION TO SUBMIT THESIS

This thesis of Kristen Sparkman, submitted for the degree of Master of Science with a Major in Food Science and titled, "Optimization of High Protein Formulations Using Wear and Mechanical Behaviors," has been reviewed in final form. Permission, as indicated by the signatures and dates below, is now granted to submit final copies to the College of Graduate Studies for approval.

Major Professor: _____ Date _____

Helen Joyner, Ph.D.

Committee Members: _____ Date _____

Girish Ganjyal, Ph.D.

_____ Date _____

Brennan Smith, Ph.D.

Department Administrator: _____ Date _____

Barbara Rasco, Ph.D., J.D.

ABSTRACT

High protein bars are popular snack items that can have significant processing issues like sticking, clogging, and cold flow. These issues are primarily problematic during formulation development as current predictive testing is reliant on empirical bench tests or pilot plant testing that is expensive and time-consuming. Due to the deformation and thus structural information that rheological testing provides, it has promise to predict high protein bar processing ability. Wear testing, which has been used in the medical field to evaluate the lifetime of soft materials used in joint replacements, may have promise in evaluating food processing ability. The objectives of this study were to determine how ingredients impact formulation processing ability, determine potential predictive bench-level testing that would give information about formulation and thus processing ability, and create predictive models for high protein bar formulations based on empirical testing and instrumental data. Two response surface designs of model high protein bars comprising whey protein isolate (WPI), high fructose corn syrup (HFCS), and either canola oil or vegetable shortening were evaluated. Rheological tests including adhesion, strain and frequency sweeps, large amplitude oscillatory shear, and wear testing were conducted to determine the impact of individual ingredients on protein bar behavior. Ingredient formulation impacted the processing ability, wear testing, and rheological behaviors. Formulations with high ratios of WPI to HFCS and either shortening or oil exhibited good processing ability, lower wear rates, and increased elastic-type behavior, indicating that both bar rheological behaviors and processing ability are related to formulation. The predictive models had relatively high accuracy rates (>85%) with only three misclassifications out of 20 samples seen for each of the oil and shortening formulations. The misclassifications created grey areas of predictive values for ingredient levels; more samples would increase model accuracy. Model validation testing showed that cold flow was best for predicting processing ability of oil formulations. For shortening formulations, wear rate and G_3'/G_1' at 4% strain and 10 rad/s best predicted processing ability. These models provide valuable information about ingredient ranges and tests that could be used to assist in the determination of processing ability.

ACKNOWLEDGEMENTS

I would first like to thank my major advisor, Dr. Helen Joyner, for her expertise, support, time, and effort throughout this work and continually encouraging professional growth through my graduate studies. I would also like to thank my committee members Dr. Smith and Dr. Ganjyal, for their knowledge, time, effort, and support throughout this work.

Thank you to the application scientists at Glanbia Nutritionals, Inc., who were invaluable resources in conducting this research and better understanding this project. I would also like to thank Dr. Lee Deobald the director of the Mass Spec Core Lab at the University of Idaho, for his expertise and assistance in running ingredient component analyses. Thank you to the Consulting Statisticians in the Statistical Programs working in the College of Agricultural and Life Science at the University of Idaho for assistance in creating the code and models for this work

This project was supported by BUILD Dairy, who throughout this project provided a great network of experts in the dairy industry to further my knowledge in the field.

DEDICATION

To my family: this work was only possible through your continual support and encouragement. Particular thanks to my parents, Stephen and Georyl Sparkman, who provided the best education I could have asked for and continue to be an invaluable support system for every new endeavor I take on. And to Megan Berge: you are my forever cheerleader and sounding board and I don't know what I would do without you. I am so incredibly lucky and thankful to have all of you in my life. Without your combined guidance, this work would not exist.

TABLE OF CONTENTS

LIST OF TABLES

LIST OF FIGURES

CHAPTER 1: INTRODUCTION

With the growing high protein bar market, a greater number of new bar formulations have been produced to better meet consumer preferences (Franco, 2015). New formulations can create processing challenges including material sticking to processing surfaces, clogging of the equipment, and cold flow, where the bar does not hold its shape under its own weight prior to packaging (Tilghman, 2017). These processing difficulties are likely related to formulation ratios. Current testing of processing ability of new formulations are highly empirical, and the food industry needs quantitative and predictive testing that would better assess the processing ability of new high protein bar formulations. The overall goal of this study was to determine the feasibility of instrumental testing as predictors for high protein bars processing ability.

There were three main objectives of this study. The first objective was to determine how ingredients impact formulation mechanical behaviors, which was addressed in Chapter 3. The second objective was to determine potential predictive bench-level testing that would give information about formulation and thus processing ability, which was addressed in Chapter 4. The third objective was to determine predictive testing methods and ingredient ranges that would produce food processing ability high protein bar formulations, which was addressed in Chapter 5.

The model bar system used in this work was composed of high fructose corn syrup (HFCS), whey protein isolate (WPI), and either canola oil or vegetable shortening to provide a simplified version of current commercial bar formulations. Because rheology provides deformation properties and thus structural characteristics of a material, a range of rheological tests, wear testing, and subjective cold flow testing were used to evaluate the rheological, wear, and processing behaviors of model high protein bar formulations. The rheological tests used in this study were chosen based on their high likelihood of predicting processing ability based on deformation behavior they provide (Steffe, 1996). Frequency and strain sweeps give insight to the extent of elastic versus viscous behavior and critical strain of a sample, respectively; both have the potential to relate to processing ability. Adhesion tests provide information on how sticky or adhesive a material is, which is a processing issue as material sticking to rollers can clog machinery. Wear testing was selected based on its ability to evaluate the effectiveness of semisolid materials like hydrogels as artificial cartilage in joint

replacements (Yarimitsu,Sasaki,Murakami,&Suzuki,2016; Freeman, Furey, Love, & Hampton, 2000; Kyomoto, Moro, Takatori, Kawaguchi, & Ishihara, 2011; Li, Wang, & Wang, 2016). Artificial cartilages are soft solids, similar to high protein bars. Additionally, wear testing provides information about the durability of the artificial cartilage in joints, which could relate to high protein bar durability in processing equipment, determining processing ability.

The use of predictive model is beneficial to this project because it would provide ranges of good processing ability for new formulations. This would allow high protein bar manufacturers to rapidly assess new formulations without needing large amounts of sample, long periods of time, or extensive experience. Predictive modeling was used to evaluate the ability of these testing methods to predict the processing ability of a given high protein bar formulation. Validation of models was done using previously untested formulations. By using rheology and wear to better understand how ingredients impact processing ability, this study is the first step in closing the gap between the variability of new formulations and processing ability.

CHAPTER 2: LITERATURE REVIEW

High protein bars are relatively new but have been continually adapting and expanding in the consumer market where they have found a strong foothold. More recently, adaptability has been key, with 67% of consumers preferring simple ingredient labels (Manufacturing & May, 2016). Changes in food label preference are challenging food companies to adjust formulations to meet consumer demands, while also ensuring smooth production. Protein bar production has become increasingly complex with the continuous change of bar formulations, leading to processing issues. The goal of this work is to demonstrate a connection between protein bar processing and wear behaviors.

2.1.1 MARKETPLACE RELEVANCE OF HIGH PROTEIN BARS

Marketplace prevalence of high protein bars has grown significantly in recent years and their popularity does not appear to be waning. The consumer market is wide, with segments looking for snacks, meals on the go, and athletic replenishment. These bars are attractive due to the variety of proteins used and the vast ingredient combinations that can meet many consumer segments' nutritional needs. Along with these consumer segments, the convenience of bars makes them popular because mealtime structure has changed to snacks supplementing and integrating into meals (Institute of Food Technologists, 2016). Consumers are looking for more snacks that are high in nutrients but not calories, which makes high protein bars popular (Forgrieve, 2015). An estimate for food bar sales in 2016 was $8.3 billion, a 6.6% increase from 2015 sales (Franco, 2015). Although there are many types of food bars that serve different nutritional needs, such as cereal, granola, energy, and high protein bars, high protein bars are generally chosen as a quick source of protein.

The nutritional benefits for high protein bars are often highlighted through labeling to improve marketability. With labeling claims, the amount of protein dictates the degree of the claim. According to the FDA, when labeling a product "high" it must exceed 20% of the daily value per serving (Nutrition, 2013a), which is 50 g for protein. This means high protein products should contain at least 10 g of protein per serving (Nutrition, 2013b). When using the claim "beneficial nutrient," the product must contain 10% of the daily value of that nutrient per serving; for protein, the product should contain at least 5 g of protein per serving (Nutrition, 2013a). Currently, there are no standards of identity for high protein bars, but

manufacturers have established common protein values between 10 or 20g of protein per bar, which range between 40 to 60g.

2.1.2 MANUFACTURING OF HIGH PROTEIN BARS

Food manufacturing is vital to maintaining an adequate food supply. For protein bars, processing techniques vary depending on composition (Nutrition Bar Confectioners, n.d.). Two main techniques are used for processing high protein bars, slab-forming and extrusion (Nutri-Nation Functional Foods, n.d.). With the ability of extruders to manufacture different products and product shapes, they are more prevalent in the food industry. This availability allows smaller bar manufacturers access to processing equipment. Both screw and roller extrusion methods are performed at ambient temperature and without applied pressure, which allows the material to cool during processing (Koch, 2008). Slab-forming techniques are used for granola bars, nut bars, protein bars, fruit bars, and layered bars (Nutri-Nation Functional Foods, n.d.). Processing generally begins in a hopper, where the mixed ingredients are pushed into a forming device. These devices form the appropriate thickness and width, typically followed by a cutting step to finish the sizing process (Figure 2.1). Differences in processing techniques generally stem from the forming device. In slab-forming (Figure 2.2 a.) a conveyor belt and a series of rollers flatten and form the material to the producers' specifications. This is done by slicing strips, then cutting the desired length by guillotine. The number of rollers is dependent on the machine set up. This technique of manufacturing bars is common because it can process many different formulations and is less likely to crush ingredients, like puffs or crisps. In screw extrusion (Fig.2. 2 b.), the internal screw moves the material to a die that shapes the material, while roller extrusion (Fig. 2.2 c.) uses large rollers to flatten the material in a manner similar to a pasta machine. Many machines have a feedback adjustment system for improved control and use weight specifications to obtain the desired thickness and density of the final product (Production Techniques Ltd., 2015).

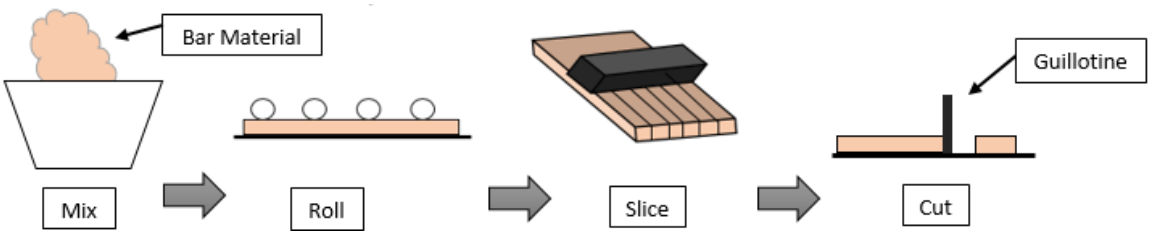

Figure 2.1. Processing steps for cold pressing nutrition bars before packaging steps.

Generally, in screw extrusion, pressure is applied to the system prior to the die, enhancing the volume expansion on the other side and, producing puffed products like, puffed cereals, candies, and pet food (Fig. 2.2b). Products manufactured using screw extrusion enter the hopper and proceed through the extruder via an internal screw. Innate back pressure occurs in the extruder as the material is pushed through a smaller die at the end of the screw (Reiser, 2017). The die gives the product its final shape and come in a wide range of die shapes and sizes give unique product dimensions and appearances (Imperial Design Technologies, 2015). Following die output, there is a cutting step to yield individual bars. While screw extrusion is versatile, there are processing challenges associated with certain higher fat protein bar formulations. Bars with peanut butter, for example, tend to leach fat as they pass through the die (Bond, 2017). This leaching, caused by mechanical force, leaves the bar dry, giving it a less desirable texture (Bond, 2017). Additionally, it is likely that slip could be an issue with screw extrusion because leached fat would make a slippery layer between the bar and extruder wall, but the main problem is primarily the leaching of fat as the material passes through the die. For this reason, methods for bar processing are often chosen by formula.

Roller extruders are versatile and are used for many bar types (Fig. 2.2c). Roller extrusion uses a hopper that feeds the material between two rollers (Tilghman, 2017). Once the material is past the rollers, it can either be pushed through a row of dies or sliced and cut as in slab forming. Some of these machines have the capability for multiple die outputs and can produce multiple rows of bars (Reiser, 2017). Like screw extrusion and slab-forming, thickness and height can be adjusted depending on the desired dimensions of the final product. What makes roller extrusion unique is its potential to use multiple rollers to yield

different bars. A three-roller system has greater control over the weight of the bar material

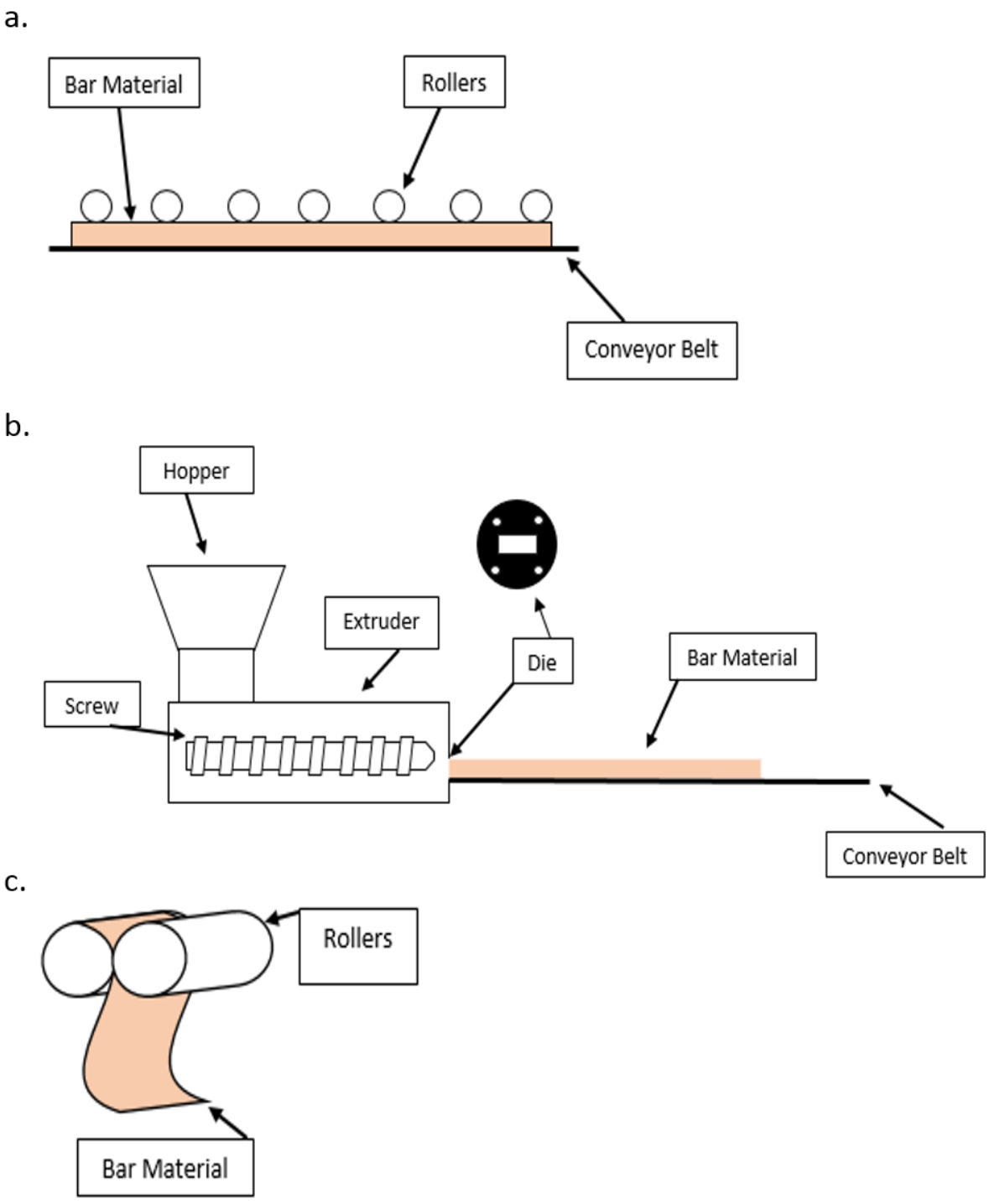

Figure 2.2. Illustrations of main types of bar manufacturing a. slab-form or cold pressing, b. screw extrusion, and c. roller extrusion.

and can adjust the density without altering the appearance (Whitaker, 2010). A four-roller system can produce filled bars with jams or peanut butter by taking multiple inputs and creating layers of bar material and filling (Figure 2.3) (Whitaker, 2010). While roller extrusion is versatile, it still has limits. For roller extrusion, processing high fat material can result in the rollers becoming coated with fat, which can cause slip during the feeding process (Bond, 2017).

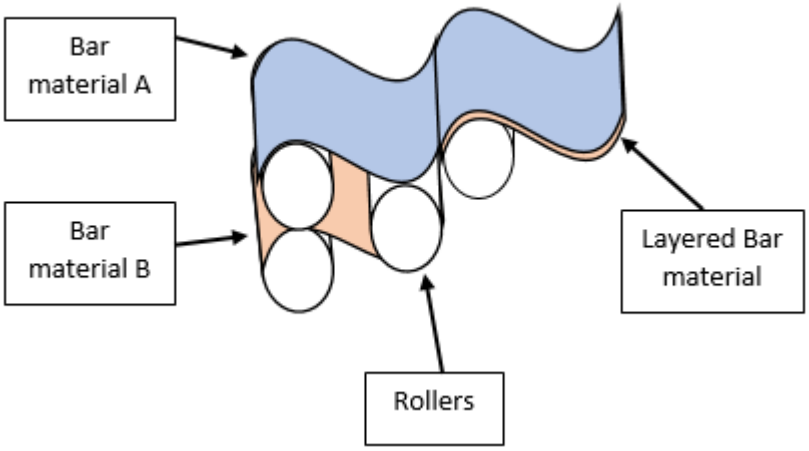

Figure 2.3. Multiple roller extrusion.

Both extrusion and slab-forming are complex unit operations that utilize processing variables to obtain the bar producers want. One of the main variables for high protein bar processing is the speed of the process line and pressure or force on the bar material (Imperial Design Technologies, 2015). In screw extrusion, there are additional variables of die size and shape (Reiser, 2017). Optimizing these variables can help reduce potential processing issues that can result in significant financial and time loss for companies. Common issues include clogging, sticking, slip, cold flow, and difficulty cleaning the processing equipment post operation. Equipment focused issues, such as sticking have been resolved for some manufacturers by changing the equipment to non-stick material. For example, Baker Technologies Enterprises switched from stainless steel rollers to Teflon rollers to resolve sticking (Tilghman, 2017). Cold flow, where the bar does not hold its shape after cutting, causes issues getting the bars into the packaging. Sticking and cleaning ability may be

controlled, but not eliminated through processing factors, such as switching materials used for rollers or contact surfaces.

Adjusting the formulation of high protein bars can have a significant impact on processing ability. This is especially true for higher-fat formulas which will likely slip or leach fat no matter what material is used for the processing surfaces (Bond, 2017). Changes in ingredient and/ or ingredient ratios can significantly impact rheological behavior by creating a more solid- or fluid-like product. The impact of the type and amount of sugar and protein used can also have a marked effect on rheological behavior. Therefore, an improved understanding of component interaction could improve protein bar processing.

2.2 FUNCTIONALITY OF COMPONENTS IN HIGH PROTEIN BARS

A combination of proteins, fats, carbohydrates, and inclusions are used to create the high protein bars consumers purchase. Each component plays a functional role in the physicochemical, rheological, and sensory properties of the bars.

2.2.1 PROTEIN

2.2.1.1TYPE OF PROTEIN

As the name “high protein bar” implies, protein is a major component of the formulation. Protein choice plays a significant role in making a functional, palatable bar. The type of protein chosen is often based on the target market, as there is a wide range of options and protein functionalities. High protein bars may contain one or more types of protein including whey, peanut, and pulse proteins. Pulse proteins typically include soy, pea, bean, and lentil proteins. One of the more popular proteins used in protein bars is whey protein. Whey protein is a group of proteins (Park & Haenlein, 2013) containing β-lactoglobulin, α-lactalbumin, bovine serum albumin, immunoglobulins, and cryoglobulins (Brady, 2013). Common forms of whey proteins found in high protein bars include whey protein hydrosylate, whey protein concentrate, and whey protein isolate. The functional properties of these proteins vary based on heat or acidification treatments during processing. Acidified whey proteins extruded at different temperatures demonstrate functional differences, above 21.1°C protein had improved cold-set gel strength and heat stability, and protein aggregates had lower solubility (Nor Afizah & Rizvi, 2014).

Sensory properties of whey protein powders are also important in high protein bars. Most whey products, both liquid and dry, contain lipids (Carunchia-Whetstine, Croissant, & Drake, 2005). Over time, whey products are susceptible to lipid oxidation, which can result in unpleasant sensory characteristics, including cardboard, soapy, and bitter flavors (Wright, Zevchak, Wright, & Drake, 2009; Evans, Zulewska, Newbold, Drake, & Barbano, 2010). The proteins themselves can also contribute to unpleasant flavors. Some of these disagreeable flavors are from bitter peptides proteins which may be exaggerated by the degree of hydrolysis or can be due to flavor binding (Leksrisompong, Miracle, & Drake, 2010). For example, in whey protein concentrate, the level of flavor binding is dependent on the type of chemical bond between the flavor volatile and the protein (Stevenson & Chen, 1996). For proteins, consumer acceptance pivots around bitter taste and aroma (Leksrisompong et al., 2010). Knowing that consumers control product success, care should be taken in formulating with whey protein to ensure a palatable flavor profile.

Globular proteins found in whey or serum include β-lactoglobulin, α-lactalbumin, bovine serum albumin, immunoglobulins, and cryoglobulins (Brady, 2013 & Kilara & Vaghela, 2018). The two main proteins are β-lactoglobulin and α-lactalbumin, which comprise approximately 70% of the protein content (Foegeding, Luck, & Vardhanabhuti, 2011). Since β-lactoglobulin has many desirable functionalities, whey protein is commonly used in food products. Applying shear to β-lactoglobulin changes its secondary structure, resulting in greater perceived viscosity (Qomarudin et al., 2015). β-lactoglobulin is also noted for its emulsion capacity and can form emulsions at 0.5% w/w concentration (Bouyer et al., 2011). β-lactoglobulin can also form gels, but salt is required to form a self-supported gel (Mulvihill & Kinsella, 1988). α-lactalbumin also has gelling capabilities, but its gelation time is much longer than β-lactoglobulin (Loveday, Rao, Creamer, & Singh, 2009). Along with its structural properties, α-lactalbumin has shown benefits for mammary gland health through bactericidal activity and initiating apoptosis in tumor cells (Permyakov & Berliner, 2000).

While whey proteins are popular in food products, there are advantages for using alternative proteins. One advantage is that these other proteins can be vegan, which opens a larger consumer market. Peanut proteins are generally made from peanut meal cakes, a waste product from processing peanut oil (Kain & Chen, 2010). The use of peanut proteins in protein bars could reduce a significant amount of waste, especially in developing countries

(Kain & Chen, 2010). Peanut flour made from peanut meal cakes contains about 50% w/w protein (Kain & Chen, 2010), while peanut protein concentrate contains approximately 85% w/w protein (Yu, Ahmedna, & Goktepe, 2007). Peanut protein is a beneficial nutrient because of its amount of protein and amino acids composition (Kholief, 1987). Functionally, peanut proteins offer emulsification abilities (Kain & Chen, 2010).

Another legume protein is soy. Soy proteins are composed of 90% globulin proteins, which are soluble in salt water (Brady, 2013). This solubility makes soy proteins ideal for tofu and meat substitutes, which utilize their gelling and emulsification properties (Brady, 2013). One protein with comparable emulsifying properties to soy is walnut protein (Mao & Hua, 2012). The investigation into walnut and other protein sources show promise for use of these proteins in the high protein industry.

While these proteins are useful alternatives, one of their main drawbacks is their allergen potential. Soy, peanut, and other nut proteins are all included in the eight major allergens, making them problematic in formulations. Pulse proteins, such as peas, beans, and lentils, can be used as a substitute for proteins that are major allergens. The pulse category has a general protein range of 17-30% w/w; peas have a protein content of 23-30% (Zare & Pletch, 2010). Pulse proteins' functional properties include water and fat binding, foaming, and gelation (Zare & Pletch, 2010). Compared to soy protein, pea proteins have lower emulsion stability, likely resulting from differences in amino acid composition (Tomoskozi, Lasztity, Haraszi, & Baticz, 2001). Unfortunately pulse proteins are associated with strong beany flavors which are unpalatable to consumers (Gelski, 2014). Overall, pulse protein functionality makes it a suitable replacement for the more major proteins.

2.2.1.2 PROTEIN FUNCTIONALITY

With the plethora of protein options for bars, protein selection is often based on protein functionality. Protein functionality plays a key role in the texture and appearance of high protein bars. Functional properties include water binding, fat binding, solubility, emulsifying abilities, and in food systems, gelling and dispersion (Zayas, 1997d). Because cohesive bars hold their shape, water and fat binding are the most impactful protein functionalities in high protein bars. Water binding is generally associated with the amount of water retained by protein, and sorption isotherms are often used to measure the extent of water binding (Zayas,

1997d). Protein configuration and amino acid composition directly affect water binding, which plays a significant role in determining water–protein interactions (BeMiller et al., 1996). Milk proteins have effective water binding capacities (Kneifel & Seiler, 1993). For caseins, water binding increases with heat treatment; variation is due to water-protein-solute equilibrium (Kneifel & Seiler, 1993). Variation in water-binding of globular proteins, like β-lactoglobulin, is dependent on interactions with other proteins, aggregation, denaturation, and degree of hydration (Kneifel & Seiler, 1993). This reinforces that protein composition and configuration affect water–protein interactions, and thus the functionality of the system.

Protein composition also impacts fat binding, which affects bar texture and appearance. Protein bars have a wide range of lipid content, between 4-16g per serving depending on formulation, to provide nutritional content and flavor, and improve bar appearance (Evolution Nutrition, 2016; Dugan et al., 2013). Protein structure and composition determine the amount of fat interaction. Having more nonpolar groups in protein increases the number of potential interaction sites and thus, overall fat binding ability (Zayas, 1997c). Similarly, protein surface area also plays a role in fat binding ability. Smaller particles with lower density have a greater ability to trap and interact with lipids than larger particles with higher density, which is likely due to the increased surface area to volume ratio and the increased exposure of hydrophobic regions in smaller, less dense particles (Zayas, 1997c). Fat binding has been correlated with surface hydrophobicity and protein solubility, which are impacted by protein configuration and composition (Zayas, 1997c).

Protein gelling ability can have a major influence on a food system's firmness, fracture stress, and overall mouthfeel (Foegeding, 2005). Gelation can affect viscoelastic behavior, viscosity, water and fat binding, cohesiveness, stickiness, adhesiveness, and hardness of a food system (Zayas, 1997b). For protein bars, protein gelling ability may not be a substantial portion of their desired functionality, but gelation may prevent cold flow. By altering the charged groups within the protein, the texture and rheological properties of food systems can be modified through gelation. The gelling abilities of protein are not universal and are directly affected by the charged groups on the protein (BeMiller et al., 1996). On a structural level, gelling requires partial unfolding of proteins' secondary structure, which is generally achieved through heat, acid, or alkaline treatment (Zayas, 1997b). Through protein and solvent interactions three-dimensional protein networks can form in the gelling process (Zayas,

1997b).

Protein emulsion capacity can help maintain a homogenous distribution of ingredients in protein bars, particularly when mixing hydrophobic and hydrophilic ingredients like lipids and sugar syrups. Proteins stabilize newly-formed emulsions by reducing the surface tension between components in the food system, such as carbohydrates and lipids (Zayas, 1997a). To create a stable emulsion good solubility and evenly-distributed positive and negative charges are needed (Zayas, 1997a); this is shown in partially denatured whey proteins and their increased emulsion capacity (Mantoviani, Cavallieri, & Cunha, 2011).

A major problem in the protein bar industry is bar hardening, which has been linked to a few factors, most notably protein. Protein aggregation, whether by moisture, pH, or temperature changes during storage was proposed to be the main cause (Zhou, Guo, Liu, Liu, & Labuza, 2013). In the protein–sugar–lipid matrix of protein bars, the protein and lipid droplets are suspended in a continuous sugar phase (Adams, 2008). The bar-hardening mechanism is believed to be due to protein hydration over time, creating a protein-sugar bicontinuous phase that disrupts the continuous sugar phase and increases hardening (Adams, 2008). The use of hydrolyzed proteins was suggested to reduce phase separation due to their smaller molecular weight, maintaining the continuous sugar phase resulting in giving softer bars (Adams, 2008). This bar hardening mechanism supports the hypothesis that protein size, charge, and composition have an impact on bar texture and functionality.

2.2.2 LIPIDS

In high protein bars, lipids play a key role in both nutrition and functionality. Lipids are organized into two groups, oils and fats. Oils are generally categorized as being liquid at ambient temperature. This property is related to the structure of the unsaturated hydrocarbon tails, which are kinked due to the presence of double bonds (BeMiller et al., 1996). These kinks make stacking the hydrocarbon chains difficult, preventing crystalline structures and solid formation (McClements & Decker, 2017). Fats tend to have fewer *cis* bonds along their hydrocarbon fatty acid chains, increasing packing density. With tightly packed hydrocarbon chains, a crystalline formation occurs, allowing the lipid to be solid at ambient temperatures (Powar & Chatwal, 2008). The differences in lipid behavior caused by chemical structures can impact air incorporation and melting point. This makes lipid selection important to achieving

the desirable characteristics for a food system.

A mix of oils, shortenings, and butters are used in high protein bars. Common oils in these bars include palm kernel, palm, soybean, safflower, and canola oil. Fats such as cocoa butter and shortenings are often used to help give the bars more structure at ambient temperatures. Shortenings are commonly used in food products that require solid fats for structure, including baked goods such as pies, cakes, and puff pastries (Rajah, 2014). Shortenings are generally manufactured from a blend of vegetable oils, undergo multiple processing steps and often fatty acid modifications to obtain the desired lipid crystallization (Ghotra, Dyal, & Narine, 2002). Processing of shortening involves the basic steps of degumming, neutralization, drying, bleaching, filtration, deodorization, polishing, and cooling (Rajah, 2014). Recently, shortening manufacturing has shifted from partial or total hydrogenation to fractionation modification to reduce *trans* fatty acids due to their associated health risks (Rajah, 2014). Fractionation separates triglycerides by crystallization once the lipid is melted. It is also performed to winterize an oil, to enrich a lipid with unsaturated triglycerides, or to sharpen the melting point of a lipid (Hamm, 1995). These modifications give specific nutritional and functional properties (Ghotra et al., 2002).

Lipid functionality is generally based on the ratio of solid to liquid fat, which dictates the plasticity, oxidative stability, and final attributes of the shortening (Ghotra et al., 2002, Rajah, 2014). One of the main attributes that affects the functional properties of shortening is the crystal structure and network of fat molecules rather than the solid fat content (Braipson-Danthine & Deroanne, 2004). Manipulation of the crystalline structure to obtain desired melting and crystallization characteristics can be done through applied shear and cooling rate. Crystallization characteristics are often determined by the end use of shortenings as they impact functionality of texture, hardness, and mouthfeel (Humphrey & Narine, 2004 & Humphrey, Moquin, & Narine, 2003).

Due to the high level of control in shortening functionality, the application range in foods is comprehensive. Understanding the food products desired functionality, processing steps, and its use provides selection criteria for shortenings used in food formulations. For example, additional free fatty acid esters can be added to shortenings for emulsification, which often helps with aeration for products like cakes and icings (Rajah, 2014; Ghotra et al., 2002). Foods like crackers and cookies or applications, such as frying, do not require aeration and

thus no emulsifiers are added (Ghotra et al., 2002). All-purpose shortenings are often emulsified and typically contain 5 to 8% mono- and diglycerides (Ghotra et al., 2002). For protein bars, shortenings are important for maintaining texture and appropriate firmness at ambient temperatures.

2.2.3 CARBOHYDRATES

The two main categories of carbohydrates used in high protein bars are fiber and sugars. Dietary fiber, such as non-starch polysaccharides, lignin, non-digestible oligosaccharides, or resistant starches, promotes nutrition and gastrointestinal health, helps maintain blood sugar levels, and reduces low-density lipoproteins when consumed at a level of 25-35 g per day (Lomer, 2015). Cellulose is a common fiber found in whole grains and may be present in multiple forms on an ingredient label such as carboxymethylcellulose or microcrystalline cellulose. Cellulose is a polysaccharide chain with linear β-1-4 D-glucose polymers (Dhingra, Michael, Rajput, & Patil, 2012). This molecular structure affects water binding (Kuntz, 1996) and creates different textural characteristics in food systems, most notably viscosity increases when used as a thickener (Dhingra et al., 2012). Cellulose can come in two different grades: bulking grade used to replace sugar and fat, or functional grade used for dietary purposes, such as to promote gastrointestinal health (Kuntz, 1996). Bulking grade cellulose is often considered a hydrocolloid, serving as a bulking agent in beverages, and can promote satiety by filling the stomach (Sannino et al., 2010). While bulking grade celluloses are typically used to swell and act as a filler, functional grade celluloses' functionality is primarily about non-digestibility to aid in digestive health.

The functionality of fiber is much different from digestible carbohydrates that are used in protein bars for sweetness. Sweetening carbohydrates can come from a variety of sources such as sucrose, glucose (dextrose), and high fructose corn syrup. Sugars, along with non-carbohydrate sweeteners like sugar alcohols and artificial sweeteners, provide sweetness and water binding in high protein bars (Brady, 2013). In most food systems, the main function of sugar is to provide sweetness. The scale used to measure sweetness is dextrose equivalent (DE), which shows the level of starch hydrolysis and measures the reducing power of a starch-based sugar. Using the DE scale, the longest chain referenced is starch and is given a value of zero (Rong, Sillick, & Gregson, 2009). The shortest reference on the DE scale is

glucose, which has a value of 100 (Rong et al., 2009). The DE scale takes advantage of the fact that saccharide (glucose) chains are the backbone of all sugars. Typically, the presence of more glucose and short saccharide chains results in a sweeter carbohydrate than one with longer saccharide chains.

Along with sweetness, sugars, especially reducing sugars, are a key element in non-enzymatic browning reactions, which provide many flavor and color compounds (Brady, 2013). Such browning reactions include caramelization and Maillard reactions, which produce desirable flavors and aromas like caramelizing onions, or contribute to negative sensory attributes, like burnt toast flavors (Davis, 1995). For caramelization, sugar and heat are required and the resulting color, flavor, and aromas are known as caramel (Davis, 1995). In Maillard reactions, water, an amine molecule, and a reducing sugar are the reagents (Davis, 1995). These reactions are integral to sensory characteristics of a food system by providing color, aroma, and flavor. In protein bars, Maillard reactions can occur during storage, resulting in darker bar appearance that could be desirable depending on consumer preferences (Adams, 2008).

Other properties of sugars have a larger impact on the functional properties of protein bars, such as water binding and crystallization. Sugars can bind water, reducing water activity or the unbound water in food that is available for reaction (Belitz, Grosch, & Schieberle, 2004). By reducing water activity, sugars reduce the rate of microbial growth, which in turn can improve shelf stability (Davis, 1995). Sugar's sweetness and ability to bind water are the main reasons it is added to many products. Another functional property of sugar is crystallization, which can be tied to water uptake and texture (Belitz et al., 2004). Crystallization is also utilized in sugar production to separate out molasses from granular sugars (Belitz et al., 2004). Sugar crystallization has been a suggested theory for bar hardening due to the high concentration of sugar in most formulations, but experimental results are inconclusive (Adams, 2008).

2.2.4 INCLUSIONS

Inclusions provide visual and textural contrast, flavor enhancement, and nutritional benefits in high protein bars (Berry, 2016). While they may not be found in large quantities, generally 8-10% by weight, inclusions affect the texture of the final product and its processing

ability (Mihalos & Schwartzberg, 2002). Most of the inclusions found in commercial high protein bars add crunch to an otherwise chewy texture. Puffs and nuts are common inclusions because of their crunch and neutral taste, so they can be used in both savory and sweet flavor profiles (Berry, 2016). Puffs are generally made from cereals such as rice, quinoa, and millet. Ingredients such as quinoa and millet are gluten-free and may also be used to promote a cleaner label, both of which are increasing in popularity with consumers (Berry, 2016) (Walters, 2016). Like puffs, nuts help provide crunch, but due to allergen concerns facilities are looking at nut alternative (Berry, 2016).

2.3 MECHANICAL PROPERTIES

Rheology is the study of deformation and flow of matter. Rheometry looks at a materials response to applied strain and stress (Steffe, 1996), giving quantitative data that can be useful in modeling material behavior (Böhm, Brehmer, & Kraume, 2016). Studying high protein bars using rheometry allows for a better fundamental understanding of high protein bars mechanical properties and can help reduce future processing issues.

In rheometry, deformation can result from force or torque applied material surface and vice versa. Normal force is applied perpendicular to the material surface and shear force is applied parallel to the material surface (Tabilo-Munizaga & Barbosa-Cánovas, 2005; Steffe, 1996). In protein bar processing, bar thickness can be adjusted using normal or shear forces to cause deformation and achieve the desired bar thickness.

Many solid materials exhibit primarily linear elastic behavior, in which stress and strain remain linearly proportionate under applied force, which can be described by Hooke's Law (Eqn. 2.1) (Steffe, 1996). Upon removal of the force, the material returns to its original state (Steffe, 1996). As viscoelastic materials, protein bars will likely exhibit nonlinear elastic type behavior, particularly under industrial and oral processing conditions, limiting the effectiveness of Hooke's Law to fully describe their behavior.

$$\sigma_{12} = E\gamma \tag{2.1}$$

2.3.1 SMALL STRAIN RHEOLOGICAL TESTING

There are many tests used to give a well-rounded picture of the extent of elastic and

viscous behaviors of a material. Materials generally exhibit viscoelastic behavior, showing both elastic and viscous responses to stimuli. Elastic materials store stress until the stress is removed, then the material promptly returns to its original form. Viscous materials dissipate stress rather than store it, making it difficult for the material to return to its original form once the stress is removed. Viscoelastic materials display behaviors that partially store or dissipate stress, so they cannot be complete characterized by being elastic or viscous. High protein bars can exhibit a range of viscoelastic behaviors depending on formulation.

Some tests, like creep and step relaxation, give an estimate of the degree of viscous and elastic behavior (Steffe, 1996). Creep testing looks at how a material responds to applied stress over time, flow over long time periods, or behavior at very low frequencies (Steffe, 1996). Creep or cold flow in the bar industry is where the bar does not hold the desired shape during prosessing or in packaging. Similar to creep testing, stress relaxation or step strain gives an approximation of the elastic or viscous behavior in a material. Stress relaxation looks at how a material behaves in response to a set amount of deformation that is then removed (Steffe, 1996). An elastic material would have little change after such a test, a viscoelastic solid would slowly relax to its orignial state, and a viscoelastic liquid would slowly relax to zero (Steffe, 1996). In high protein bars, relaxation and cold flow tests give a rough estimation of long-time viscoelastic behavior of the formulation. Temperature sweeps can also be useful in illustrating food rheological behaviors important to processing. Temperature sweeps evaluate the change of material behavior with temperature, which is important for foods that undergo significant temperature changes during processing (Steffe, 1996). In the case of protein bars, all processing is done at ambient temperatures, putting such a test outside of the scope of this current project.

Small amplitude oscillatory shear (SAOS) tests include stress relaxation test, creep tests, and start-up flow tests (Steffe, 1996). SAOS tests provide information about the viscoelastic nature of a material under small stresses and strains (Steffe, 1996). Depending on the test parameters, either strain or stress is changed while frequency is held constant, giving strain or stress sweeps, respectively (Steffe, 1996). To demonstrate the full behavior of the material, the strain must cover the linear viscoelastic region (LVR), where the viscoelastic behavior is strain-independent, as well as strains beyond the LVR to determine the critical strain along with the extent of structure of the material (Fig. 2.4) (Franck, 2016). Critical

strain is the point at which the LVR ends, the material becomes strain-dependent, and the microstructure is permanently deformed, often calculated by the point of suddenly increased strain multiplied by 0.75 (Steffe, 1996). To demonstrate the full behavior of the material, the strain must cover the linear viscoelastic region (LVR), where the viscoelastic behavior is strain-independent, as well as strains beyond the LVR to determine the critical strain along with the extent of structure of the material (Fig. 2.4) (Franck, 2016). Critical strain is the point at which the LVR ends, the material becomes strain-dependent, and the microstructure is permanently deformed, often calculated by the point of suddenly increased strain multiplied by 0.75 (Steffe, 1996). x When G' is larger than G", the material demonstrates elastic-dominant behavior (Steffe, 1996). For viscous-dominant behavior, G" is larger than G' (Steffe, 1996).

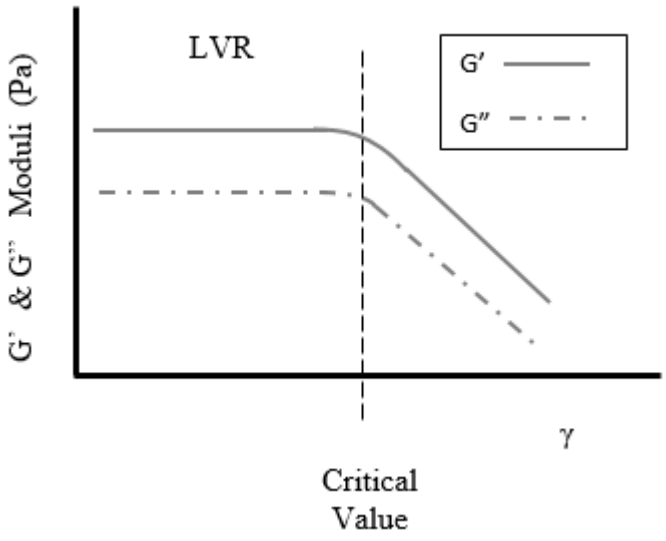

Figure 2.4. Amplitude sweep showing the LVR and critical point of a viscoelastic material.

$$G' = \left(\frac{\sigma}{\gamma}\right)\cos(\delta) \tag{2.2}$$

$$G'' = \left(\frac{\sigma}{\gamma}\right)\sin(\delta) \tag{2.3}$$

Frequency sweeps are another common oscillatory test. Frequency sweeps maintain constant stress or strain while the frequency increases, providing information on how viscous

and elastic behavior change with the rate of applied stress or strain (Steffe, 1996). Knowing the changes in viscous and elastic behavior at certain strains makes frequency sweeps useful for comparison of ingredient or processing changes (Steffe, 1996).

2.3.2 LARGE STAIN OSCILLATORY TESTING METHODS

Looking at nonlinear behavior gives a much wider picture of a materials deformation behavior under high stresses and strains, allowing for better understanding for processing applications. In food, LAOS has been used to better understand the microstructure of gluten-free flour doughs (Yazar, Duvarci, Tavman, & Kokini, 2017), hard wheat flour dough (Yazar, Duvarci, Tavman, & Kokini, 2016), blue cheese (Helen S. Joyner (Melito), Francis, Luzzi, & Johnson, 2017), food gels (H.S. Joyner (Melito), Daubet, & Foegeding, 2013), tomato paste, and mayonnaise (Duvarci, Yazar, & Kokini, 2017). A large part of the rheological study of foods focuses on SAOS tests performed in the LVR. One of the main reasons for this is that the equations to interpret G' and G" require assumptions that are only valid in the LVR, like the linear calculation for stress and phase shift (Hyun, Kim, Ahn, & Lee, 2002; Steffe, 1996). Due to how strain is computed from displacement the description of strain is limited, leading to misinterpretation outside of the LVR (Caswell, 1980).

The evolution of LAOS analysis has minimized this misinterpretation outside of the LVR. One category of LAOS analyses, Fourier transform rheology, was made possible by Fourier computing (Melito, 2012). Fourier transform rheology uses harmonics to describe frequency and time domain relationship (C. Klein, Venema, Sagis, & van der Linden, 2008; Läuger & Stettin, 2010). Fourier analysis assumes sinusoidal strain input are used, configuring inputs relative to time and converts these outputs into harmonics (Melito, 2012). LAOS produces higher-order harmonics while SAOS does not (Ewoldt, McKinley, & Hosoi, 2007). By applying Fourier transformation of the rheology spectrum to the time and stress relationship, the odd harmonics are given for viscoelastic materials (Wilhelm, 2002). Improvement of this analysis was shown by Klein et al. (2007), who demonstrated that super positioning Fourier spectra can provide improved separation at higher harmonics, clarifying interpretation of various types of LAOS data (C. O. Klein, Spiess, Calin, Corneliu Balan, & Wilhelm, 2007). This analysis helps differentiate between materials based on their behavior characteristics (Wilhelm, 2002).

Viscoelastic decomposition is another category of LAOS analysis. An example of this is Ewoldt et al. (2008) who elaborated on the initial Fourier analysis by adding Chebyshev polynomials. Adding Chebyshev polynomials of the first kind to elastic (e) and viscous (v) stress response vs. strain inputs provides separate Fourier series which can be analysis separately and simultaneously (Ewoldt, Hosoi, & McKinley, 2008). When applied to raw waveform data from LAOS testing, Chebyshev polynomials can be used to separate nonlinear viscoelastic behavior into strain-softening, strain-hardening, shear-thinning, and shear-thickening based on the third-order Chebyshev coefficients (e_3 and v_3) (Ewoldt et al., 2008). The third-order Chebyshev coefficients relate third-harmonic viscoelastic moduli (G_3' and $G_3^{"}$) and third-harmonic phase angle (δ_3), giving them physical meaning outside of the LVR (Table 2.1) (Ewoldt et al., 2008; Melito, 2012; Melito, Daubert, & Foegeding, 2013). The ability of Chebyshev analysis to give physical meaning to LAOS data is what makes it a unique analysis.

Table 2.1. Interpretation from modulus ratios.

Value	G'_L/G'_M	η'_L/η'_M
>0	Strain stiffening	Shear thickening
0	Linear elastic	Linear viscous
<0	Strain softening	Shear thinning
	G'_3/G'_1	G''_3/G''_1
≥0.01	Nonlinear viscoelastic behavior	Nonlinear viscous behavior
<0.01	Linear viscoelastic behavior	Linear viscous behavior

Another main category of LAOS analysis is geometric interpretation, which gave a visual representation of material behaviors. One example of the classification of complex fluids is strain hardening, strain thinning, weak strain and strong strain overshoot represented by G' and G" either both increasing, both decreasing, one increasing then decreasing, or one initially increases then decreases, respectively (Hyun et al., 2002). Another example of geometric interpretation is the use Lissajous-Bowditch curve shapes to determine structural behaviors which produced similar conclusions to the classification of complex fluids, giving the data a physical interpretation (Hyun, Nam, Wilhelm, Ahn, & Lee, 2003). Lissajous-Bowditch curves are plots of stress vs strain and are visual depictions of the linear and

nonlinear viscoelastic material behaviors (Ewoldt, McKinley, & Hosoi, 2007). When Lissajous plots are used to determine the ratio of large strain elastic modulus to minimum strain elastic modulus (G'_L/G'_M) for strain-hardening or -softening behavior and corresponding instantaneous viscosities (η'_L/η'_M) for shear-thickening or -thinning behavior, the analysis is viscoelastic decomposition (Table 2.2) (Ewoldt et al., 2008). To add another dimension of nonlinear material characteristics to Lissajous curves, they can be plotted with relation to frequency on Pipkin diagrams (Ewoldt et al., 2008).

Using these various methods of LAOS analysis gives meaningful information the nonlinear behaviors of materials (Table 2.2). Since these LAOS analysis methods vary, their results may be different. Regardless of the analysis method, the obtained LAOS information can still be used in determining texture-structure-function relationships in materials.

Table 2.2. Comparison of LAOS analysis methods.

Analysis Categories	Examples within Category	Understanding from Analysis	Reference
Fourier Analysis	Fourier transformation	Fourier spectra provides a unique characterization of material behavior, which is used to distinguish between samples	(Wilhelm, 2002)
Geometric Interpretations	Lissajous plots and Pipkin diagrams	Visually shows material response, giving a "rheological fingerprint"	(Rogers & Lettinga, 2012 & Ewold et al., 2008)
Viscoelastic Decomposition	Chebyshev polynomials	Gives physical interpretation of both nonlinear viscous and elastic behavior simultaneously and separately	(Ewoldt et al., 2007 & Ewoldt et al., 2008)

Another useful test for understanding material behavior is adhesion or tack testing, a large-strain rheological test frequently used for understanding polymer behaviors. For a material to have adhesive properties, it must demonstrate both elastic and viscous behaviors (Grillet, Wyatt, & Gloe, 2012). Though there are other factors that may affect adhesion, the viscous behavior is needed for surface contact and molding and the elastic properties allow the material to resist applied stress preventing material flow (Grillet et al., 2012). On the molecular level, polymers, particularly proteins, are noted for their adhesive potential (Wall &

Huebner, 1980). This is often due to the hydrophobic surface interactions, which are useful in biological functions such as DNA synthesis (Dorh et al., 2016). Since proteins and sugar syrups often contribute to adhesive qualities of materials, adhesion testing can improve understanding of high protein bar formulations and help indicate potential sticking issues in processing equipment.

2.3.3 TRIBOLOGY

Tribology is the study of wear, friction, and lubrication. To best examine tribological behaviors of any material, the entire system should be considered to give a more holistic understanding of what is happening and improves data interpretation (Bayer, 2002). The elements that are considered part of a tribosystem include relative motion, loading, lubrication, environment, surface topography, geometry of the contacting pairs, contact configuration, and contact materials (Bayer, 2002). In industry, tribology has been used mainly in machinery to study wear, but there is increased focus on biotribology of prosthetics and tissue replacement, nanotribology of surface interactions of biodetectors and lasers, and green tribology of renewable lubricants (Ricci, 2011). In food, tribology has been used to investigate friction and lubrication behaviors to better understand oral processing and textural attributes not described by rheological properties (Chen & Stokes, 2012). By exploring these new possibilities for tribometry and gaining a better understanding of food wear behaviors, more palatable food textures and more effective and usable products, processes, and technologies can be created.

Lubricants can be used to minimize the effects of friction and wear on sliding surfaces. Depending on the tribosystem, the sliding surfaces, and the testing environment, the lubricant can have a variety of impacts on wear and friction behaviors. These may include increasing or decreasing wear and friction—not necessarily simultaneously—depending on the lubricant and the system (Bayer, 2002). The main types of lubricants are dry or solid phase, fluid or liquid phase, and boundary which is within the system (Bayer, 2002). Often lubrication can be thought of as a visible layer, like grease between gears, but it can also be provided by molecules in the sliding or stationary material. A thin film, five to ten molecules thick, can have fluid-like behavior due to molecular interactions (Cushman, 1990). This molecular-level lubrication could be of interest for food interactions, as lubrication and friction play a role in

sensory perceptions such as mouthfeel. In addition to food, saliva also plays a role in oral lubrication (Malone, Appelqvist, & Norton, 2003). Along with mouthfeel, lubrication of oral surfaces and mouth coating have also been studied (Morris & Groves, 2013), leading to the observation that aspects of chewdown and swallowing can be described with tribology (Chen & Stokes, 2012). Most of these studies focus on friction and lubrication; there has been one study on the effects of oral cavity processing on lozenge decay, which is considered wear, but this study mainly focused on oral processing (Keck, 2015). Most current publications on food tribology focus on oral friction and lubrication of foods and relate data to sensory attributes, leaving the aspect of wear during industrial and oral processing relatively untouched. Food wear behaviors may be used to better understand how foods move through processing equipment and improve production. Wear is the removal of material from a surface over time by sliding against another surface. The degree of wear is dependent on material interactions and lubrication (Bayer, 2002). Since wear is the removal of material from a surface, connecting high protein bar wear and the ability of the bars to move through processing equipment has potential to predict processability of bar formulations.

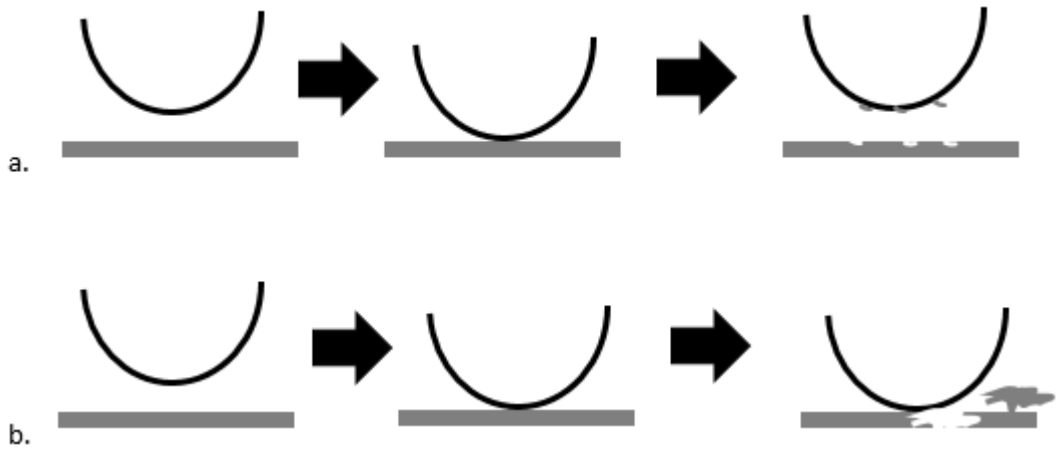

Figure 2.5. Common types of wear a. adhesive wear, b. abrasive wear.

For hard materials, there are four main mechanisms of wear: abrasion, adhesion, surface fatigue, and tribology chemical reaction (Poulachon, Bandyopadhyay, Jawahir,

Pheulpin, & Seguin, 2004). Abrasive wear is common in the metal industry and often found in grinding mechanics (Fig. 2.5 a.) (Li, 2004). Adhesive wear involves two surfaces that stick together while moving in opposite directions or one moving faster relative to the other; weak spots on one of the surfaces allows a small piece of the weaker material to be removed (Fig. 2.5 b.) (Li, 2004). Surface fatigue wear, in which the material surface is worn to the point of fatigue and pieces start to be removed from the surface, results from repeated cycles which weakens the material. Chemical reaction wear is often due to corrosive surroundings. An example of this is oxidative wear, beginning with the metal being covered in an oxide, which often acts as a lubricant. Friction can remove this oxide layer, resulting in adhesive or abrasive wear (Li, 2004). These four wear mechanisms may stand alone or be coupled depending on the system (Bayer, 2002).

Friction can impact the wear on sliding surfaces and is one of the many factors affecting system interactions. For viscoelastic materials, adhesion and deformation directly impact the response to an applied load (Bayer, 2002). To ensure accurate data, the inputs for wear testing of applied load, sliding distance, sliding speed, temperature, humidity, contact area, and the number of contacts must be carefully selected (Bayer, 2002). The relationship between load and the resulting wear can be seen in Archard's wear law (Eqn. 2.4).

$$V = \frac{K}{3}\frac{PS}{p} \tag{2.4}$$

Here, P is load (N), K is the probability of transfer (unitless), K/3 is the dimensionless wear rate, p is the material hardness (Pa), V is the volume of wear (m^3), and D is the sliding distance (m) (Bayer, 2002.). According to Archard's wear law, more wear will occur on softer materials that have higher loads placed on them. Additionally, Archard's wear law assumes that the material volume removed through wear is directly proportional to friction force. This assumption holds for most hard surfaces, but with more viscoelastic materials that are more susceptible to deformation under an applied load, the assumption that force is proportional to material removed may not hold.

Current soft material wear studies focus on joint replacement and advances in biotechnology, such as artificial cartilage and contact lens improvements. These studies highlight the potential to apply wear measurements to food products, as materials like

hydrogels are viscoelastic, similar to many food products. Hydrogels offer a close analog to foods compared to hard materials. The wear behavior of polyethylene and hydrogels is providing significant advances in biotechnology. In joint replacement research, polyethylene has shown good lubrication properties that improve artificial joint wear resistance and increased life span (Kyomoto, Moro, Takatori, Kawaguchi, & Ishihara, 2011; Kocen, Gasik, Gantar, & Novak, 2017). Hydrogels have been used as artificial cartilage because of their lubrication properties (Freeman, Furey, Love, & Hampton, 2000), making them a material of interest for contact lenses to reduce friction against the eye during use (Bettuelli et al., 2013). Though tribology of soft materials is currently centered around the medical field, it could also be used to study wear of food products, assisting in advances in food science and engineering. In the case of high protein bars, these advances could provide a tool to determine the processing ability of novel bar formulations.

2.4 CONCLUSION

By studying the wear behavior of foods, such as high protein bars, greater insight into food processing behaviors may be discovered. These insights may be used to optimize processing operations such as extrusion, rolling, and slicing. However, there is no published literature on the wear and rheology of high protein bar formulations to date. Gaining knowledge of high protein bar wear and rheology could have significant benefits, including saving companies time, money, and materials, particularly when developing new bar formulations. For high protein bar production, the benefits of better understanding how wear relates to processing behaviors are twofold. First, solving processing issues results in a more cost-effective operation, providing consumers with palatable products at a reasonable cost. Additionally, research on high protein bar wear and rheological behaviors has significant potential to advance the understanding of how food wear contributes to food processing behaviors, providing new insights into factors controlling food behaviors under processing conditions.

2.5 REFERENCES

Bayer, R. (2002). *Wear Analysis for Engineers* (1st ed.). Vestal: HNB Publishing.

Brady, J. (2013). *Introductory Food Chemistry* (1st ed.). Ithaca, New York: Cornell University Press.

Caswell, B. (1980). Computation of Large Strain in the Simulation of Memory Fluids. In *Rheology* (pp. 313-0314). New York.

Chen, J., & Stokes, J. R. (2012). Rheology and tribology: Two distinctive regimes of food texture sensation. *Trends in Food Science & Technology*, *25*(1), 4–12. https://doi.org/10.1016/J.TIFS.2011.11.006

Dorh, N., Zhu, S., Dhungana, K. B., Pati, R., Luo, F.-T., Liu, H., & Tiwari, A. (2016). BODIPY-Based Fluorescent Probes for Sensing Protein Surface-Hydrophobicity. *Scientific Reports*, *5*(1), 18337. https://doi.org/10.1038/srep18337

Duvarci, O. C., Yazar, G., & Kokini, J. L. (2017). The comparison of LAOS behavior of structured food materials (suspensions, emulsions and elastic networks). *Trends in Food Science & Technology*, *60*, 2–11. https://doi.org/10.1016/J.TIFS.2016.08.014

Ewoldt, R., Hosoi, A. E., & McKinley, G. H. (2008). New measures for characterizing nonlinear viscoelasticity in large amplitude oscillatory shear. *Journal of Rheology*, *52*(6), 1427–1458. https://doi.org/10.1122/1.2970095

Ewoldt, R., McKinley, G., & Hosoi, A. E. (2007). Fingerprinting Soft Materials: A Framework for Characterizing Nonlinear Viscoelasticity.

Franck, A. (2016). *Understanding Rheology of Structured Fluids*. Retrieved from http://www.tainstruments.com/pdf/literature/AAN016_V1_U_StructFluids.pdf

Gelski, J. (2014). Masking proteins undesirable flavors | Food Business News | July 18, 2014 10:49. Retrieved September 9, 2018, from https://www.foodbusinessnews.net/articles/4597-masking-protein-s-undesirable-flavors

Hyun, K., Kim, S. H., Ahn, K. H., & Lee, S. J. (2002). Large amplitude oscillatory shear as a way to classify the complex fluids. *Journal of Non-Newtonian Fluid Mechanics*, *107*(1–3), 51–65. https://doi.org/10.1016/S0377-0257(02)00141-6

Hyun, K., Nam, J. G., Wilhelm, M., Ahn, K. H., & Lee, S. J. (2003). Nonlinear Response of Complex Fluids Under LAOS Flow. *Korea_Australia Rheology Journal*, *15*(2), 97–105. Retrieved from http://citeseerx.ist.psu.edu/viewdoc/download?doi=10.1.1.901.8060&rep=rep1&type=pdf

Joyner (Melito), H. S., Daubet, C. R., & Foegeding, E. A. (2013). Relationships Between Nonlinear Viscoelastic Behavior and Rheological, Sensory and Oral Processing Behavior of Commercial Cheese. *Journal of Texture Studies*.

Joyner (Melito), H. S., Francis, D., Luzzi, B., & Johnson, J. R. (2017). The effect of storage temperature on blue cheese mechanical properties. *Journal of Texture Studies*. https://doi.org/10.1111/jtxs.12301

Keck, M. E. (2015). Tribological and Thermodynamic Analysis of Lozenge Decay during Oral Processing. Retrieved from https://repository.lib.ncsu.edu/handle/1840.16/10350

Kilara, A., & Vaghela, M. N. (2018). Whey proteins. *Proteins in Food Processing*, 93–126. https://doi.org/10.1016/B978-0-08-100722-8.00005-X

Klein, C. O., Spiess, H. W., Calin, A., Corneliu Balan, § and, & Wilhelm, M. (2007). Separation of the Nonlinear Oscillatory Response into a Superposition of Linear, Strain Hardening, Strain Softening, and Wall Slip Response. https://doi.org/10.1021/MA062441U

Klein, C., Venema, P., Sagis, L., & van der Linden, E. (2008). Rheological discrimination and characterization of carrageenans and starches by Fourier transform-rheology in the non-

linear viscous regime. *Journal of Non-Newtonian Fluid Mechanics*, *151*(1–3), 145–150. https://doi.org/10.1016/J.JNNFM.2008.01.001

Kocen, R., Gasik, M., Gantar, A., & Novak, S. (2017). Viscoelastic behaviour of hydrogel-based composites for tissue engineering under mechanical load. *Biomedical Materials*, *12*(2), 025004. https://doi.org/10.1088/1748-605X/aa5b00

Läuger, J., & Stettin, H. (2010). Differences between stress and strain control in the non-linear behavior of complex fluids. *Rheologica Acta*, *49*(9), 909–930. https://doi.org/10.1007/s00397-010-0450-0

Leksrisompong, P. P., Miracle, R. E., & Drake, M. (2010). Characterization of Flavor of Whey Protein Hydrolysates. *Journal of Agricultural and Food Chemistry*, *58*(10), 6318–6327. https://doi.org/10.1021/jf100009u

Li, C. X. (2004). Wear and Wear Mechanism. Retrieved January 12, 2018, from http://emrtk.uni-miskolc.hu/projektek/adveng/home/kurzus/korsz_anyagtech/1_konzultacio_elemei/wear_and_wear_mechanism.htm

Malone, M. ., Appelqvist, I. A. ., & Norton, I. . (2003). Oral behaviour of food hydrocolloids and emulsions. Part 1. Lubrication and deposition considerations. *Food Hydrocolloids*, *17*(6), 763–773. https://doi.org/10.1016/S0268-005X(03)00097-3

McClements, D. J., & Decker, E. A. (2017). Lipids. In S. Damodaran & K. L. Parkin (Eds.), *Fennema's Food Chemistry* (5th ed., pp. 171–233). Boca Raton: CRC Press Taylor & Fransis Group.

Melito, H. (2012). *Large Amplitude Oscillatory Shear Behavior of Food Systems*. North Carolina State University.

Morris, V. J., & Groves, K. (2013). *Food Microstructures : Microscopy, Measurement And Modelling*. Elsevier Science. Retrieved from https://books.google.com/books?hl=en&lr=&id=k2NEAgAAQBAJ&oi=fnd&pg=PA292&dq=food+tribology&ots=8Q437kHyTz&sig=5ljizDz5FtFk-cpp7zqBlAq4uwY#v=onepage&q=food tribology&f=false

Rong, Y., Sillick, M., & Gregson, C. M. (2009). Determination of Dextrose Equivalent Value and Number Average Molecular Weight of Maltodextrin by Osmometry. *Journal of Food Science*, *74*(1), C33–C40. https://doi.org/10.1111/j.1750-3841.2008.00993.x

Steffe, J. F. (1996). *Rheological Methods in Food Process Engineering* (2nd ed.). East Lansing: Freeman Press. Retrieved from https://bblearn.uidaho.edu/bbcswebdav/pid-1105998-dt-content-rid-9580077_1/courses/201610_38230/STEFFE.pdf

Tabilo-Munizaga, G., & Barbosa-Cánovas, G. V. (2005). Rheology for the food industry. *Journal of Food Engineering*, *67*, 147–156. https://doi.org/10.1016/j.jfoodeng.2004.05.062

Wilhelm, M. (2002). Fourier-Transform Rheology. *Macromolecular Materials and Engineering*, *287*(2), 83–105. https://doi.org/10.1002/1439-2054(20020201)287:2<83::AID-MAME83>3.0.CO;2-B

Yazar, G., Duvarci, O. C., Tavman, S., & Kokini, J. L. (2016). Effect of mixing on LAOS properties of hard wheat flour dough. *Journal of Food Engineering*, *190*, 195–204. https://doi.org/10.1016/J.JFOODENG.2016.06.011

Yazar, G., Duvarci, O., Tavman, S., & Kokini, J. L. (2017). Non-linear rheological behavior of gluten-free flour doughs and correlations of LAOS parameters with gluten-free bread properties. *Journal of Cereal Science*, *74*, 28–36. https://doi.org/10.1016/J.JCS.2017.01.008

CHAPTER 3: IMPACT OF FORMULATION ON HIGH PROTEIN BAR RHEOLOGICAL AND WEAR BEHAVIORS

3.1 ABSTRACT

Due to the popularity of high protein bars, many new formulations are being generated to meet consumer preferences. New formulations may have different mechanical behaviors that can impact processing ability, which makes determining the effect of ingredients on processing ability important. Thus, the objective of this study was to determine the effects of major ingredients in high protein bars on their rheological and tribological behaviors. Two response surface designs of model high protein bars comprising whey protein isolate (WPI), high fructose corn syrup (HFCS), and either canola oil or vegetable shortening were evaluated. Rheological tests, including adhesion, strain and frequency sweeps, large amplitude oscillatory shear, and wear testing, were conducted to determine the impact of individuals on protein bar behavior. Oil formulas had greater adhesion at higher levels of HFCS, while shortening formulations were affected by shortening more than HFCS, resulting in lower overall adhesive maximum forces. Formulas with higher levels of WPI had lower phase angles and greater nonlinear viscoelastic and strain-hardening behaviors, while formulas with higher lipid and HFCS levels had higher phase angles. Ingredient ratio had a notable impact on high-protein bar rheological and wear behaviors, suggesting that rheological and tribological testing could be useful for indicating processing ability of high protein bars.

3.2 INTRODUCTION

High protein bars have been a growing industry the last few years (Franco, 2015). To keep current with consumer preferences and expectations, the food industry has developed many new formulations. The rheological and tribological behavior of these new formulation may be important for manufacturing high protein bars that meet consumer expectations. High protein bar formulations consist of three basic ingredients: protein powder, a sweetener, and some form of lipid. From the observation of most commercial high protein bar labels, the variety of each basic ingredient used is extensive; this study used a model system composed

of HFCS, WPI, and a liquid and solid lipid, i.e. canola oil and vegetable shortening, respectively. It is likely that the level of each ingredient has impact on the rheological and tribological behavior of high protein bars (Hogan, O'Loughlin, & Kelly, 2016).

Rheological tests have been used to better understand the mechanical behavior of many semisolid foods (Böhm, Brehmer, & Kraume, 2016). These rheological tests include adhesion, which provides information on stickiness or adhesiveness, frequency sweeps, which provide information on viscoelastic behavior over different timescales, and strain sweeps, which provide information on critical strain, which marks the end of the linear viscoelastic region (LVR) and the onset of permanent definition to the sample structure. (Steffe, 1996) While these rheological tests give valuable information about material information, large amplitude oscillatory strain (LAOS) tests can give additional behavioral information because they probe material viscoelastic behavior beyond the LVR (Ewoldt, Hosoi, & McKinley, 2008). LAOS has been used in many semisolid foods to better understand their microstructures and large-strain viscoelastic behaviors. Such foods include gluten-free flour dough (Yazar, Duvarci, Tavman, & Kokini, 2017), blue cheese (Helen S. Joyner (Melito), Francis, Luzzi, & Johnson, 2017), mashed potatoes (Helen S. Joyner (Melito) & Meldrum, 2015), locust bean gum gels (Sousa & Gonçalves, 2015), tomato paste, and mayonnaise (Duvarci, Yazar, & Kokini, 2017).

The field of rheology encompasses a subsection called tribology, the study of wear, friction, and lubrication. Recently, the wear of soft solid foods has been modeled to better understand how wear is related to food rheological behaviors (Tan & Joyner, 2018). Wear testing has been used to determine possible effectiveness of artificial cartilage in joint prosthetics (Yarimitsu, Sasaki, Murakami, & Suzuki, 2016; Kyomoto, Moro, Takatori, Kawaguchi, & Ishihara, 2011; Li, Wang, & Wang, 2016). Because wear testing is effective in determining the durability of artificial cartilage in actions similar to those observed in high-protein bar processing, e.g. compression and rubbing contacts, wear testing could be effective in predicting processing ability of high protein bars. Artificial cartilage and high protein bars are both soft solids, which makes wear testing feasible on high protein bars. The objective of this study was to determine the effects of major ingredients in high protein bars on their rheological and tribological behaviors.

3.3 MATERIALS AND METHODS

3.3.1 MATERIALS

Proximate content validation of whey protein isolate, (90% protein, dry basis) (Glanbia Nutritionals, Inc. Fitchburg, WI, USA) was done using combined SDS-PAGE and chromatography with an Agilent Bioanalyzer 2100 (Agilent, Santa Clara, CA). Protein 230 chips with a 4.5-240kDa molecular weight range were used for analysis (Smith et al., 2010). Chip and sample preparation were done according to Agilent protocols. Briefly, protein samples were vortexed and centrifuged at 11,000 RPM in a urea buffer, samples were added to a buffer containing an equal ratio of sodium phosphate and sodium chloride, then the solution was denatured, and a ladder standard was added. Samples were then heated to 95°C for 5 min and added to chip wells. The presence of β-lactoglobulin, α-lactalbumin, and casein was confirmed.

Proximate content validation of high fructose corn syrup (42% fructose) (Batory Foods, Inc. Hopkins, MN, USA) was completed through HPLC analysis according to a modified version of the compositional sugar analysis of Ng & Reuter (2015). Adjustments to the protocol included using a 72:28 acetonitrile/water dispersion to improve resolution at a flow rate of 0.5 ml/min. Despite solvent and HFCS concentration adjustments, percentages were approximate due to poor peak resolution; major sugars fond included fructose (36%), maltose (15%), glucose (12%), and sucrose (11%).

Fatty acid profiles for canola oil and vegetable shortening (Crisco, both purchased form a local retailer in Moscow, ID, USA) were determined using unsaturated fatty acid methyl ester (FAME) analysis using gas chromatography and C14-C22 FAME mix (Sigma-Aldrich/Millipore Sigma, Saint Louise, MI, USA) as a standard (AOAC, 2001). Both oil and shortening contained primarily palmitic and stearic fatty acids. No further purification of ingredients was done before testing.

3.3.2 FORMULATION PREPERATION

Twenty formulations created for two central composite center-faced response surface designs one for oil and the other for shortening based formulations these were prepared using the weights for WPI, HFCS, and either oil or shortening specified in Table 3.1. A KitchenAid Classic 275W stand mixer (KitchenAid; St. Joseph, MI, USA) was used to mix ingredients at

speed 1 for 2 min. Samples were then wrapped tightly in plastic wrap and placed in zippered plastic bags, which were stored at room temperature (22±2°C) prior to testing. Testing was completed within 8 hrs to minimize the impact of sample aging and new batches were made as needed; batch variation was minimal according to preliminary testing (data not shown).

For wear testing, 20 g of each sample was weighed and wrapped in plastic. Samples were placed in a freezer (-18°C) for 20 min prior to testing, removed, and transferred to the tribology base of the rheometer (Fig. 3.1 a.). A plastic tool of ultra-high molecular weight polyethylene was used to level sample surfaces (Fig. 3.1 b. and c.). To ensure samples were at room temperature prior to testing, they were equilibrated at room temperature (22°C±2°C) for 5 min in the tribology base plate (Fig. 3.1 d.).

Table 3.1. RSM experimental designs for oil and shortening.[1]

Experimental Design for Oil				**Experimental Design for Shortening**			
	Coded Levels				**Coded Levels**		
Treatment	WPI	HFCS	Canola Oil	Treatment	WPI	HFCS	Shortening
W37.F40.C23	0 (37)	0 (40)	0 (23)	W46.F29.S26	0 (46)	-2 (29)	0 (26)
W43.F47.C10	1 (43)	1 (47)	-1 (10)	W26.F45.S29	-1 (26)	1 (45)	1 (29)
W41.F43.C15	-1 (41)	-1 (43)	-1 (15)	W42.F28.S30	1 (42)	-1 (28)	1 (30)
W46.F50.C4	0 (46)	0 (50)	-2 (4)	W33.F56.S12	-1 (33)	1 (56)	-1 (12)
W25.F44.C31	-1 (25)	1 (44)	1 (31)	W38.F41.S21	0 (38)	0 (41)	0 (21)
W37.F40.C23	0 (37)	0 (40)	0 (23)	W32.F34.S34	0 (32)	0 (34)	2 (34)
W53.F35.C12	1 (53)	-1 (35)	-1 (12)	W38.F41.S21	0 (38)	0 (41)	0 (21)
W31.F33.C36	0 (31)	0 (33)	2 (36)	W38.F41.S21	0 (38)	0 (41)	0 (21)
W44.F28.C28	0 (44)	-2 (28)	0 (28)	W32.F49.S18	0 (32)	2 (49)	0 (18)
W27.F46.C27	-2 (27)	0 (46)	0 (27)	W53.F35.S12	1 (53)	-1 (35)	-1 (12)
W32.F56.C12	-1 (32)	1 (56)	-1 (12)	W38.F41.S21	0 (38)	0 (41)	0 (21)
W41.F27.C32	1 (41)	-1 (27)	1 (32)	W46.F50.S4	0 (46)	0 (50)	-2 (4)
W35.F38.C27	1 (35)	1 (38)	1 (27)	W38.F41.S21	0 (38)	0 (41)	0 (21)
W37.F40.C23	0 (37)	0 (40)	0 (23)	W42.F43.S15	-1 (42)	-1 (43)	-1 (15)
W32.F48.C20	0 (32)	2 (48)	0 (20)	W36.F39.S25	1 (36)	1 (39)	1 (25)
W37.F40.C23	0 (37)	0 (40)	0 (23)	W32.F33.S35	-1 (32)	-1 (33)	1 (35)
W44.F35.C21	2 (44)	0 (35)	0 (21)	W38.F41.S21	0 (38)	0 (41)	0 (21)
W37.F40.C23	0 (37)	0 (40)	0 (23)	W43.F47.S10	1 (43)	1 (47)	-1 (10)
W37.F40.C23	0 (37)	0 (40)	0 (23)	W45.F36.S19	2 (45)	0 (36)	0 (19)
W31.F32.C38	-1 (31)	-1 (32)	1 (38)	W28.F47.S25	-2 (28)	0 (47)	0 (25)

[1] Values are stated as x (% w/w), where x is the relative position to the center point, 0. The anchor points -2 and 2 in the design are the lowest and highest amount of each ingredient. Formulation codes were denoted by W for whey, F for HFCS, C for canola oil, and S for shortening; the number after each letter is the percentage of that ingredient.

3.3.2 ADHESION TESTING

Adhesion tests at 25°C, were performed on the TwinDive setting of an Anton Paar MCR 702 TwinDive rheometer (Anton Paar; Ashland, VA, USA); the TwinDrive setting was required for the adhesion testing protocol. Smooth parallel plates (25 mm upper diameter, 60 mm lower diameter) were used. Testing was done at 1 mm gap; samples were trimmed at 1.25 mm. Samples were held at a measurement gap of 1 mm for 5 min before testing to allow the sample to relax; then the upper plate was raised for 4 s at 5.0 mm s^{-1}. A minimum of 4 replicates per treatment were conducted.

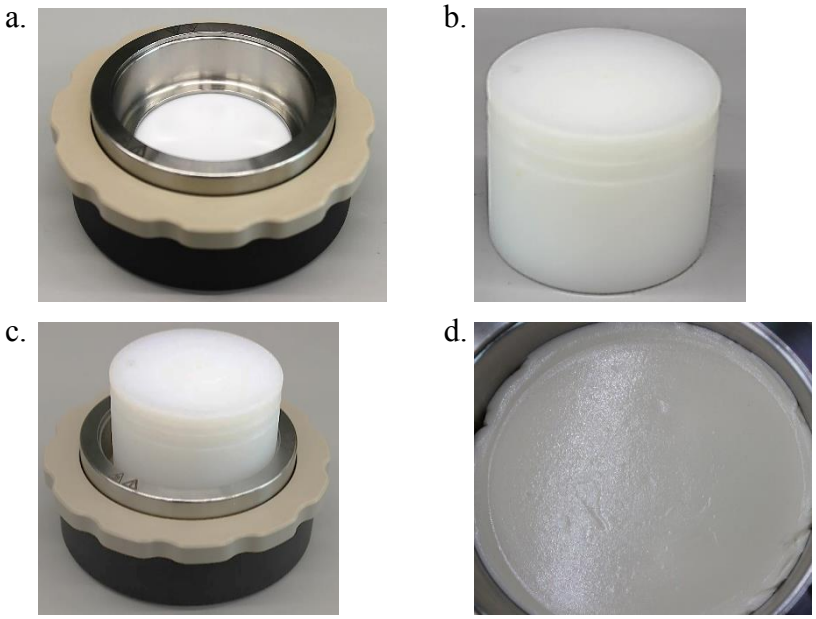

Figure 3.1. Sample preparation for wear testing, including a. tribology base plate, b. plastic tool, c. plastic tool used to flatten material, and d. flattened material left to acclimate to room temperature.

3.3.3 STRAIN SWEEP & LARGE AMPLITUDE OCILLAROTY SHEAR TESTING

For oscillatory testing on an Anton Paar MCR 702 TwinDrive rheometer (Anton Paar; Ashland, VA, USA), the same geometry and pre-test setup was used for each test. Slip was minimized by using cross-hatched parallel plates (25 mm diameter). A 1 mm gap was used for testing. Samples were trimmed at a gap of 1.25 mm; petroleum jelly (Unilever; Trumbull, CT, USA) was applied to the sample sides to prevent sample drying. Samples were held at a gap

of 1 mm for 5 min before the start of the test to allow the sample to relax. A minimum of 3 replicates per samples were conducted at 25°C.

Strain sweeps (0.0015%-350% strain) were conducted at three frequencies for 3 separate strain sweeps at 10, 1, and 0.1 rad s^{-1}. Tests were stopped when material cracking, material escape, or severe gapping occurred. Rheocompass software was used to collect raw strain, stress, and LAOS data. Frequency sweeps were conducted at 0.1-100 rad $s^{-1,}$ and 0.0379% strain (based off preliminary testing of the softest sample's critical strain determined by the Rheocompass software). A minimum of 3 replicates per sample were conducted at 25°C.

3.3.4 WEAR TESTING

Wear testing using at 25°C using a pin-in-disk attachment with 8 mm stainless steel balls (McMaster-Carr, Santa Fe Springs, CA, USA) was performed on an Anton Paar MCR 702 TwinDive rheometer (Anton Paar; Gratz, Austria). An initial gap of 13 mm was used, which allowed the balls to just touch the sample surface. Samples were held at this gap height for 2 min to allow sample relaxation prior to testing. Testing was performed using a normal force of 0.1 N and a sliding speed of 10 mm s^{-1}. The end time of the test was determined to be when the wear track was marred by the pin holders, (Appendix A.1). Three to five preliminary runs were used to determine the end time. The total test end time for each sample was divided into five runs of equal time. For example, a total test end time of 100 s would separate into runs of 20 s, 40 s, 60 s, 80 s, and 100 s. Imaging of the tribology plate containing the sample was done with a DSLR camera (Cannon Rebel T3i (Cannon, Ōta, Tokyo, Japan), 18MP with an 18-55 mm lens).

3.3.7 DATA ANALYSIS

Because a response surface design was used for both sets of formulations, it was not practical to run ANOVA on the data collected in this study. Rather, the data were organized in Microsoft Excel and examined for notable trends. Response surface models were analyzed in a companion paper (Chap. 4).

3.4 RESULTS AND DISCUSSION

The proposed structure of the ingredients used in the model high protein bar formulations is a matrix. composed of fructose and glucose sugar molecules in HFCS, WPI protein polymers, either longer fatty acid chains and emulsifiers from shortening or shorter oil fatty acid chains, and inherent water. We propose that in oil formulations, the protein polymers form a network structure that contains the sugar molecules and smaller oil fatty acid chains, creating a viscoelastic solid material. For shortening formulations, the longer fatty acid chains and emulsifiers would assist the WPI in providing structure to the three-dimensional matrix. Because each ingredient has a different structural contribution to the matrix, ingredient ratios would impact how the structure deforms under applied force or deformation and thus mechanical and wear results (Hogan et al., 2016).

In the following sections, only five selected formulations for both oil and shortening that represent the overall data set are shown because presenting the full data sets for each series of formulation would result in an overwhelming amount of data. The full data sets are included in the Appendices.

3.4.1 ADHESION RESULTS

Maximum adhesive force, defined as the maximum force recorded as the upper plate was raised during adhesion testing, for the selected oil formulations was highest at high levels of HFCS compared to both oil and WPI (Table 3.2). The results from all formulations followed similar trends (Appendix A.2). The amount of oil also had a large impact between formulations with similar HFCS levels, where greater oil decreased the maximum adhesive force. This result was attributed to the hydrophobic properties of oil, which would result in reduced interaction with the hydrophilic steel plate, reducing the adhesive force (Brady, 2013). The impact of WPI on adhesive force was unclear, as the other ingredient had much greater impacts on adhesive force. For the selected shortening formulations, maximum adhesive force was lower for formulations with shortening levels >4%, which was likely due to the emulsifiers in all-purpose shortening and the hydrophobic lipid reducing interaction with the hydrophilic steel plate (Table 3.2), as noted for the oil formulations. Shortening level had the greatest effect on maximum adhesive force, followed by the amount of HFCS; WPI had little impact on maximum adhesive force for shortening formulations.

Table 3.2 Selected adhesion results.

Oil	Treatments	Time of max. force (s)	Max. adhesive force (N)
	W46.F50.C4	0.24	20.70±0.8
	W44.F28.C28	0.12	9.330±0.8
	W44.F35.C21	0.18	11.32±0.7
	W37.F40.C23	0.22	18.79±0.7
	W27.F46.C27	0.22	11.87±1.1
Shortening	**Treatments**	**Time of max. force (s)**	**Max. adhesive force (N)**
	W46.F50.S4	0.22	19.02±4.2
	W46.F29.S26	0.12	6.247±1.0
	W45.F36.S19	0.14	6.910±0.8
	W38.F41.S21	0.20	6.408±2.2
	W28.F47.S25	0.18	3.682±0.5

3.4.2 STRAIN SWEEP RESULTS

Critical stress values for formulations were greater for formulations with a higher ratio of WPI to both HFCS and either oil or shortening (Table 3.3, Appendix A.3 and A.4), which was likely because the WPI strengthened the bar matrix structure, requiring greater stress to achieve permanent deformation. The impact of HFCS and either oil or shortening on critical stress was unclear. Oil formulation critical stress values generally increased with increased frequency, except at a high ratio of WPI to HFCS and oil, which had reduced critical stress at 1 rad/s. Shortening formulations showed no notable trends in critical stress with frequency. Critical strain values for both oil and shortening formulations did not show clear trends with ingredient ratios or frequency; this was likely due to the small range of critical strain values. (Table 3.3).

G* values at critical strain for both oil and shortening formulations increased with increased frequency and high ratios of WPI to HFCS and both oil and shortening. Similar tends were seen in the full data set (Appendix A.3 and A.4). The increased WPI content would strengthen the matrix structure, resulting in increased G* values. The impact of HFCS and either oil and shortening were unclear. G* values increased with increased frequency, likely due to the increased elastic-type behavior exhibited at higher frequencies, which is expected in viscoelastic materials (Leroy, Pitura, Scanlon, & Page, 2010).

Formulations with higher WPI levels had lower values for phase angle at critical strain (Table 3.3), likely due to the structure the WPI provided to the bar matrix. Shortening

formulations had lower phase angle at critical strain values than oil formulations, which expected and attributed to the longer shortening fatty acid chains. Similar trends were seen in the full data set (Appendix A.3 and A.4). The impact of HFCS was unclear for both oil and shortening treatments. Phase angle values for oil and shortening decreased at 1 rad/s, then increased slightly at 10 rad/s, likely due to structural disruption at the higher frequency, which would manifest as increased viscous-type behavior (Table 3.3).

3.4.3 LAOS RESULTS

Lissajous-Bowditch plots, which are individual stress versus strain curves, were arranged into Pipkin diagrams to show how individual Lissajous-Bowditch plots changed shape with changes in strain and frequency. Pipkin diagrams can be used to evaluate material viscoelastic behaviors over a wide range of strains and frequencies (Paul, Kalelkar, & Pullarkat, 2017). Elliptical Lissajous-Bowditch plots denote linear viscoelastic behavior, while plots that are distorted from an elliptical shape denote nonlinear viscoelastic behavior (Helen S. Joyner (Melito) & Meldrum, 2015). Nonlinear elastic behaviors can also be quantified using G_3'/G_1' values, or the ratio of the third to the first harmonic elastic modulus (Tables 3.5 and 3.6; Ewoldt et al., 2008). Values >0.01 denote nonlinear viscoelastic behavior (H.S. Joyner (Melito), Daubet, & Foegeding, 2013). Strain-softening versus strain-hardening behaviors can be quantified using G_L'/G_M' values, or the ratio of large strain to minimum strain of elastic modulus (Ewoldt et al., 2008). Strain-hardening behavior is denoted by values >1.1, and strain-softening behavior id denoted by values <0.9 (Joyner (Melito) et al., 2013). (Ewoldt et al., 2008; Melito, 2012). Shear-thinning versus shear-thickening behavior can be quantified using η_L'/η_M' values, or the ratio of maximum to minimum shear rate of instantaneous viscosity, where values >1.1 denote shear-thickening behavior and shear-thinning behavior is denoted by values <0.9 (Ewoldt et al., 2008; H.S. Joyner (Melito) et al., 2013).

Nonlinear viscous behavior can be quantified by $G_3^{"}/G_1^{"}$ values, or the ratio of third to the first harmonic viscous modulus, where nonlinear viscous behavior is denoted at values >0.01 Regardless of formulation, all samples showed increased nonlinear viscoelastic behavior with increased strain (Fig. 3.10 and 3.11). Phase angles of all formulations at 0.052% strain indicated elastic-dominant behavior (Table 3.4). As strain increased, the extent

of viscous-type behavior increased due to permeant structural deformation; at 60% strain, all formulations showed viscous-dominant behavior (Table 3.4)

Table 3.3 Selected strain sweep results.

Oil	Test Responses	Critical Stress (Pa)	Critical Strain (%)	G* at Critical Strain (kPa)	δ at Critical Strain (degrees)
0.1 rad/s	W46.F50.C4	8.45±3.4	0.039±0.0	21.9±6.7	48.2±1.4
	W44.F28.C28	208±93	0.016±0.0	1284±440	14.2±2.6
	W44.F35.C21	16.5±4.6	0.007±0.0	249.3±52	32.5±1.8
	W37.F40.C23	1.28±0.2	0.039±0.0	3.31±0.04	42.0±1.7
	W27.F46.C27	4.11±0.5	0.094±0.0	4.39±0.04	37.4±0.4
1 rad/s	W46.F50.C4	14.0±9.4	0.016±0.0	87.36±44	38.8±3.6
	W44.F28.C28	97.8±32	0.007±0.0	1485±370	10.5±0.9
	W44.F35.C21	37.3±9.0	0.007±0.0	562.1±100	17.8±0.9
	W37.F40.C23	3.35±0.5	0.039±0.0	8.624±0.09	41.7±0.9
	W27.F46.C27	7.30±1.5	0.094±0.0	7.77±1.2	37.1±0.8
10 rad/s	W46.F50.C4	36.5±13	0.016±0.0	321.1±61	24.8±4.1
	W44.F28.C28	285±66	0.016±0.0	1793±310	12.2±1.3
	W44.F35.C21	84.7±18	0.016±0.0	533.1±85	24.1±1.7
	W37.F40.C23	4.21±1.0	0.016±0.0	26.5±4.7	43.5±1.1
	W27.F46.C27	6.63±2.0	0.038±0.0	17.3±3.9	36.2±0.8
Shortening	**Test Responses**	**Critical Stress (Pa)**	**Critical Strain (%)**	**G* at Critical Strain (Pa)**	**δ at Critical Strain (degrees)**
0.1 rad/s	W46.F50.S4	30.4±11	0.039±0.0	78.7±22	43.0±1.6
	W46.F29.S26	120±42	0.016±0.0	749.2±200	17.6±1.9
	W45.F36.S19	90.7±16	0.016±0.0	566.8±75	21.4±1.4
	W38.F41.S21	4.36±1.9	0.003±0.0	158.8±52	33.6±4.6
	W28.F47.S25	11.8±0.5	0.094±0.0	12.6±0.04	33.0±0.3
1 rad/s	W46.F50.S4	32.4±8.6	0.016±0.0	201.9±40	28.5±1.9
	W46.F29.S26	45.6±23	0.007±0.0	688.2±36	13.7±1.2
	W45.F36.S19	84.5±19	0.007±0.0	1276±210	11.0±1.3
	W38.F41.S21	7.92±2.0	0.003±0.0	288.7±54	17.7±1.6
	W28.F47.S25	5.08±0.1	0.016±0.0	31.6±0.02	24.1±0.4
10 rad/s	W46.F50.S4	27.5±7.5	0.007±0.0	417.9±85	18.0±5.1
	W46.F29.S26	74.3±37	0.007±0.0	1132±420	14.6±2.1
	W45.F36.S19	85.7±38	0.007±0.0	1305±430	12.8±1.8
	W38.F41.S21	19.8±2.2	0.007±0.0	301.2±25	17.1±1.1
	W28.F47.S25	6.29±1.0	0.016±0.0	39.6±4.8	27.7±0.7

[1] Full values were <0.0.

The Pipkin diagram for the oil treatments (Fig. 3.10) showed linear viscoelastic behavior at 0.052% strain and nonlinear viscoelastic behavior at ≥1.8% strain. At lower strains, oil samples W44.F35.C21 and W44.F28.C28 showed elastic-dominant behavior according to their phase angles (Table 3.4) and visually from the Pipkin diagram of Lissajous-Bowditch plots (Fig. 3.2). At 60%, the phase angle for these samples indicated viscous-type behavior, which was concurrent with other oil formulations and similar phase angle trends were seen through the entire data set (Table 3.4 and Appendix A.5). W44.F35.C21 and W44.F28.C28 had high WPI and lower HFCS and oil compared to the other oil formulations, the additional structural strength provided by WPI was likely why these formulations exhibited elastic-dominant behavior. The other formulations with higher levels of HFCS and oil had phase angles (Table 3.4) on the border of elastic- and viscous-dominant behavior. However, these samples did show notable nonlinear behavior at 60% strain (Fig. 3.2). This viscous-dominant behavior was likely due to the HFCS and oil contributing little to the matrix structure, resulting in increased permanent deformation and flow, as previously discussed.

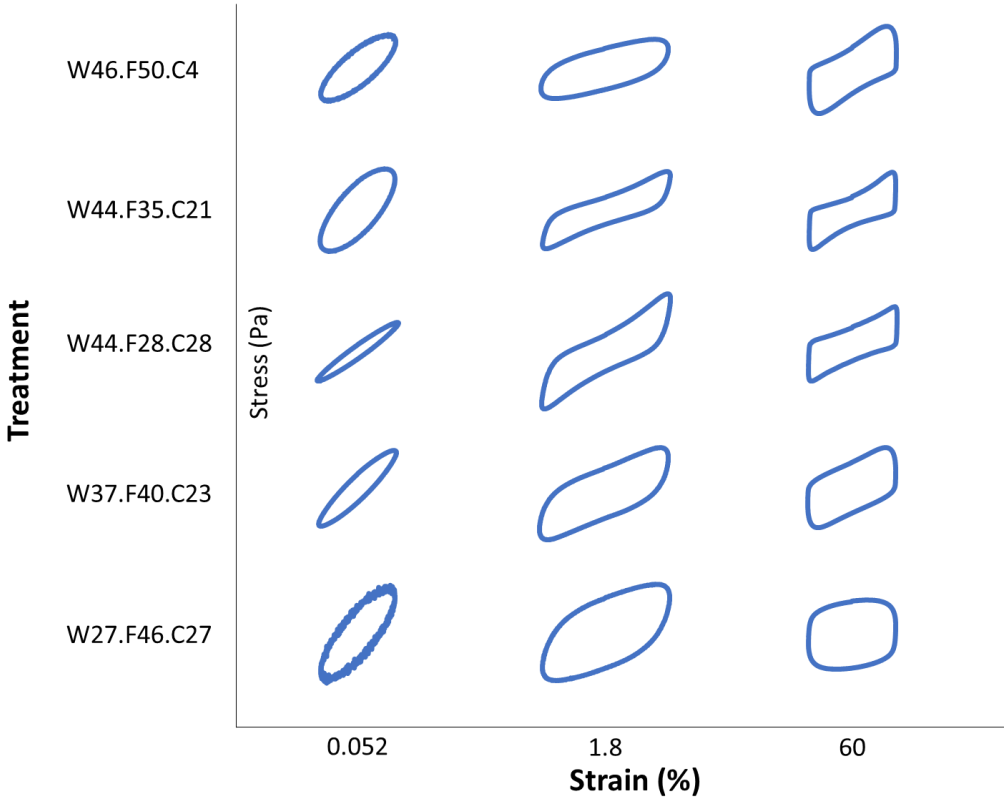

Figure 3.2. Pipkin diagram for oil treatments at 1 rad/s.

Table 3.4 Phase angles from LAOS testing for oil and shortening treatments.

Model	Treatments	Phase Angle (°)		
		0.052 (%)	1.8 (%)	60 (%)
Oil	W46.F50.C4	40±3.31	49±2.82	58±2.84
	W44.F35.C21	24±2.08	33±1.28	45±1.37
	W44.28.C28	14±1.11	27±2.26	48±0.60
	W37.F40.C23	42±0.86	55±1.50	61±0.81
	W27.F46.C27	40±0.51	49±2.13	58±0.64
Shortening	W46.F50.S4	30±1.75	41±2.21	51±1.42
	W46.F29.S26	18±1.65	30±1.19	45±2.68
	W45.F36.S19	16±1.28	27±1.88	48±3.47
	W38.F41.S21	21±1.40	31±0.13	46±0.62
	W28.F47.S21	25±0.60	34±1.33	49±1.30

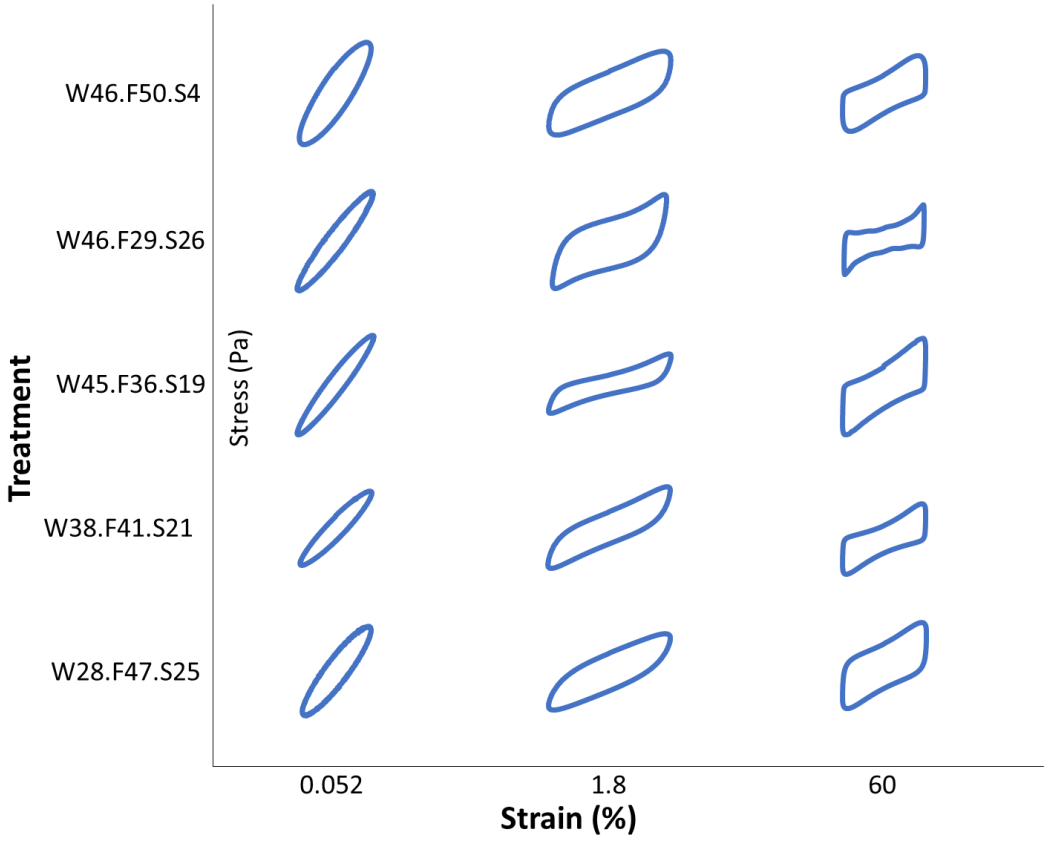

Figure 3.3. Pipkin diagram for shortening treatments at 1 rad/s.

Shortening formulations showed greater elastic-dominant behavior at higher WPI and lower HFCS levels, similar to the oil formulations (Fig. 3.3, Table 3.4, and Appendix A.5). These WPI ratio trends were similar to those in the selected phase angle data, which was also seen in the entire data set (Table 3.4 and Appendix A.5). Unlike oil treatments, which showed lower phase angle with increased oil ratio, increased shortening ratio resulted in decreased phase angle. As the only viscous-dominant behavior for shortening samples was seen at 60% strain which was likely due to permanent structural deformation. In both oil and shortening Pipkin diagrams (Fig. 3.3 and 3.4), there were distinct differences among the Lissajous plots for each treatment and strain, indicating that LAOS was an acceptable method for distinguishing among treatments.

Table 3.5. LAOS data at 60% strain for oil treatments.

Frequency (rad/s)	Treatment	G'_3/G'_1	G'_L/G'_M	G''_3/G''_1	η'_L/η'_M
0.1	W46.F50.C4	0.143±0.02	0.520±0.02	0.244±0.01	0.274±0.02
	W44.F35.C21	0.048±0.02	0.724±0.10	0.322±0.03	0.209±0.01
	W44.F28.C28	0.006±0.03	0.834±0.08	0.265±0.02	0.310±0.05
	W37.F40.C23	0.132±0.01	0.490±0.02	0.239±0.02	0.319±0.02
	W27.F46.C27	0.027±0.03	0.652±0.05	0.155±0.01	0.431±0.01
1	W46.F50.C4	0.098±0.01	0.766±0.04	0.264±0.03	0.766±0.03
	W44.F35.C21	0.077±0.05	1.382±0.17	0.432±0.03	0.206±0.02
	W44.F28.C28	0.068±0.03	1.287±0.13	0.328±0.04	0.293±0.04
	W37.F40.C23	0.116±0.02	0.717±0.06	0.297±0.01	0.225±0.01
	W27.F46.C27	0.065±0.01	1.098±0.03	0.148±0.00	0.478±0.01
10	W46.F50.C4	0.147±0.02	1.681±0.08	0.272±0.03	0.413±0.03
	W44.F35.C21	0.312±0.03	2.717±0.20	0.280±0.04	0.467±0.03
	W44.F28.C28	0.300±0.06	2.912±0.42	0.299±0.03	0.691±0.14
	W37.F40.C23	0.205±0.01	2.268±0.42	0.250±0.01	0.405±0.02
	W27.F46.C27	0.388±0.04	14.96±9.76	0.114±0.01	0.606±0.02

The selected treatments showed nonlinear elastic behavior at 60% and all frequencies based on G'_3/G'_1 values, except for one oil and two shortening formulations at 0.1 rad/s; similar trends were seen in the whole data set (Table 3.5, 3.6, Appendix A.6 and A.7). At higher frequencies, formulations switched from strain-softening behavior to strain-hardening behavior based on G'_L/G'_M values (Table 3.5 and 3.6). For all frequencies, all samples showed

both nonlinear viscous and shear-thinning behaviors based on their $G_3^{"}/G_1^{"}$ and η_L'/η_M' values, respectively (Table 3.5 and 3.6). The exception was oil formulation W44.F28.C28 at 0.1 rad/s, which showed linear viscoelastic behavior. This result was likely due to the ratio of WPI to oil and HFCS being higher than the WPI ratio in the other oil formulations; WPI would provide more structure to the matrix, and the sample would show less permanent structural change at this low frequency. Strain-softening behavior (Table 3.5) was shown at 0.1 rad/s for oil all treatments, which was likely because low frequencies promote increased viscous-type behavior. At 1 rad/s, only two of the oil formulations shown, W46.F50.C4 and W37.F40.C23, showed strain-softening behavior (Table 3.5). For these formulations, the strain-softening behavior was likely due to the high HFCS:WPI ratio. Similar trends for linear and shear-softening behavior were seen for shortening treatments (Table 3.6 and Appendix A.7). Shortening formulations W45.F36.S19 and W38.F41.S2 had relatively high ratios of WPI to HFCS and shortening, which was probably why they showed linear viscoelastic behavior at 0.1 rad/s (Table 3.6). This result was also seen in the Pipkin diagram (Fig. 3.3). Strain-softening behavior was seen at 0.1 rad/s for all formulations and one formulation at 1 rad/s, W46.F50.S4, which was likely due to the high level of HFCS (Table 3.6). As frequency increased, strain-hardening behavior was seen in most formulations between 0.1 and 1 rad/s, the remaining formulations switch from strain-softening to strain-hardening behavior at 1 and 10 rad/s for all formulations and W46.F50.S4.Regardless of frequency, all formulations showed nonlinear viscous and shear-thinning behavior except one formulation for that had a high standard deviation. The structural matrix provided by the WPI likely reduced the instantaneous viscosity by preventing sugar molecules and fatty acids from escaping and thus material flow which resulted in lower $G_3^{"}/G_1^{"}$ and η_L'/η_M' values (Table 3.3 and Appendix A.7).

Table 3.6. LAOS data at 60% strain for shortening treatments.

Frequency (rad/s)	Treatment	G'_3/G'_1	G'_L/G'_M	G''_3/G''_1	η'_L/η'_M
0.1	W46.F50.S4	0.146±0.02	0.524±0.06	0.269±0.03	0.229±0.01
	W46.F29.S26	0.032±0.02	0.850±0.05	0.335±0.02	0.206±0.01
	W45.F36.S19	0.009±0.04	0.765±0.11	0.310±0.06	0.277±0.07
	W38.F41.S21	0.003±0.01	0.874±0.02	0.381±0.02	0.161±0.01
	W28.F47.S25	0.065±0.01	0.998±0.03	0.269±0.01	0.294±0.01
1	W46.F50.S4	0.103±0.02	0.731±0.16	0.312±0.06	0.216±0.02
	W46.F29.S26	0.186±0.03	2.114±0.67	0.446±0.04	0.196±0.04
	W45.F36.S19	0.128±0.11	1.121±0.35	0.334±0.08	0.331±0.05
	W38.F41.S21	0.037±0.01	1.242±0.06	0.392±0.02	0.199±0.01
	W28.F47.S25	0.090±0.01	1.353±0.06	0.285±0.00	0.305±0.01
10	W46.F50.S4	0.238±0.08	2.576±0.78	0.327±0.01	0.360±0.04
	W46.F29.S26	0.263±0.02	2.607±0.18	0.307±0.03	0.595±0.11
	W45.F36.S19	0.333±0.03	2.527±0.13	0.356±0.01	0.547±0.13
	W38.F41.S21	0.245±0.01	2.325±0.11	0.288±0.00	0.392±0.01
	W28.F47.S25	0.219±0.01	2.643±0.11	120.42±12.2	0.492±0.01

3.4.4 WEAR TRACKS

The effects of ingredients were seen in the wear track patterns for each formulation (Fig. 3.4). At WPI levels > 45%, the wear tracks were clearly distinguishable. In formulations with oil levels >21%, the tracks had a shiny, reflective layer likely caused by surface oil combined with oil expressed during wear testing due to the applied normal force. Shortening formulations did not show this reflective layer. As all-purpose shortening contains emulsifiers, it is possible that a surface lipid layer was not present due to the emulsifiers stabilizing the emulsions in those samples. For treatments W37.F40.C23 and W38.F41.S21, the wear track became thinner and less defined than samples with ingredients at moderate levels. As the amount of WPI decreased, the wear track became less visible, e.g. the wear tracks observed for W27.F46.C27 and W28.F47.S25. In treatment W27.F46.C27, the image showed a tail of material created as the attachment was raised at the completion of testing, indicating increased adhesive and flow behaviors. These behaviors were likely due to the high ratio of HFCS, which is both adhesive and viscous.

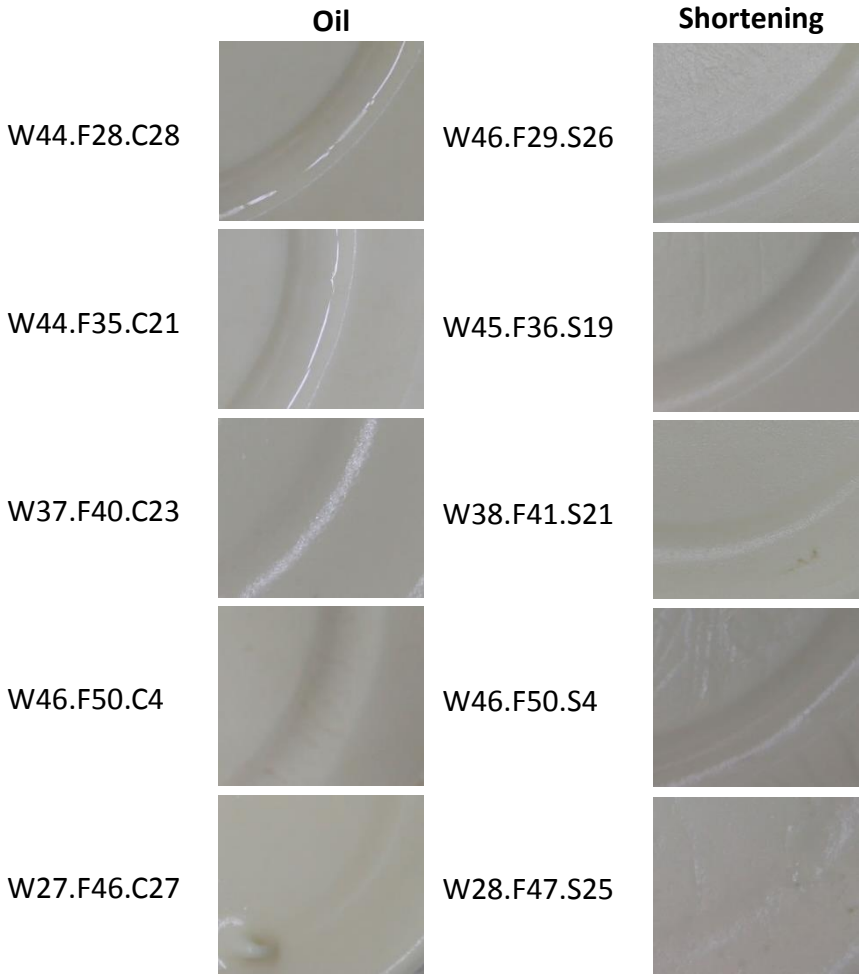

Figure 3.4. Selected images of wear tracks for oil and shortening formulations.

3.5 CONCLUSIONS

Formulation clearly impacted the mechanical and wear behaviors of high-protein bars. For oil treatments, HFCS had the greatest impact on adhesion. For shortening treatments, shortening ratio had the greatest impact, where higher HFCS related to greater adhesion and greater shortening resulted in lower adhesion. For both oil and shortening formulations, critical stress, G*, and phase angle at critical stress were greatly impacted by the ratio of WPI, where higher levels of WPI resulted in higher critical stress and G* at critical stress values and lower phase angle values indicating that elastic and rigid behavior were connected to WPI

ratio. The impact of WPI was also seen in the LAOS results for both oil and shortening formulations, where formulations with higher WPI levels showed more elastic-dominate behavior across all strains, linear viscoelastic behavior at lower frequencies and all strains, and strain-hardening behavior at higher frequencies. Formulation also affected wear testing, resulting in wear tracks with greater definition and deeper tracks for formulations with greater levels of WPI. Over all, this study indicated a relationship between high-protein bar formulation and mechanical and wear behaviors.

3.6 ACKNOWLEDGEMENTS

This project was funded by BUILD Dairy. The authors would like to thank the Consulting Statisticians in the Statistical Programs working in the College of Agricultural and Life Science at the University of Idaho for their assistance in statistical evaluation. Additional thanks to Dr. Lee Deobald, Director of the Mass Spec Core Lab at the University of Idaho for his assistance on proximate ingredient analysis.

3.7 REFERENCES

AOAC. (2001). *AOAC Official Method 996.06 Fat (Total, Saturated, and Unsaturated) in Foods*. https://doi.org/http://down.40777.cn/stardard/8/41.1.28A%20AOAC%20Official%20Method%20996.06%20Fat(Total,Saturated.pdf

Böhm, L., Brehmer, M., & Kraume, M. (2016). Comparison of the Single Bubble Ascent in a Newtonian and a Non-Newtonian Liquid: A Phenomenological PIV Study. *Chemie Ingenieur Technik*, *88*(1–2), 93–106. https://doi.org/10.1002/cite.201500105

Brady, J. (2013). *Introductory Food Chemistry* (1st ed.). Ithaca, New York: Cornell University Press.

Duvarci, O. C., Yazar, G., & Kokini, J. L. (2017). The comparison of LAOS behavior of structured food materials (suspensions, emulsions and elastic networks). *Trends in Food Science & Technology*, *60*, 2–11. https://doi.org/10.1016/J.TIFS.2016.08.014

Ewoldt, R., Hosoi, A. E., & McKinley, G. H. (2008). New measures for characterizing nonlinear viscoelasticity in large amplitude oscillatory shear. *Journal of Rheology*, *52*(6), 1427–1458. https://doi.org/10.1122/1.2970095

Franco, V. (2015). Press Release for U.S. Food Bars.

Hogan, S. A., O'Loughlin, I. B., & Kelly, P. M. (2016). Soft Matter Characterisation of Whey Protein Powder Systems. *Elsevier Science Ltd*, *52*(January 2016), 1–9. Retrieved from https://ida.lib.uidaho.edu:2116/science/article/pii/S0958694615001417

Joyner (Melito), H. S., Daubet, C. R., & Foegeding, E. A. (2013). Relationships Between Nonlinear Viscoelastic Behavior and Rheological, Sensory and Oral Processing Behavior of Commercial Cheese. *Journal of Texture Studies*.

Joyner (Melito), H. S., Francis, D., Luzzi, B., & Johnson, J. R. (2017). The effect of storage temperature on blue cheese mechanical properties. *Journal of Texture Studies*. https://doi.org/10.1111/jtxs.12301

Joyner (Melito), H. S., & Meldrum, A. (2015). Rheological Study of Different Mashed Potato Preparations Using Large Amplitude Oscillatory Shear and Confocal Microscopy. *Journal of Food Engineering*, *169*, 326–337.

Kyomoto, M., Moro, T., Takatori, Y., Kawaguchi, H., & Ishihara, K. (2011). Cartilage-mimicking, High-density Brush Structure Improves Wear Resistance of Crosslinked Polyethylene: A Pilot Study. *Clinical Orthopaedics and Related Research®*, *469*(8), 2327–2336. https://doi.org/10.1007/s11999-010-1718-5

Leroy, V., Pitura, K. M., Scanlon, M. G., & Page, J. H. (2010). The complex shear modulus of dough over a wide frequency range. *Journal of Non-Newtonian Fluid Mechanics*, *165*(9–10), 475–478. https://doi.org/10.1016/J.JNNFM.2010.02.001

Li, F., Wang, A., & Wang, C. (2016). Analysis of friction between articular cartilage and polyvinyl alcohol hydrogel artificial cartilage. *Journal of Materials Science: Materials in Medicine*, *27*. https://doi.org/10.1007/s10856-016-5700-y

Melito, H. (2012). *Large Amplitude Oscillatory Shear Behavior of Food Systems*. North Carolina State University.

Ng, C. M., & Reuter, W. M. (2015). *Application Note: Liquid Chromatography*.

Paul, S., Kalelkar, C., & Pullarkat, P. A. (2017). Oscillatory extensional rheology of microscale fluid filaments. *Rheologica Acta*, *56*(2), 113–122. https://doi.org/10.1007/s00397-016-0986-8

Smith, B. M., Bean, S. R., Schober, T. J., Tilley, M., Herald, T. J., & Aramouni, F. (2010). Composition and Molecular Weight Distribution of Carob Germ Protein Fractions. *Journal of Agricultural and Food Chemistry*, *58*(13), 7794–7800. https://doi.org/10.1021/jf101523p

Sousa, A. M. M., & Gonçalves, M. P. (2015). The influence of locust bean gum on native and alkali-modified agar gels. *Food Hydrocolloids*, *44*, 461–470. https://doi.org/10.1016/J.FOODHYD.2014.10.020

Steffe, J. F. (1996). *Rheological Methods in Food Process Engineering* (2nd ed.). East Lansing: Freeman Press. Retrieved from https://bblearn.uidaho.edu/bbcswebdav/pid-1105998-dt-content-rid-9580077_1/courses/201610_38230/STEFFE.pdf

Tan, J., & Joyner, H. S. (2018). Characterizing wear behaviors of k-carrageenan and whey protein gels by numerical modeling. *Journal of Food Engineering*.

Yarimitsu, S., Sasaki, S., Murakami, T., & Suzuki, A. (2016). Evaluation of lubrication properties of hydrogel artificial cartilage materials for joint prosthesis. *Biosurface and Biotribology*, *2*(1), 40–47. https://doi.org/10.1016/j.bsbt.2016.02.005

Yazar, G., Duvarci, O. C., Tavman, S., & Kokini, J. L. (2017). LAOS behavior of the two main gluten fractions: Gliadin and glutenin. *Journal of Cereal Science*, *77*, 201–210. https://doi.org/10.1016/J.JCS.2017.08.014

CHAPTER 4: RESPONSE SURFACE ANALYSIS

4.1 ABSTRACT

High protein bars are popular snack items that can have significant processing issues like sticking, clogging, and cold flow. These issues are primarily problematic during formulation development because current predictive testing is reliant on highly empirical bench tests or pilot plant testing, which is expensive and time-consuming. Wear testing, which has been used in the medical field to evaluate the lifetime of soft materials used in joint replacements, may have promise in evaluating food processing ability. Wear and rheological testing were used to better understand high-protein bar processing ability. The objective of this study was to determine bench-level instrumental tests that would be able to predict processing ability for a given formulation. Two response surface designs were used for formulations of model bar systems comprising whey protein isolate (WPI), high fructose corn syrup (HFCS), and either canola oil or vegetable shortening. Ingredient formulation affected processing ability, wear behaviors, and rheological behaviors. Formulations with high ratios of WPI to HFCS and either shortening or oil exhibited good processing ability, lower wear rates, and increased elastic-type behavior, indicating that processing ability is related to formulation. The results of this study indicated that material mechanical and wear behaviors were related to processing ability; both were controlled by formulation. Because it was shown to be a good indicator of high protein bar processing ability, wear testing of food has potential significance in benchtop testing.

4.2 INTRODUCTION

The market for high protein bars has grown significantly because snacking and protein trends are on the rise (Franco, 2015). Because of this growth, manufacturers are making more new formulations to meet consumer needs. The addition or substitution of different ingredients like protein, lipid, sweetener, and inclusions can potentially increase the chance of manufacturing issues. Common issues include sticking of material to processing surfaces, clogging of machinery, and cold flow, where the bar sags under its own weight after cutting and no longer fits into the intended packaging (Tilghman, 2017). These issues are related to

ingredient ratios, making testing of high protein bar formulations highly empirical. The protein bar industry needs predictive, quantitative tests that allow targeted formulation of high-protein bars. Because rheology probes a material's deformation behavior and thus its structural characteristics, and ingredient ratios will likely have an impact on structure and deformation, a range of rheological tests, including wear, may be used to determine the behavior–ingredient and behavior–processing ability relationships, as well as link high protein bar properties to processing ability.

Rheological tests have a high likelihood of predicting processing ability based on the information on deformation behavior that they provide (Steffe, 1996). Frequency and strain sweeps give insight to the extent of elastic versus viscous behavior and critical strain of a sample, respectively; both have the potential to relate to processing ability. Adhesion tests provide information on how sticky or adhesive a material is, which is a processing issue as material sticking to rollers can clog machinery. Additionally, wear testing has been used in artificial cartilage studies to determine the possible effectiveness of novel joint prosthetics (Yarimitsu, Sasaki, Murakami, & Suzuki, 2016). Because the artificial cartilage materials used in these studies are often hydrogels or other soft materials, it is possible wear testing could be an effective measure in predicting processing ability of a high protein bar, a soft solid. Thus, wear testing has potential applications in soft solid foods for determining their ability to be successfully processed.

The objectives of this study were to determine potential predictive bench-level testing that would give information about processing ability of a given high protein bar formulation. By using rheology to better understand how ingredients affect processing ability, this study is the first step in closing the gap between the variability of new formulations and processing ability.

4.3 MATERIALS

Whey protein isolate (WPI, 90% protein, dry basis) was obtained from Glanbia Nutritionals, Inc. (Fitchburg, WI, USA). Proximate content validation of WPI was completed using an Agilent Bioanalyzer 2100 (Agilent, Santa Clara, CA), which combines SDS-PAGE and chromatography, using Protein 230 chips with a molecular weight range of 4.5-240kDa (Smith et al., 2010). Preparation of the chip and samples were done according to Agilent

protocols. Briefly, protein samples were prepared using a urea buffer which was vortexed then centrifuged at 11,000 RPM, followed by adding 0.5 ml of the protein solution to an equal quantity of a sodium phosphate and sodium chloride buffer. The buffer solution was vortexed, mixed with denaturing solution and the ladder standard, and heated to 95°C for 5 min. Samples were then transferred to the Protein 230 chip wells. The results confirmed the presence of major milk proteins β-lactoglobulin, α-lactalbumin, and casein.

High fructose corn syrup (HFCS, 42% fructose) was obtained from Batory Foods, Inc. (Hopkins, MN, USA). Sugar content of HFCS was done through HPLC analysis following the protocols from Ng & Reuter (2015). To get better peak resolution, the analysis used a 72:28 acetonitrile/water dispersion and was run on an amino column (35641, Alltech associates, Deerfield, IL, USA) with a flow rate of 0.5 ml/min. The analysis indicated that the weight percentages of common sugars in HFCS were approximately 36% fructose, 12% glucose, 11% sucrose, and 15% maltose.

Store-brand canola oil and Crisco vegetable shortening were obtained from a local grocer (Moscow, ID, USA). The fatty acid profiles of the canola oil and vegetable shortening were determined by unsaturated fatty acid methyl ester (FAME) testing using gas chromatography with C14-C22 FAME mix (Sigma-Aldrich/Millipore Sigma, Saint Louise, MI, USA). FAME testing determined that the major fatty acids in oil were palmitic, stearic, and oleic. The major fatty acids in shortening were palmitic and stearic. All ingredients were used as-is with no further purification.

4.3.1 FORMULATION PREPARATION

All formulations were composed of WPI, HFCS, and either shortening or oil. Twenty formulations were created for each of oil- and shortening-based formulations using a central composite center-faced response surface design (Table 4.1). Ingredient boundaries were determined by preliminary testing. Ingredients were mixed using a KitchenAid Classic 275W stand mixer (KitchenAid; St. Joseph, MI, USA) at speed 1 for 2 min. The sample was then tightly wrapped in plastic wrap (Winco Foods Inc.; Boise, ID, USA), placed in a zippered plastic bag, and stored at room temperature (22±2°C) until tested. Formulations were tested within 8 hrs to minimize the impact of sample aging. New batches were made as needed for

testing; variation between batches was determined to be minimal by preliminary testing (data not shown).

Table 4.1. RSM experimental designs for oil and shortening.[1]

Experimental Design for Oil				Experimental Design for Shortening			
	Coded Levels				Coded Levels		
Treatment	WPI %(w/w)	HFCS %(w/w)	Canola Oil %(w/w)	Treatment	WPI %(w/w)	HFCS %(w/w)	Shortening %(w/w)
W37.F40.C23	0 (37)	0 (40)	0 (23)	W46.F29.S26	0 (46)	-2 (29)	0 (26)
W43.F47.C10	1 (43)	1 (47)	-1 (10)	W26.F45.S29	-1 (26)	1 (45)	1 (29)
W41.F43.C15	-1 (41)	-1 (43)	-1 (15)	W42.F28.S30	1 (42)	-1 (28)	1 (30)
W46.F50.C4	0 (46)	0 (50)	-2 (4)	W33.F56.S12	-1 (33)	1 (56)	-1 (12)
W25.F44.C31	-1 (25)	1 (44)	1 (31)	W38.F41.S21	0 (38)	0 (41)	0 (21)
W37.F40.C23	0 (37)	0 (40)	0 (23)	W32.F34.S34	0 (32)	0 (34)	2 (34)
W53.F35.C12	1 (53)	-1 (35)	-1 (12)	W38.F41.S21	0 (38)	0 (41)	0 (21)
W31.F33.C36	0 (31)	0 (33)	2 (36)	W38.F41.S21	0 (38)	0 (41)	0 (21)
W44.F28.C28	0 (44)	-2 (28)	0 (28)	W32.F49.S18	0 (32)	2 (49)	0 (18)
W27.F46.C27	-2 (27)	0 (46)	0 (27)	W53.F35.S12	1 (53)	-1 (35)	-1 (12)
W32.F56.C12	-1 (32)	1 (56)	-1 (12)	W38.F41.S21	0 (38)	0 (41)	0 (21)
W41.F27.C32	1 (41)	-1 (27)	1 (32)	W46.F50.S4	0 (46)	0 (50)	-2 (4)
W35.F38.C27	1 (35)	1 (38)	1 (27)	W38.F41.S21	0 (38)	0 (41)	0 (21)
W37.F40.C23	0 (37)	0 (40)	0 (23)	W42.F43.S15	-1 (42)	-1 (43)	-1 (15)
W32.F48.C20	0 (32)	2 (48)	0 (20)	W36.F39.S25	1 (36)	1 (39)	1 (25)
W37.F40.C23	0 (37)	0 (40)	0 (23)	W32.F33.S35	-1 (32)	-1 (33)	1 (35)
W44.F35.C21	2 (44)	0 (35)	0 (21)	W38.F41.S21	0 (38)	0 (41)	0 (21)
W37.F40.C23	0 (37)	0 (40)	0 (23)	W43.F47.S10	1 (43)	1 (47)	-1 (10)
W37.F40.C23	0 (37)	0 (40)	0 (23)	W45.F36.S19	2 (45)	0 (36)	0 (19)
W31.F32.C38	-1 (31)	-1 (32)	1 (38)	W28.F47.S25	-2 (28)	0 (47)	0 (25)

[1] Values are stated as x (% w/w), where x is the relative position to the center point, 0. The anchor points -2 and 2 in the design are the lowest and highest amount of each ingredient.

For wear testing, 20g of each sample was weighed out and wrapped tightly in plastic. Prior to testing the wrapped samples were placed in a freezer (-18°C) for 20 min, then removed and transferred to the tribology base (Fig. 4.1 a.). An ultra-high molecular weight polyethylene plastic tool was used to even out the sample surface (Fig. 4.1 b. and c.).

Flattened samples were left to acclimate to room temperature (22°C±2°C) for 5 min prior to testing (Fig. 4.1 d.).

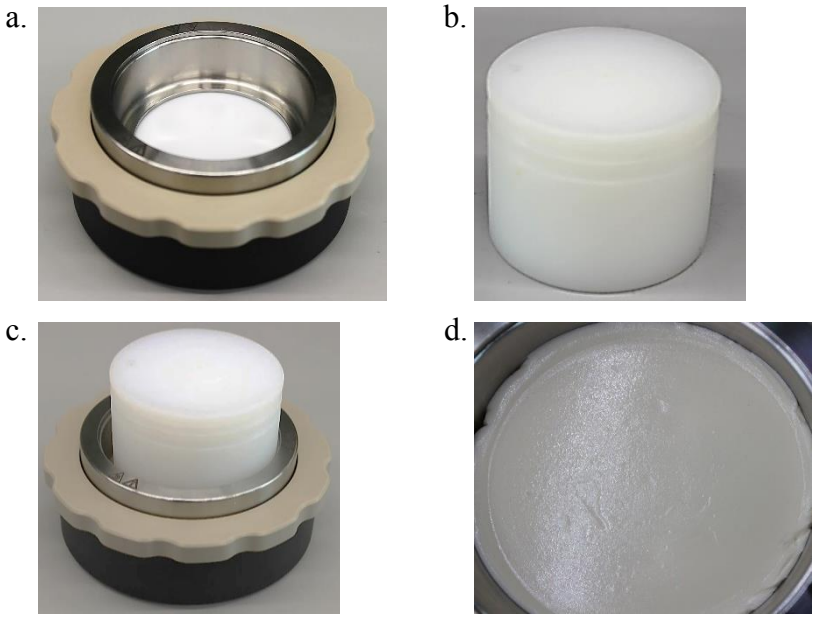

Figure 4.1. Wear testing sample preparation including a. tribology base plate, b. plastic tool, c. plastic tool used to flatten material, and d. flattened material left to acclimate to room temperature.

4.3.2 ADHESION TESTING

Adhesion tests were performed on an Anton Paar MCR 702 TwinDive rheometer (Anton Paar; Ashland, VA, USA) on the TwinDrive setting according to the protocols in the Rheocompass software (Anton Paar version 1.20.449). Smooth parallel plates (25 mm upper diameter, 75 mm lower diameter) at a 1 mm gap were used for testing; samples were trimmed at a gap of 1.25 mm. Samples were held at a gap of 1 mm for 5 min before the start of the test to allow them to relax. After the hold period, the upper plate was raised at a constant crosshead velocity of 5.0 mm s^{-1} for 4 s. All tests were conducted at 25°C with a minimum of 4 replicates per formulation.

4.3.3 STRAIN SWEEP & LARGE AMPLITUDE OSCILLATORY SHEAR TESTING

All oscillatory testing was performed on an Anton Paar MCR 702 TwinDrive rheometer (Anton Paar; Ashland, VA, USA); the same geometry and pre-test setup were used for each test. To minimize slip, cross-hatched parallel plates (25 mm diameter) were used, and a 1 mm gap was used for testing. Petroleum jelly (Unilever; Trumbull, CT, USA) was applied to the sides of each sample to prevent sample drying during testing. Samples were held at a gap of 1 mm for 5 min before the start of the test to allow them to relax.

Strain sweeps were conducted over a strain range of 0.0015%-350% at three different frequencies (10, 1, and 0.1 rad s^{-1}). Tests were stopped when material began to escape from between the plates, or severe gapping and cracking of the sample occurred. Raw strain, stress, and large amplitude oscillatory shear (LAOS) data were collected from the Rheocompass software. Frequency sweeps were conducted from 0.1-100 rad s^{-1} at 0.0379% strain (below the critical strain of the softest sample as determined by the Rheocompass software during preliminary testing). All tests were conducted at 25°C with a minimum of 3 replicates per formulation.

4.3.4 WEAR TESTING

Wear testing was performed on an Anton Paar MCR 702 TwinDive rheometer (Anton Paar; Gratz, Austria) at 25°C using a pin-in-disk attachment with stainless steel balls (8 mm diameter; McMaster-Carr, Santa Fe Springs, CA, USA). An initial gap of 13 mm, allowing the balls to just touch the sample surface, was used. Samples were held at this gap for 2 min prior to testing to allow relaxation. A normal force of 0.1 N and a sliding speed of 10 mm s^{-1} were used for testing. The end time of the test was determined when the pin holders dug into the sample, marring the wear track, (Appendix A.1). Three to five preliminary runs were used to determine the test end time, each using a new sample of the same formulation. To better determine the wear rate, the total test time for each sample was separated into five runs of equal time. For example, a total test time of 50 s would separate into runs of 10 s, 20 s, 30 s, 40 s, and 50 s. Each run was performed with a fresh sample. The tribology plate containing the sample was removed from the machine after each run for imaging with a DSLR camera (Cannon Rebel T3i (Cannon, Ōta, Tokyo, Japan), 18MP with an 18-55 mm lens).

4.3.5 ASSESSMENT OF COLD FLOW AND PROCESSING ABILITY

Checks for processing ability were performed by personnel at Glanbia Nutritionals, Inc. (Twin Falls, ID, USA) who had over 4 years of experience in the protein bar formulation and processing. 400 g of each formulation was prepared using the procedure detailed in Section 4.2.1. Samples were manipulated by hand, mimicking the processing force of hoppers and rollers, movement of between belts, corners, and belt speed. After manipulation, the suitability of each formulation for processing was evaluated using a yes/no responses.

Cold flow of each formulation was determined by packing a 2" circular cookie cutter with material to make uniform cylinders. A permanent marker was used to mark the initial size of the material with the sample in the mold, then the mold was removed. Once the cookie cutter was removed, the material was allowed to rest at ambient temperatures (22±2°C) for 10 min. Cold flow occurred when the material sagged over the marker line during the rest period.

4.3.6 PILOT PLANT TESTING

Pilot scale testing was executed on four of the formulations deemed suitable for processing; 2000 g of each of oil formulations W46.F50.C4, W41.F27.C32 and shortening formulations W42.F28.S30, W46.F50.S4 (Table 4.1) were run. Ingredients were mixed using an industrial-sized Hubert mixer (Markham, ON, Canada) for 2 min at ambient temperature (22±2°C). Samples were directly fed into the hopper of a Hosokawa Confectionary & Bakery Technology System (Summit, NJ, USA) for processing at ambient temperature (22°C±2°C), with the hopper, belt, roller, and cutter speeds set at middle-speed setting. Formulations were considered successfully processed if no material was left on the roller, if the bar showed good cohesion after being rolled, if the bar was cut without adhering to the slicing blade, and if the bar could be removed from the conveyor without it breaking or not able to hold its shape.

4.3.7 DATA ANALYSIS

Analysis of the central composite center-faced response surface design was done using Design Expert v.11 (Taylor&Francis/CRC/Productivity Press, New York, NY). Diagnostics, predicted vs. actual, and three-dimensional response surface plots were generated using the software. Analysis of variance (ANOVA) was run for the model of each response (α=0.05) using Design Expert v. 11.

4.4 RESULTS AND DISCUSSION

The theorized structure of the HFCS, WPI, and shortening or lipid is a matrix comprising protein polymers, fatty acid chains, fructose and glucose molecules, and the inherent water in HFCS and the lipids used. The protein polymers form a more rigid three-dimensional structure that traps the sugar molecules and smaller fatty acid chains (Y. Zhou & Roos, 2011); the larger fatty acid chains contribute to this protein network. Because the matrix structure was dependent on bar formulation, the rheological and wear behaviors, which are dependent on material structure, were also impacted by formulation (Hogan, O'Loughlin, & Kelly, 2016).

Individual test results were discussed in Chapter 3. These data were used in this study to develop response surface plots and investigate their predictive ability for high protein bar processing ability.

4.4.1 OVERVIEW OF MODEL SIGNIFICANCE

All rheological response in Table 4.2 were derived from oscillatory shear testing; several parameters are from LAOS evaluation. In particular, G_3'/G_1' is the ratio of the third harmonic to the first harmonic elastic modulus and is a measure of the extent of nonlinear elastic behavior (Ewoldt, Hosoi, & McKinley, 2008). G_L'/G_M' is the ratio of large-strain to minimum-strain elastic modulus and is a measure of strain-hardening and strain-softening behaviors. (Ewoldt et al., 2008). Nonlinear viscoelastic is denoted at values of G_3'/G_1' >0.01, and strain-hardening behavior is denoted at values of G_L'/G_M' >1.1 and values <0.9 denotes strain-softening behavior (Joyner (Melito), Daubet, & Foegeding, 2013).

In oil formulations (Table 4.2), the responses for G_3'/G_1', at 4% and 0.1, 1, and 10 rad/s had significant models. Other responses with significant models (Table 4.2) were the phase angle at critical strain and, G_L'/G_M' at 10 rad/s, maximum adhesive force, and wear rate. In 4 of the 7 significant response models (Table 4.2), WPI and HFCS were significant ingredients, as were the interactions between them. This interaction suggested synergistic behavior between those ingredients. Oil was the only significant ingredient for wear rate and phase angle at critical strain.

In shortening formulations (Table 4.3), significant models included responses at 10 rad/s for G* and phase angle at critical strain, G_3'/G_1' at 4% strain and 10 rad/s, and G_L'/G_M' at

4% strain and 10 rad/s, phase angle and G* values from frequency sweep data at 1 rad/s, and wear rate. HFCS was significant in four of the eight models, shortening was significant for three, and WPI was significant for two. This suggests that the ratio of WPI had a greater impact on the behaviors of bars made with oil (Table 4.2), whereas HFCS had a greater impact on the behaviors of bars made with shortening (Table 4.3). Significant ingredient interactions among the models for shortening formulations were between WPI and HFCS (4 of 8 models), and HFCS and shortening (3 of 8 models).

Table 4.2. ANOVA for oil response surface models.

						Interactions		
Response		**Model**	**WPI**	**HFCS**	**Oil**	**WPI-HFCS**	**WPI-Oil**	**HFCS-Oil**
Phase angle at critical strain at 10 rad/s	p-value	Quadratic <0.001	NS	NS	0.001	0.005	0.033	0.044
	R^2	0.918						
G'3/G'1 at 4% and 10 rad/s	p-value	Linear 0.003	NS	<0.001	NS	NS	NS	NS
	R^2	0.574						
G'L/G'M at 4% and 10 rad/s	p-value	2FI[1] <0.001	0.002	NS	NS	NS	0.003	0.004
	R^2	0.823						
G'3/G'1 at 4% and 1 rad/s	p-value	Quadratic 0.006	NS	NS	NS	<0.001	NS	NS
	R^2	0.839						
G'3/G'1 at 4% and 0.1 rad/s	p-value	Quadratic 0.001	0.049	0.028	NS	0.005	NS	NS
	R^2	0.886						
Maximum adhesive force	p-value	Quadratic <0.001	0.036	0.022	NS	<0.001	NS	NS
	R^2	0.967						
Wear rate	p-value	Linear <0.001	<0.001	0.002	0.003	NS	NS	NS
	R^2	0.729						

[1]2FI: two factor interaction model type.

Within the significant models for both oil and shortening (Table 4.2 and 4.3), more models were significant at 10 rad/s than at 1 and 0.1 rad/s. This was likely because higher frequencies promote greater elastic-type behavior. Specific results will be addressed later in subsequent sections.

4.4.2 SMALL AMPLITUDE OSCILLATORY SHEAR AND FREQUENCY SWEEP RESULTS

For oil formulations (Fig. 4.2 a. and b.), oil had the most impact on the value of phase angle at critical strain and 10 rad/s. WPI and HFCS appeared to have an interaction effect as indicated by the change of phase angle values as WPI and HFCS levels changed concurrently (Fig 4.2 a. and b.).

Table 4.3. ANOVA for shortening response surface models.

						Interactions		
Response		**Model**	**WPI**	**HFCS**	**Shortening**	**WPI-HFCS**	**WPI-Shortening**	**HFCS-Shortening**
G* at critical strain at 10 rad/s	p-value	Quadratic <0.001	NS	NS	NS	<0.001	NS	NS
	R^2	0.983						
Phase angle at critical strain at 10 rad/s	p-value	2FI <0.001	NS	<0.001	NS	0.019	NS	0.031
	R^2	0.864						
G'3/G'1 at 4% and 10 rad/s	p-value	Linear <0.001	<0.001	<0.001	<0.001			
	R^2	0.897						
Phase angle at critical strain at 1 rad/s	p-value	Quadratic <0.001	NS	NS	NS	NS	NS	0.002
	R^2	0.956						
G'L/G'M at 4% and 0.1 rad/s	p-value	Quadratic <0.001	NS	NS	0.021	0.043	NS	NS
	R^2	0.921						
G* at 1 rad/s	p-value	Quadratic <0.001	NS	NS	NS	<0.001	0.045	0.001
	R^2	0.971						
Phase angle at 1 rad/s	p-value	2FI <0.001	NS	0.002	NS	NS	NS	0.035
	R^2	0.899						
Wear rate	p-value	Linear <0.001	<0.001	<0.001	<0.001			
	R^2	0.856						

[1]CG^*_{CS}: G* at critical strain. [2]2FI: two-factor interaction model type. [3]G^*_{FS}: G* value from frequency sweep data. [4]$phase\ angle_{FS}$: phase angle values form frequency sweep data.

At lower oil levels (Fig. 4.2 a.), higher phase angles were seen at the highest level of both WPI and HFCS. As oil content increased (Fig. 4.2 b.), phase angle decreased with

decreased levels of WPI and HFCS. The impact of oil on phase angle values was likely due to its ability to flow through the matrix structure, contributing to increased viscous-type behavior. WPI increased elastic-type behavior by containing the oil and sugar molecules; thus, there was increased viscous-type behavior seen at lower WPI levels (Fig 4.2 b.). Phase angles were lower at high levels of both HFCS and WPI for formulations at low oil levels (Fig. 4.2 a.). This was attributed to the disrupting effect of HFCS on the WPI structure in the bar matrix. At high oil levels, the opposite trend was observed: phase angles were higher at low levels of HFCS and WPI. It is likely that the oil played a dominant role in bar rheological behavior under these conditions, promoting a more fluid structure and increasing phase angles.

For all shortening formulations, increased WPI (Fig. 4.2 c-f.) decreased phase angle values, in agreement with the oil formulation results. At 10 rad/s (Fig. 4.2 e. and f.), phase angle values were most affected by HFCS. HFCS likely had the most influence on phase angle because its plasticizing effect on the matrix structure, resulting in softer, more fluid structure and higher phase angle values (Paramita, Piccolo, & Kasapis, 2017). At 1 rad/s, WPI appeared to have the greatest effect on phase angle, while at 10 rad/s HFCS did (Fig. 4.2 c-f.). shortening had less impact on phase angle values than other ingredients at both frequencies. At 1 rad/s (Fig. 4.2 c. and d.), there was an interaction between shortening and HFCS (Table 4.3), where the material had higher phase angle values at high levels of HFCS and low levels of shortening, or vice versa. It is likely that WPI provided most of the matrix structure and shortening strengthened the structure when present at lower levels. Lower phase angle values were also seen at higher frequencies, which is typical of viscoelastic materials (Fig. 4.2 e. and f.) (Franck, 2016).

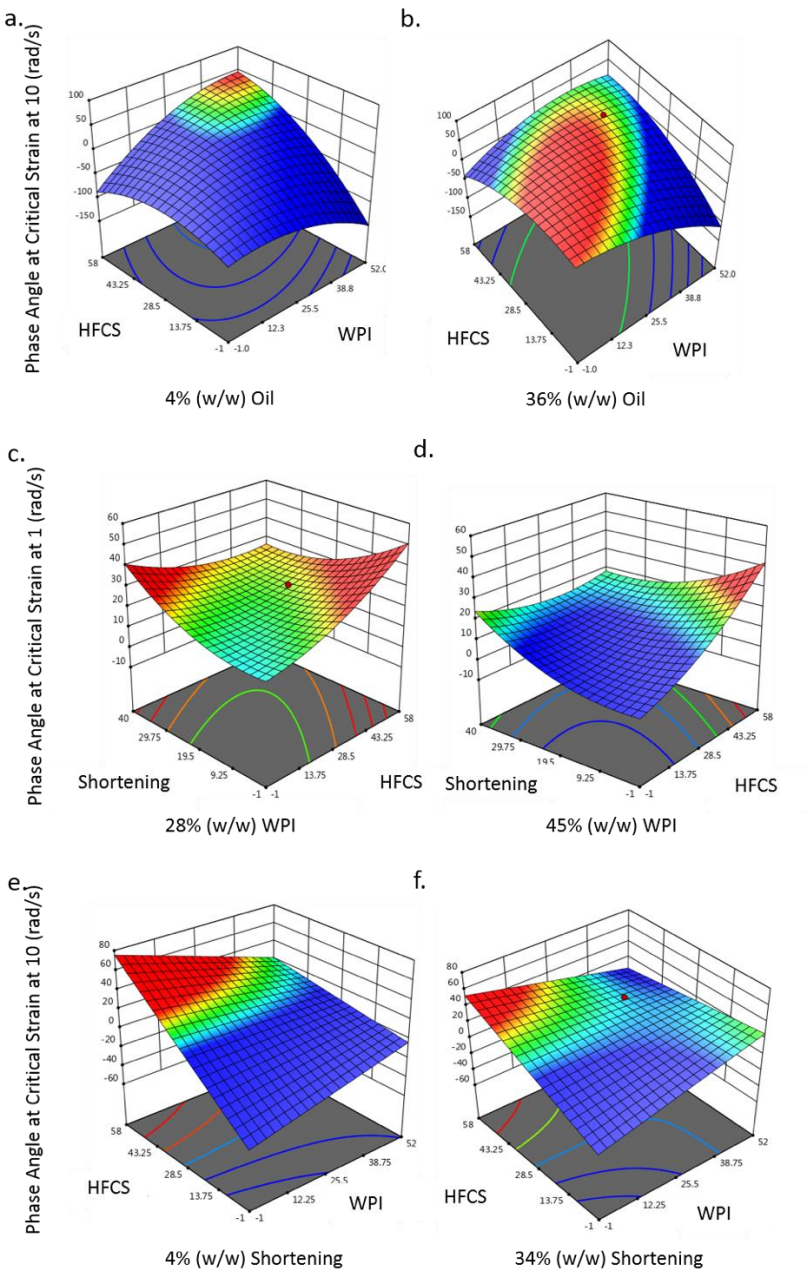

Figure 4.2. Response surface plots for phase angle at critical strain for a) oil formulations at 10 rad/s and 4% oil, b) oil formulations at 10 rad/s and 36% oil, c) shortening formulations at 1 rad/s and 28% WPI, d) shortening formulations at 1 rad/s and 45% WPI, e) shortening formulations at 10 rad/s and 4% shortening, and f) shortening formulations at 10 rad/s and 34% shortening.[1]

[1] Red dots seen in some of the response surface plots are data points which the program was unable to fit using the selected model.

For G^*_{CS} at 10 rad/s (Fig. 4.3), the ingredients that impacted the values of G^*_{CS} most were WPI and HFCS, indicating an interaction between them, although the effect of the individual ingredients was not significant (Table 4.3). Regardless of shortening level, increased WPI resulted in increased G* values, especially at lower HFCS. The lowest G* values appeared at high HFCS levels and moderate WPI levels. As shortening levels increased, an interaction was seen between the HFCS and WPI, where low G* values appeared at moderate to low WPI levels and moderate to high HFCS levels. Additionally, higher shortening levels resulted in decreased G* values, which was attributed to weaker bar matrix structure (Fig. 4.3).

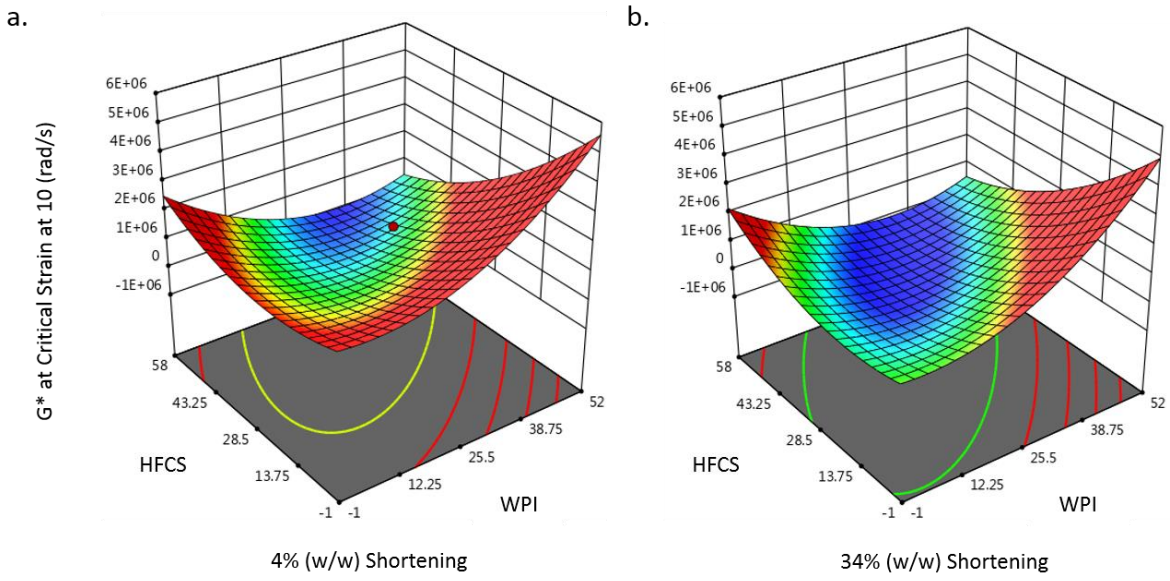

Figure 4.3. Response surface plot for G^*_{CS} at 10 rad/s for a) shortening formulations at 4% shortening and b) shortening formulations at 34% shortening.[1]

[1] Red dots seen in some of the response surface plots are data points which the program was unable to fit using the selected model.

For G^*_{FS} at 1 rad/s for shortening formulations (Fig. 4.4 a. and b.), WPI had the most impact on G^*_{FS} values at low shortening levels (Fig 4.6 a.), and both WPI and HFCS had the most impact on G^*_{FS} values at high shortening levels (Fig. 4.6 b). At higher levels of WPI, G^*_{FS} increased markedly, which was emphasized at lower levels of both HFCS and shortening (Fig. 4.6 a.). The cause of this was likely the WPI providing added matrix

structure, increasing the rigidity of the material. At higher shortening levels (Fig. 4.6 b.), there was an interaction between WPI and HFCS (Table 4.3 and Fig. 4.4 b.) where G^*_{FS} was highest at low HFCS and high WPI, and low WPI and high HFCS. There was suggested synergy based on the ingredient interaction between WPI and HFCS, as the ingredients were not significant in the model (Table 4.3). Lower G* values were seen when HFCS and WPI were at similar levels. The differences in response between shortening levels were attributed to increased shortening, which would trap some of the sugar molecules even at lower WPI levels (Fig. 4.4 b.). As mentioned earlier, HFCS likely contributed to less rigid behavior.

In the phase angle models at 1 rad/s from frequency sweep data (Fig. 4.4 c. and d.), phase angle values were greatly affected by HFCS, particularly at lower WPI levels (Fig. 4.4 c.). At higher WPI levels (Fig. 4.4 d.), HFCS had less impact on phase angle, likely because the matrix structure provided by WPI was better able to form a stronger structure at higher WPI levels (Zhou & Roos, 2011). Shortening, on the other hand, did not appear to have a strong effect on phase angle values, especially at lower WPI (Fig. 4.4 c.). At higher levels of WPI (Fig. 4.4 d.), higher levels of shortening did show higher phase angles than lower levels of shortening at low WPI levels. It is likely that at low WPI levels (Fig. 4.4 c.), shortening had a larger contribution to the matrix structure (Fig. 4.4 d.) than at high WPI levels, where WPI would provide most of the structure.

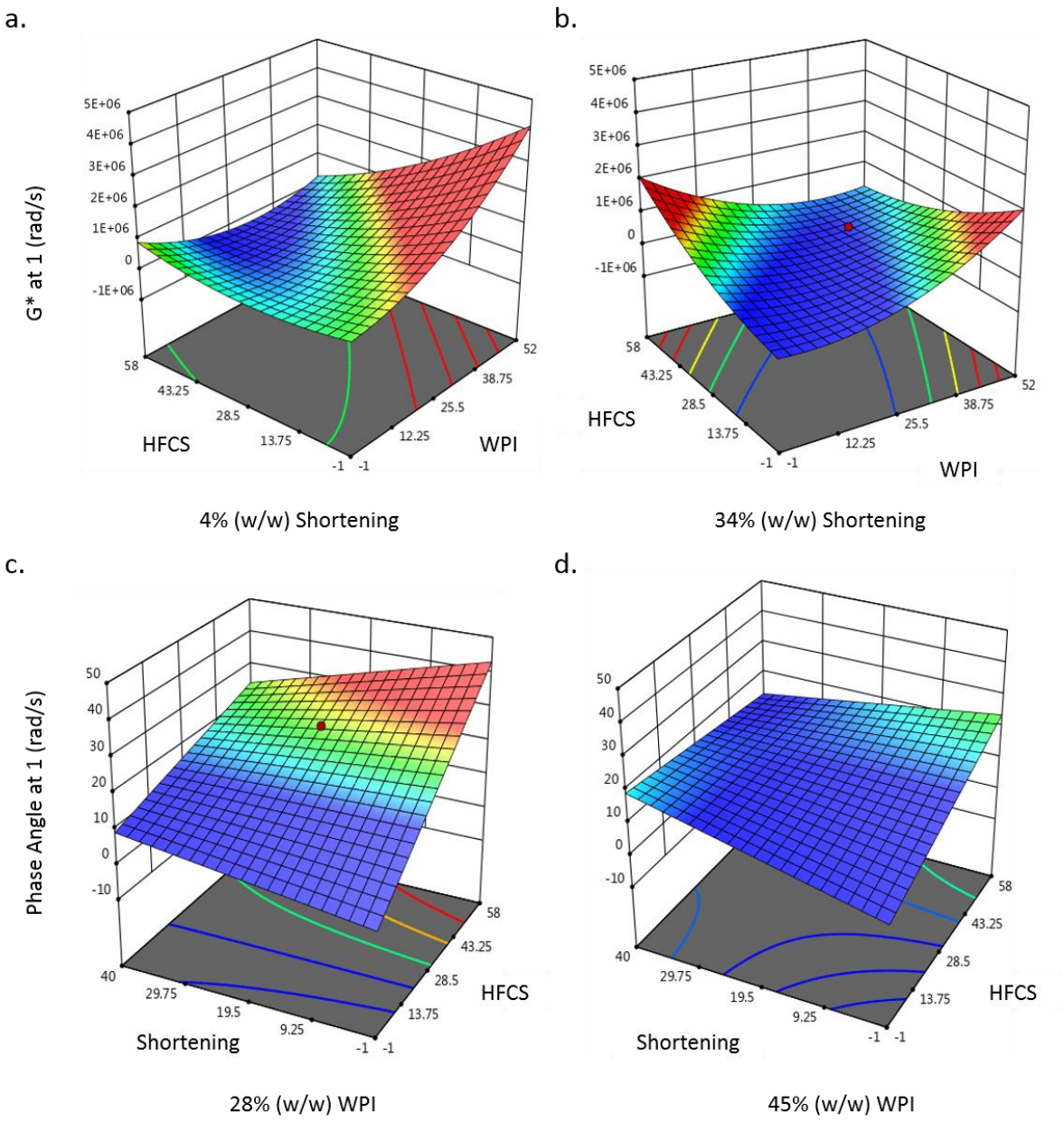

Figure 4.4. Response surface plots for shortening formulations frequency sweeps at 1 rad/s for a) G^*_{FS} at 4% shortening, b) G^*_{FS} at 34% shortening, c) phase angle$_{FS}$ at 1 rad/s at 28% WPI, and d) phase angle at 1 rad/s from frequency sweep data at 45% WPI.[1]

[1] Red dots seen in some of the response surface plots are data points which the program was unable to fit using the selected model.

4.4.3 LAOS RESULTS

An interaction between WPI and HFCS was seen in oil formulations even though the individual ingredients were not significant in the models which indicate synergy between the ingredients (Table 4.2 and Fig. 4.5 a-c). At 0.1 rad/s, this interaction resulted in higher G_3'/G_1' values at equal amounts of WPI and HFCS. However, as WPI decreased, maximum G_3'/G_1' values were primarily across the middle range of HFCS (Fig. 4.5 a. and b.). At 1 rad/s, an equal amount of WPI and HFCS resulted in the highest G_3'/G_1' values, which indicated an interaction and was supported by the ANOVA (Fig. 4.6 c., d., and Table 4.2). Both WPI and HFCS had a large impact on G_3'/G_1' values at 1 rad/s (Fig. 4.5 c. and d.). At 10 rad/s, HFCS had the most effect on G_3'/G_1' values (Fig. 4.5 e. and f.). This transition from WPI to HFCS having the most impact on G_3'/G_1' values as frequency increased was likely because the difference in relaxation times between structures dominated by HFCS versus WPI, which would result in different nonlinear viscoelastic behaviors.

For oil formulations, models for G_3'/G_1' values at 4% strain were notably impacted by frequency. For G_3'/G_1' at 4% strain, WPI had the greatest effect on the response at 0.1 rad/s (Fig. 4.5 a. and b.). At 0.1 rad/s; the highest G_3'/G_1' values were seen at lower WPI levels across most HFCS levels (Fig. 4.5 a. and b.). As frequency increased, lower oil levels showed higher values of G_3'/G_1' (Fig. 4.5 a-d.). However, at 10 rad/s (Fig. 4.5 e. and f.), oil had little effect on G_3'/G_1' values. The smaller molecular size of HFCS and oil likely promoted lower G_3'/G_1' values as the molecules are able to realign quickly. In oil formulations at 10 rad/s (Fig. 4.5 a. and b.), WPI level had less effect on G_3'/G_1' values as frequency increased, and HFCS level appeared to have the most effect on G_L'/G_M' values at high frequencies. The rapid realignment with an oscillating shear field would result in low permanent deformation and thus low G_3'/G_1' values. However, increased protein–protein interactions at higher WPI levels would result in a stiffer structure that would prevent rapid realignment of HFCS and oil molecules. The combination of the stiffer structure and lack of molecular alignment with the shear field would result in increased permanent deformation and thus higher G_3'/G_1' values (Cifre, Hess, & Kröger, 2004; Malkin, 1995).

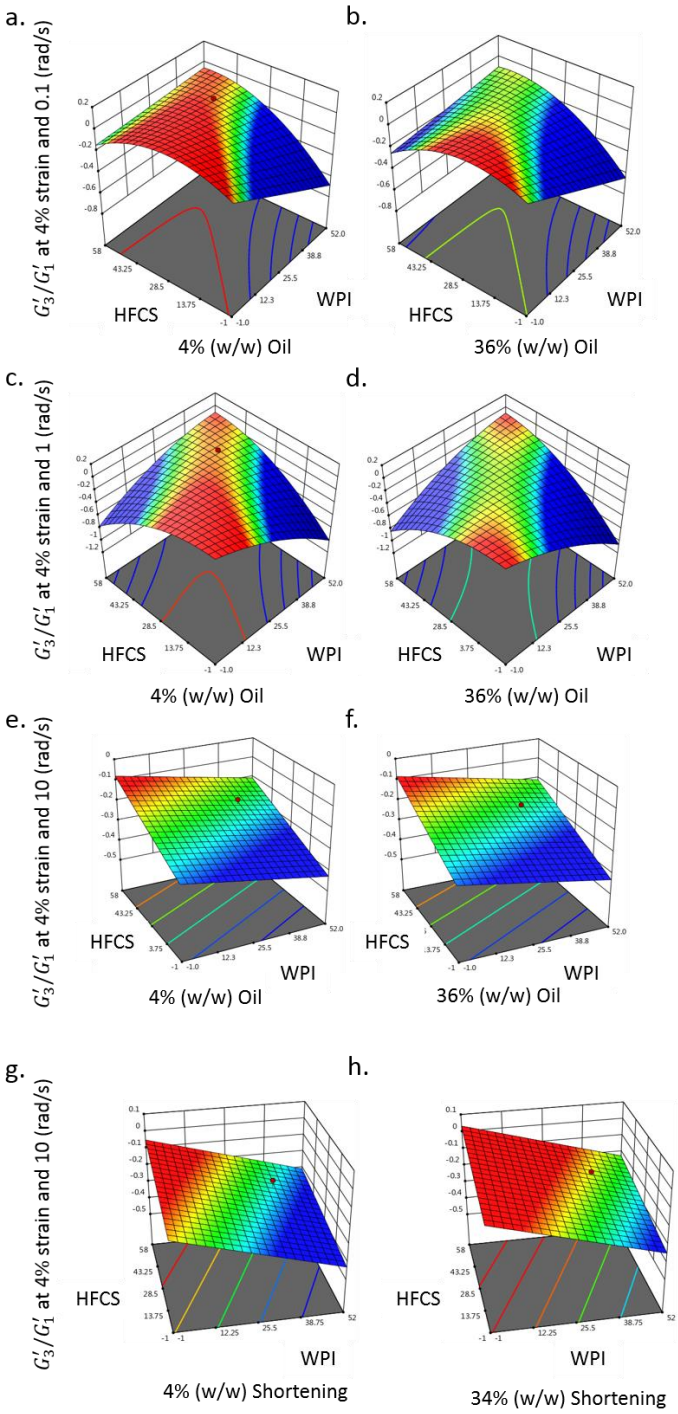

Figure 4.5 Response surface plots for G_3'/G_1' values at 4% strain for a) oil formulations at 0.1 rad/s and 4% oil, b) oil formulations at 0.1 rad/s and 36% oil, c) oil formulations at 1 rad/s and 4% oil, d) oil formulations at 1 rad/s and 36% oil, e) oil formulations at 10 rad/s and 4% oil, f) oil formulations at 10 rad/s and 36% oil g) shortening formulations at 10 rad/s and 4% shortening, and h) shortening formulations at 10 rad/s and 34% shortening.[1]

[1] Red dots seen in some of the response surface plots are data points which the program was unable to fit using the selected model.

For shortening formulations (Fig. 4.5 g. and h.), WPI had the greatest effect on G_3'/G_1' values. The amount of HFCS in shortening formulations (Fig. 4.5 g. and h.) had little effect on G_3'/G_1' values. This could be due to HFCS contributing little to the structural matrix of the material, thus having little impact on nonlinear viscoelastic behavior. In shortening formulations (Fig. 4.5 g. and h.), higher shortening levels increased G_3'/G_1' values. However, WPI level had greater impact than shortening level on G_3'/G_1' values. It is likely that the HFCS molecules had a plasticizing effect on the bar matrix structure, which resulted in greater nonlinear behavior which was emphasized as shortening increased because the shortening exaggerated the plasticizing effect.

From the response surface plots of G_L'/G_M' at 4% at 10 rad/s (Fig. 4.6 a.), a lower level of WPI increased G_L'/G_M' values when both HFCS and oil were at either minimum or maximum levels. As the level of WPI increased (Fig. 4.6 b.), only low levels of both HFCS and oil had higher G_L'/G_M' values. Overall, WPI appeared to increase G_L'/G_M' values in oil formulations. This was likely because the matrix of ingredients had more protein polymers to contain the fatty acids and sugar molecules that would otherwise flow freely. Increased protein would strengthen the matrix structure, resulting in increased strain hardening behavior (Zhang, Daubert, & Foegeding, 2005).

G_L'/G_M' values were impacted by an interaction between oil and HFSC at low WPI levels, which was confirmed in the ANOVA table (Fig. 4.6 a., b., and Table 4.2). While there were interactions between WPI and oil, and HFCS and oil, none of the individual ingredients were significant in the models (Table. 4.2), indicating a synergy occurring between the ingredients. At high levels of HFCS and oil, the lower G_L'/G_M' values observed were probably due to the weaker matrix, which would be less resistant to deformation. At low levels of both HFCS and oil, the stiffer matrix likely fractures at low strain, leading to higher G_L'/G_M' values. With less oil and HFCS, there is less plasticizing effect resulting in a stiffer matrix which is more susceptible to fracture (P. Zhou, Liu, & Labuza, 2008; Hogan et al., 2016).

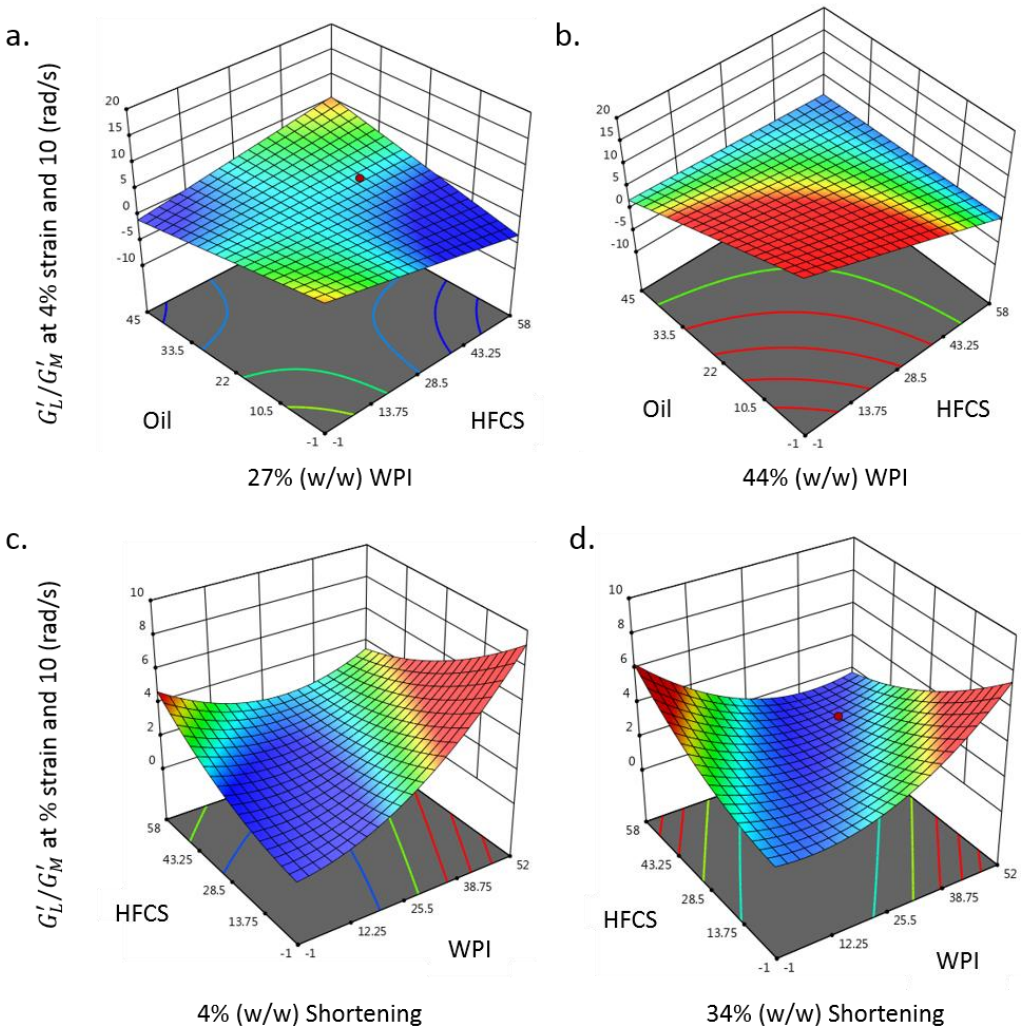

Figure 4.6 Response surface plots for G_L'/G_M' values at 4% strain and 10 rad/s for a) oil formulations at 27% WPI[1], b) oil formulations at 44% WPI, c) shortening formulations at 4% shortening, and d) shortening formulations at 34% shortening[1].

[1] Red dots seen in some of the response surface plots are data points which the program was unable to fit using the selected model.

For the shortening formulations, there was an interaction effect between WPI and HFCS regardless of shortening level (Fig. 4.6 c. and d.). Concurrent increases or decreases in WPI and HFCS produced lower G_L'/G_M' values, indicating less strain-hardening behavior. At lower levels of shortening (Fig. 4.6 c.), G_L'/G_M' values were higher with higher WPI. The increased G_L'/G_M' values at high HFCS and low WPI levels, regardless of shortening content,

was likely because the shortening, which was in a solid state, strengthened the bar matrix structure.

4.4.4 MAXIMUM ADHESIVE FORCE RESPONSE SURFACE PLOTS

For the maximum adhesive force models for oil formulations (Fig. 4.7 a. and b.), WPI and HFCS appeared to have more of an impact on adhesion behaviors than oil; they also showed interaction effects. The interaction was noted by the increased adhesive force when HFCS and WPI levels were highest, and adhesion decreased as they decreased. This was confirmed in the oil ANOVA table (Table 4.2). The increased adhesion at high WPI and HFCS was attributed to a combination of HFCS and whey proteins, which have adhesive properties (Wall & Huebner, 1980) and would increase the overall adhesion. Adhesion was greater at lower oil levels (Fig. 4.7 a.) than for higher oil levels (Fig. 4.7 b.), likely because oil is hydrophobic and would not adhere to the hydrophilic surface of the steel plate used for testing. This lack of adherence would reduce adhesion even at high WPI and HFCS levels. This reduced adhesion due to oil content may also have contributed to the shift of greatest adhesion at higher oil to slightly lower WPI and HFCS levels due to the higher ratio of oil, which likely had not been fully incorporated into the material. The poor oil incorporation would result in a thin layer of oil on the surface, reducing adhesion. Higher levels of HFCS and WPI would reduce the free oil, increasing adhesion (Brady, 2013).

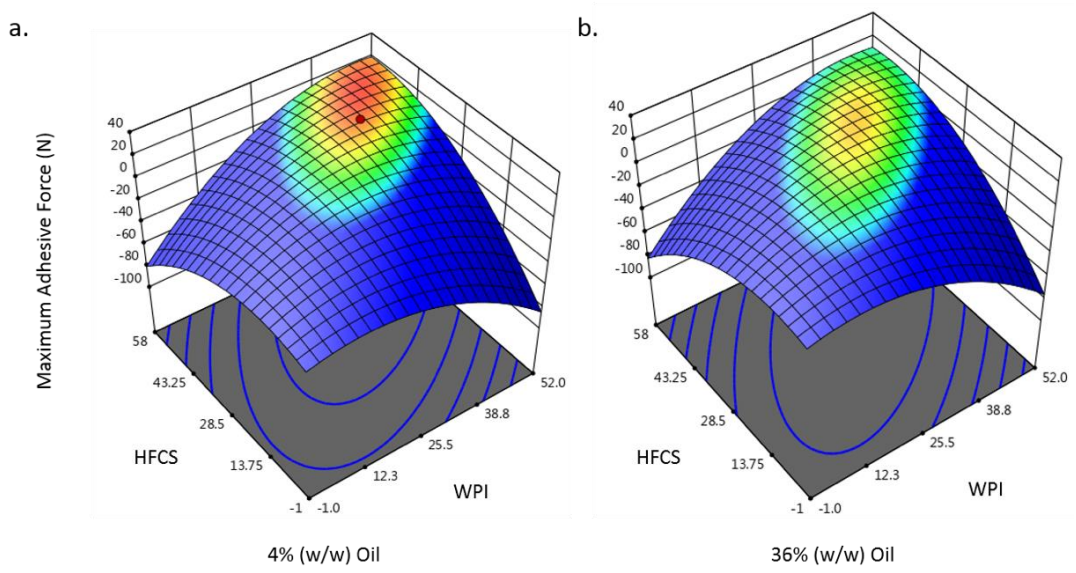

Figure 4.7. Response surface plots for maximum adhesive force for a) oil formulations at 4% oil and b) oil formulations at 36% oil.[1]

[1] Red dots seen in some of the response surface plots are data points which the program was unable to fit using the selected model.

4.4.5 WEAR RATE RESPONSE SURFACE PLOTS

For the wear rate models for both oil and shortening, all three ingredients were considered significant (Table 4.2). In both oil and shortening models, WPI appeared to contribute most to the wear rate values. As WPI increased, the wear rate decreased, indicating that the matrix structure provided by WPI slowed wear during testing. In the case of food gels, increased firmness reduced penetration depth, wear, and deformation (Tan & Joyner, 2018). As previously discussed, higher levels of HFCS weakened the matrix structure, resulting in higher wear rates. At lower levels of both oil and shortening, HFCS had a greater impact on wear rate than at higher lipid levels. This was likely due to the higher levels of both oil and shortening would create a weaker, more easily deformed material.

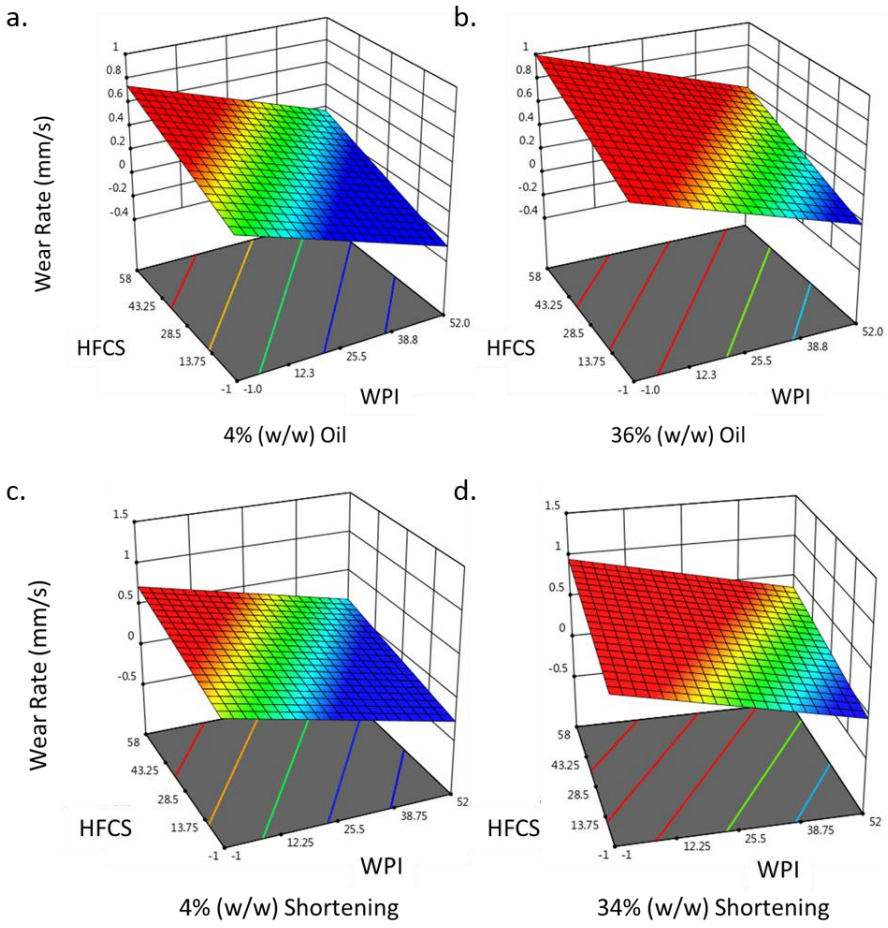

Figure 4.8 Response surface plots for wear rate for a) oil formulations at 4% oil, b) oil formulations at 36% oil, c) shortening formulations at 4% oil, and d) shortening formulations at 34% shortening.

Although increased oil or shortening in formulations increased the wear rate, the effects were lower relative to those of WPI (Fig. 4.8). As either oil or shortening increased, wear rate increased for all formulations. This was likely because increased lipids levels would increase malleability and reduced rigidity (Jacquart et al., 2016), as seen in the SAOS results.

4.4.6 ASSESSMENT OF COLD FLOW AND PROCESSING ABILITY RESULTS

Formulations with good processing ability had no cold flow (Table 4.4). These formulations had high ratios of WPI to both HFCS and either oil and shortening, indicating that good processing was likely related to less adhesion, higher critical stress, greater elastic-

type behavior, and overall greater solid-like behavior. Cold flow had similar relationships to ingredient ratios, but not all formulations that showed no cold flow showed good processing ability, indicating that the ingredient range for processing ability is smaller than that of cold flow. Further work is needed to define the relationship between processing ability and cold flow.

Table 4.4. Formulations with good processing ability and no cold flow.

Oil			**Shortening**		
Treatment	Good Processing Ability	Cold Flow	Treatment	Good Processing Ability	Cold Flow
W37.F40.C23	-	+	W46.F29.S26	+	-
W43.F47.C10	+	-	W26.F45.S29	-	+
W41.F43.C15	-	-	W42.F28.S30	+	-
W46.F50.C4	+	-	W33.F56.S12	-	+
W25.F44.C31	-	+	W38.F41.S21	-	+
W37.F40.C23	-	+	W32.F34.S34	-	-
W53.F35.C12	-	-	W38.F41.S21	-	+
W31.F33.C36	-	+	W38.F41.S21	-	+
W44.F28.C28	-	-	W32.F49.S18	-	+
W27.F46.C27	-	+	W53.F35.S12	-	-
W32.F56.C12	-	+	W38.F41.S21	-	+
W41.F27.C32	+	-	W46.F50.S4	+	-
W35.F38.C27	-	+	W38.F41.S21	-	+
W37.F40.C23	-	+	W42.F43.S15	-	-
W32.F48.C20	-	+	W36.F39.S25	-	-
W37.F40.C23	-	+	W32.F33.S35	-	-
W44.F35.C21	+	-	W38.F41.S21	-	+
W37.F40.C23	-	+	W43.F47.S10	+	-
W37.F40.C23	-	+	W45.F36.S19	+	-
W31.F32.C38	-	+	W28.F47.S25	-	+

Overall, the results of this study indicated that ingredient ratios had a significant effect on mechanical and wear behaviors. Formulation was also shown to be important for processing ability, and the connection between greater solid-like behavior, higher amounts of WPI in formulations, and good processing ability was noted. Maintaining this high ratio of WPI in bar formulations is critical for creating a structural matrix that promotes solid-like behavior by either contains the primarily viscous HFCS and oil or takes advantage of the

ability of shortening to strengthen the matrix. The connection between both lipids and HFCS, higher phase angles and poor processing ability is also important for formulation development. This impact of shortening versus oil confirms that whether the lipid used in a formulation is solid or liquid at ambient temperatures influences the material properties and thus the ingredient ratio to obtain good processing ability.

4.5 CONCLUSIONS

Having a high ratio of WPI to HFCS and either oil or shortening affected the model high protein bar linear and nonlinear viscoelastic behavior, wear rate, cold flow, and processing abilities. Because relationships were found among rheological behaviors, wear behaviors, and processing ability, instrumental testing has potential as a predictor of high protein bar processing ability. A follow-up study was performed to better relate ingredient percentages, wear rate, and mechanical behaviors determined in this study to processing ability (Chap. 5). Overall, this knowledge is important for the food industry during the development of new high protein bar formulations. While this study evaluated a simple model formulation for high protein bars, it still provides guidance for developing more complex high protein bar formulations.

4.6 ACKNOWLEDGEMENTS

This study was supported by BUILD Dairy. The authors would like to thank the application scientists at Glanbia Nutritionals, Inc for their assistance with cold flow and bar processing analyses. Thank you to Dr. Lee Deobald the director of the Mass Spec Core Lab at the University of Idaho, for his assistance in the sugar and FAME analysis.

4.7 REFERENCES

Brady, J. (2013). *Introductory Food Chemistry* (1st ed.). Ithaca, New York: Cornell University Press.

Cifre, J. G. H., Hess, S., & Kröger, M. (2004). Linear Viscoelastic Behavior of Unentangled Polymer Melts via Non-Equilibrium Molecular Dynamics. *Macromolecular Theory and Simulations*, *13*(9), 748–753. https://doi.org/10.1002/mats.200400021

Ewoldt, R. H., Hosoi, A. E., & McKinley, G. H. (2008). New measures for characterizing nonlinear viscoelasticity in large amplitude oscillatory shear. *Journal of Rheology*, *52*(6), 1427–1458. https://doi.org/10.1122/1.2970095

Franck, A. (2016). *Understanding Rheology of Structured Fluids*. Retrieved from http://www.tainstruments.com/pdf/literature/AAN016_V1_U_StructFluids.pdf

Franco, V. (2015). Market Research Analysis - Market Research Online from MarketResearch.com. Retrieved April 25, 2017, from https://www.marketresearch.com/corporate/aboutus/press.asp?view=3&article=2752&g=1

Hogan, S. A., O'Loughlin, I. B., & Kelly, P. M. (2016). Soft Matter Characterisation of Whey Protein Powder Systems. *Elsevier Science Ltd*, *52*(January 2016), 1–9. Retrieved from https://ida.lib.uidaho.edu:2116/science/article/pii/S0958694615001417

Jacquart, S., Poquillon, D., Dechambre, G., Cazalbou, S., Rey, C., & Combes, C. (2016). Mechanical properties of self-setting composites: influence of the carboxymethylcellulose content and hydration state. *Journal of Materials Science*, *51*(9), 4296–4305. https://doi.org/10.1007/s10853-016-9739-4

Joyner (Melito), H. S., Daubet, C. R., & Foegeding, E. A. (2013). Relationships Between Nonlinear Viscoelastic Behavior and Rheological, Sensory and Oral Processing Behavior of Commercial Cheese. *Journal of Texture Studies*.

Malkin, A. Y. (1995). Non-linearity in rheology ?an essay of classification. *Rheologica Acta*, *34*(1), 27–39. https://doi.org/10.1007/BF00396052

Melito, H. (2012). *Large Amplitude Oscillatory Shear Behavior of Food Systems*. North Carolina State University.

Ng, C. M., & Reuter, W. M. (2015). *Application Note: Liquid Chromatography*.

Paramita, V. D., Piccolo, J. D. Lo, & Kasapis, S. (2017). Effect of Co-soulte Concentration on the Diffusion of Linoleic Acid From Whey Protein Matrices. *Elsevier Science Ltd*, *70*(September 2017), 277–285. Retrieved from https://ida.lib.uidaho.edu:2116/science/article/pii/S0268005X17302448

Smith, B. M., Bean, S. R., Schober, T. J., Tilley, M., Herald, T. J., & Aramouni, F. (2010). Composition and Molecular Weight Distribution of Carob Germ Protein Fractions. *Journal of Agricultural and Food Chemistry*, *58*(13), 7794–7800. https://doi.org/10.1021/jf101523p

Steffe, J. F. (1996). *Rheological Methods in Food Process Engineering* (2nd ed.). East Lansing: Freeman Press. Retrieved from https://bblearn.uidaho.edu/bbcswebdav/pid-1105998-dt-content-rid-9580077_1/courses/201610_38230/STEFFE.pdf

Tan, J., & Joyner, H. S. (2018). Characterizing wear behaviors of k-carrageenan and whey protein gels by numerical modeling. *Journal of Food Engineering*.

Wall, S., & Huebner, F. R. (1980). Adhesion and Cohesion. In J. Cherry (Ed.), *Protein Functionality in Foods*. Retrieved from https://naldc.nal.usda.gov/download/26684/PDF

Yarimitsu, S., Sasaki, S., Murakami, T., & Suzuki, A. (2016). Evaluation of lubrication properties of hydrogel artificial cartilage materials for joint prosthesis. *Biosurface and Biotribology*, *2*(1), 40–47. https://doi.org/10.1016/j.bsbt.2016.02.005

Zhang, J., Daubert, C. R., & Foegeding, E. A. (2005). Characterization of polyacrylamide gels as an elastic model for food gels. *Rheologica Acta*, *44*(6), 622–630. https://doi.org/10.1007/s00397-005-0444-5

Zhou, P., Liu, X., & Labuza, T. P. (2008). Effects of Moisture-Induced Whey Protein Aggregation on Protein Conformation, the State of Water Molecules, and the

Microstructure and Texture of High-Protein-Containing Matrix. *Journal of Agricultural and Food Chemistry*, *56*(12), 4534–4540. https://doi.org/10.1021/jf073216u

Zhou, Y., & Roos, Y. H. (2011). Characterization of Carbohydrate-Protein Matrices for Nutrient Delivery. *Journal of Food Science*, *76*(4), E368–E376. https://doi.org/10.1111/j.1750-3841.2011.02126.x

CHAPTER 5: GRAPHICAL MODELING

5.1 ABSTRACT

With the growth of the high protein bar market, predictive models for good processing ability would assist bar manufactures in development of novel bar formulations. The objective of this study was to create predictive models for high protein bar model formulations based on empirical testing and instrumental data. The predictive models generated had relatively high accuracy rates (> 85%). However, three misclassifications were seen for both oil and shortening formulations, leaving grey areas of predictive values and indicating that data from additional formulations is needed to improve model accuracy. Model validation testing showed that cold flow was best for predicting processing ability of oil formulations, where cold flow was predicted accurately for 3 of the 4 validation formulations. For shortening formulations, wear rate and G_3'/G_1' at 4% strain and 10 rad/s best predicted processing ability. These models provide valuable information about ingredient ranges and instrumental tests that could be used to assist in the determination of processing ability.

5.2 INTRODUCTION

The number of new high protein bar formulations has grown significantly in recent years with the notable increase in the size of the protein bar market (Franco, 2015). It can be difficult to determine if these new formulations will process well without expert knowledge, and current testing for successful processing is highly subjective. From previous studies (Chap. 3 and 4), a wide range of formulations comprising high fructose corn syrup (HFCS) whey protein isolate (WPI) and either canola oil or vegetable shortening were tested for their mechanical and wear behaviors, and underwent subjective testing for cold flow, the ability of a material to hold its shape, and processing ability as determined by experts in the field.

The rheological tests used in these studies were selected based on the linear and nonlinear viscoelastic behavior, wear rate, and cold flow information that they provide, which could, in turn, give valuable insight to processing ability (Chap. 3 and 4; Steffe, 1996). Wear testing was conducted based on its ability to evaluate the effectiveness of soft solid materials like hydrogels as artificial cartilage in joint replacements

(Yarimitsu,Sasaki,Murakami,&Suzuki,2016; Freeman, Furey, Love, & Hampton, 2000; Kyomoto, Moro, Takatori, Kawaguchi, & Ishihara, 2011; Li, Wang, & Wang, 2016). Artificial cartilage are soft solids, similar to high protein bars. Additionally, wear testing provides information about the durability of the artificial cartilage in joints, which could relate to high protein bar durability in processing equipment, determining processing ability.

The objective of this study was to determine formulation ranges that would process well and evaluate which instrumental test responses would assist in determining good processing ability. Based on our previous results, which provided rheological and wear information for a wide range of ingredient level combinations (Chap. 4), predictive modeling was used in this study to find the ingredient ranges and testing values that would indicate ideal high protein bar formulations, similar to the way predictive modeling is used in many fields, such as in the medical field to determine appropriate materials for artificial cartilage (Euler, 2018). Additionally, we validated the accuracy of the models developed in this study with previously untested formulations.

5.3 MATERIALS AND METHODS

5.3.1 MATERIALS

Whey protein isolate provided by Glanbia Nutritionals Inc. (Fitchburg, WI, USA) (90% protein, dry basis). Protein content validation was done using the combined methods of SDS-PAGE and chromatography in Agilent Bioanalyzer 2100 (Agilent, Santa Clara, CA) (Smith et al., 2010). High fructose corn syrup provided by Batory Foods, Inc. (Hopkins, MI, USA) (42% fructose) was primarily composed of fructose, glucose, sucrose, and maltose. Sugar composition was determined by HPLC with 72:28 acetonitrile/water as the solvent (Ng & Reuter, 2015). Canola oil (store brand), and Crisco vegetable shortening were obtained via a local grocer (Moscow, ID, USA). Oil and shortening fatty acid profiles, determined by a standard C14-22 FAME mix for FAME analysis, showed that both lipids were primarily composed of palmitic fatty acid and stearic fatty acids (Sigma-Aldrich/Millipore Sigma, Saint Louise, MI, USA). All ingredients were used without further purification.

5.3.2 METHODS

Separate central composite center-faced experimental designs were used for oil- and shortening-based model high protein bars, each containing twenty formulations. Formulations were prepared at various levels of whey protein isolate (WPI), high fructose corn syrup (HFCS), and lipid (Chap. 3). Data for the predictive models included results for these formulations from adhesion, strain sweep, large amplitude oscillatory shear (LAOS), wear, and subjective testing (see Table 5.1 for a list of parameters used from each test) (chap.3). Maximum adhesive force is the peak force recorded when the samples detached form the upper plate during adhesion testing using two parallel plates. Critical strain and stress represent the amount of strain or stress applied prior to permanent deformation of the material, respectively. Crossover strain represents the strain at which the material switches from elastic-dominant to viscous-dominant behavior. Complex modulus (G*) is a measure of the rigidity of the material's microstructure. G_3'/G_1' represents the ratio of the third to first harmonic from an oscillatory testing response and is a measure of the extent of nonlinear elastic behavior. G_L'/G_M' is the ratio of large-strain elastic modulus to minimum-strain elastic modulus and is a measure of strain-hardening and -softening behavior. Phase angle indicates whether elastic or viscous behavior is dominant in a viscoelastic material. Wear rate indicates the rate at which a soft material is deformed and removed from a sample. Subjective testing done by personnel at Glanbia Nutritionals Inc. (Twin Falls, ID, USA) determined cold flow, or a material's ability to hold its shape, and processing ability, whether the formulations would roll, cut, and maintain shape on a conveyer belt without sticking (chap. 3). These results were used as data for development of the predictive model for high protein bar processing ability.

Table 5.1. List of tests and corresponding test responses.

Strain Sweep Testing	LAOS Testing	Adhesive Testing	Wear Testing	Subjective Testing
Critical stress	G_3'/G_1' inside of LVR	Maximum Forces Adhesion	Wear rate	Cold flow
Critical strain	G_3'/G_1' outside of LVR			
G* at critical strain	G_L'/G_M' inside of the LVR			
Crossover strain	G_L'/G_M' outside of the LVR			
Phase angle at critical strain				

5.3.2.1INITIAL STATISTICAL ANALYSIS

Linear discriminative analysis (LDA) and quadratic descriptive analysis (QDA) (Rstudio, Boston, MA, USA) were used for each lipid type to determine any patterns within the oil and shortening datasets. Separate analyses were performed for oil and shortening formulations. LDA resulted in similar or better analysis than QDA, so LDA results were used over QDA results. Predictions were then run for prediction for each ingredient based on their processing ability, where the average of the ingredients was selected for both poor processing or good processing (Table 5.2). Correlations (considered significant at p-value ≤0.05) among previous test responses (Chap. 3) were run to determine relationships between different test parameters and processing ability. Only correlations that met the significance criteria and had coefficients of determination (R^2 values) >|0.5| were included in the results. Confusion matrices (α=0.05), were created to validate the prediction of formulations.

5.3.3 CONSTRUCTION OF GRAPHICAL MODELS

Graphical models based on the LDA and correlation results were created using Rstudio (Rstudio, Boston, MA, USA). The LDA from the initial statistical analysis was used to construct a predictive plot to model processing ability based on ingredient inputs. Correlations from the initial statistical analysis were used to create boxplots models for processing ability and significant testing responses. These models were created to estimate acceptable ingredient ranges for good processing behaviors, as well as test responses values that would indicate good processing behaviors.

5.3.4 MODEL VALIDATION

Eight formulations that were not used in the previously tested designs (Chap. 3) were created based on the results of the LDA predictive ingredient models, four for each of the oil and shortening designs (Table 5.2). The four formulations for each model consisted of two that were within the poorly predicted processing range and the other two in the good processing predicted range. These new formulations were then compared to the LDA and boxplot model predictions to determine if their test responses agreed with predicted processing ability. Since the sample size used to create the models was small (20 samples for

each lipid design) and no expert classification for processing ability was run, it was not possible to validation each model based on processing ability.

Table 5.2 Validation formulations with expected processing ability.

Expectation	Shortening	Oil
Good	W48.F35.S17	W57.F13.C30
Good	W45.F47.S10	W52.F33.C15
Poor	W35.F50.S15	W42.F18.C40
Poor	W27.F35.S23	W35.F47.C18

5.4 RESULTS AND DISCUSSION

5.4.1 LINEAR DESCRIPTIVE ANALYSIS

For oil formulations (Table 5.3), syrup had the same average value for processing prediction, indicating that HFCS was not important for processing ability prediction, so WPI and oil were used for further analysis. In shortening formulations (Table 5.3), all ingredients had different average values and were thus all used for further analysis.

Table 5.3. p-values and mean values for LDA predictions for oil and shortening formulations.

Formulation	Analysis	p-value	Prediction	Whey	Syrup	Lipid
Oil	Linear descriptive	<0.001	0	36	41	26
			1	46	41	19
Shortening	Linear descriptive	<0.001	0	36	42	23
			1	44	38	18

For oil formulations (Fig. 5.1 a.), formulas that processed well had either moderate oil levels and high WPI levels or low oil levels and moderate WPI levels. This corresponded to the results in Chap. 3, where WPI was needed to maintain the matrix structure and thus promoted solid-like behavior and good processing ability. For shortening formulations (Fig. 5.1 b.), formulations with good processing behavior had low shortening levels and moderate to high WPI levels or moderate shortening levels and high WPI levels, which indicated a greater processing formulation range for shortening. The increased range of shortening for good processing ability was likely due to shortening providing structure to the matrix

structure discussed in Chap. 3. It should be noted that for shortening formulations, this plot did not account for the impact of HFCS on processing ability; this was resolved in further analysis. In both oil and shortening formulations (Fig. 5.1 a. and b.), there was a rather large gap between good processing and poor processing ingredient levels, which was attributed to the experimental design used for testing. Additional testing on a narrower range of ingredient percentages is needed to more finely resolve the distinction between samples with good processing behavior and samples that do not process well.

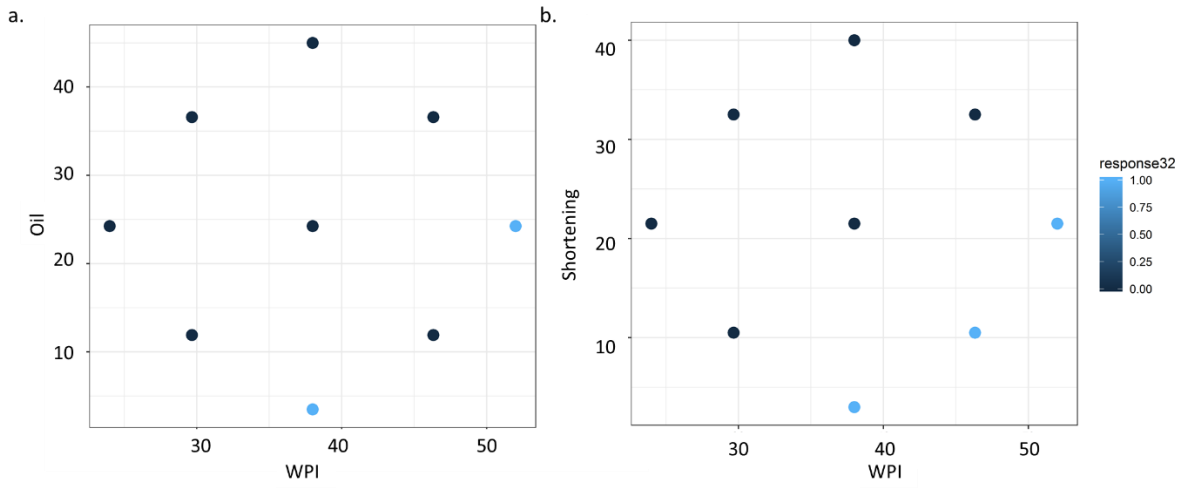

Figure 5.1. Initial processing predictions, where 1 is good processing and 0 is poor processing a) oil formulations b) shortening formulations

Correlations were run between protein bar processing ability and mechanical behaviors to gain further understand the relationships of the mechanical behaviors to determine if the behaviors could be used as predictors of processing ability (Table 5.4). Only correlations with coefficients of determination (R^2) >0.5 or <-0.5 are presented; it should be noted that all R^2 values were between 0.5 and 0.7, indicating moderate correlation between the two parameters.

Table 5.4. Test responses for oil and shortening responses with correlations >0.5 to processing ability.

Formulation	Test Response	R^2	p-value
Oil	Wear rate	-0.52	0.016
	Cold flow	-0.68	<0.001
Shortening	Critical stress at 10 rad/s	0.59	0.005
	Complex modulus at critical strain and 10 rad/s	0.61	0.003
	G'3/G'1 at 4% strain and 10 rad/s	0.54	0.012
	Crossover strain at 10 rad/s	0.61	0.003
	Wear rate	-0.66	0.001

For oil formulations, wear rate and cold flow were both negatively correlated to processing ability, which is likely because wear rate depends on the degree of malleability of the material, and cold flow depends on the ability of a material to hold its shape, a characteristic of viscoelastic solids. Hence, lower wear rate and lack of cold flow indicate less malleable structures, increasing the likelihood of the bar formulation processing well. Compared to the oil formulations, shortening formulations showed more correlations to test responses, including viscoelastic behavior measured at 10 rad/s, cold flow, and wear. These results were likely because tests at higher frequency more closely resembled actual high-protein bar processing conditions. Since shortening can assist the WPI in providing structure to the ingredient matrix compared to oil, the stronger structure paired with the increased solid-like behavior at higher frequencies provides the solid-like behavior required for processing. The correlations between all test responses were moderate, resulting in a small handful of meaningful test responses. Significant correlations indicated relationships between material rheological behaviors and processing conditions, where many of the behaviors were related to structure. For instance, critical stress is the stress value at which the linear viscoelastic region (LVR) ends and material behavior becomes nonlinear, signifying permanent deformation in the material structure. G* at critical strain indicates the stiffness of the material, and phase angle indicates the ratio of elastic-type to viscous-type behavior. Using phase angle in combination with G* provides information about both structural strength and viscoelastic nature (Steffe, 1996). G_3'/G_1' at 4% strain, the ratio of third harmonic to the first harmonic elastic modulus determines the extent of nonlinear viscoelastic behavior (Chap. 3). The crossover strain was defined as the point during strain sweep testing at which the elastic

modulus, G', and loss modulus, G", crossed and the material transitioned from elastic-dominant behavior to viscous-dominant behavior. Wear rate, which was significant for both oil and shortening formulations, is likely related to fracture properties and the extent of deformation of a material, which is related to the viscoelastic properties seen in the other test responses.

Cold flow, or the sagging of material under its own weight over time, was a significant response for oil formulations but not shortening formulations. Cold flow was probably less of an indicator of processing ability for shortening formulations because structural support from shortening would promote more solid-like behavior and reduce the occurrence of cold flow in these formulations. Since there was little structural support from the oil in oil formulations, cold flow was likely more impactful in these formulations due to the greater structural change.

5.4.1 PREDICTIVE MODELS FOR FORMULATION

More comprehensive LDA predictive plots were done based off the LDA means (Table 5.2) and the test response correlations (Table 5.4). For oil formulations, cold flow predictions were added to the original LDA plot (Fig. 5.2), as the response was binary and a prediction value for an ingredient formulation cutoff for good processing behavior would be clear. The oil LDA prediction (Fig. 5.2) showed some inconsistency with expert classification for processing ability, indicating either inconsistency between formulation duplicates or fluctuation in expert classification. Thus, the inconsistencies resulted in a grey area for processing ability, which likely reduced the preciseness of the plot for processing ability prediction. To address this issue, more samples within that range of inconsistent results should be evaluated in a subsequent study. Cold flow had similar inconsistency within the range near the predicted cutoff region of formulation levels for good processing ability, denoted by the start of the blue area. This agrees with the results seen in Chap. 3 and the grey area of cold flow results.

For shortening validation formulations, only the ingredients and processing predictions were plotted, as the plot was generated to determine the level of ingredients that would process well (Fig. 5.2 b.). Since the shortening LDA means also indicated that HFCS was a significant ingredient for processing ability (Table 5.3), HFCS was added to the prediction, creating a three-dimensional plot. However, cold flow was not a correlated test

response in shortening formulations, so was not used in the prediction plot. The predictive processing model for shortening formulations was 85% accurate according to the confusion matrix (Table 5.5) and provided ingredient ranges for both good and poor processing. Similar to the model for oil formulations, the shortening formulation model also included an area of discrepancy between LDA-predicted formulations with good processing ability and the expert classification (Fig. 5.2 b.). The reason for differences between model prediction and expert classification was likely the same as those for oil, and a narrowed range of formulations and more samples in that area should be analyzed. Shortening formulations showed good processing behavior at relatively high HFCS levels, low shortening levels, and high WPI levels, likely due to the structure provided by the WPI that contains the sugar molecules and improve the stability of the bar material (Zhou & Roos, 2011). Additionally, samples with high shortening levels, low HFCS levels, and high WPI levels showed good processing behavior, also indicating that WPI provided a degree of structural stability, as mentioned above. While the oil and shortening formulation prediction plots have shortcomings, they do offer an initial ingredient cutoff range for potential formulations. Potential formulations can be plotted to give an estimate of processing ability. If the formulation falls within the range of discrepancy between expert classification and prediction or in the poor processing region, the formulation can be adjusted to be more clearly within the ingredient range of good processing ability.

Confusion matrices were made to test the validity of the LDA predictions of processing ability for ingredients and test responses (Table 5.5). Prediction of ingredient values for both oil and shortening had an accuracy of 85% with 17 correct predictions, 1 false positive, and 2 false negatives (Table 5.5). These results indicated that the prediction for ingredients is more likely to correctly detect a good processing formulation than predict a poor processing formulation as good independent of the lipid used. The prediction accuracy of test responses of oil formulations was 85% and falsely denoted a poor processing formulation as having good processing ability only 3 out of 17 times. Prediction accuracy of test responses for shortening was 90%, with only a single false positive and false negative. Overall predictions accuracy was relatively good considering the small sample size (N=20) used to create the predictions.

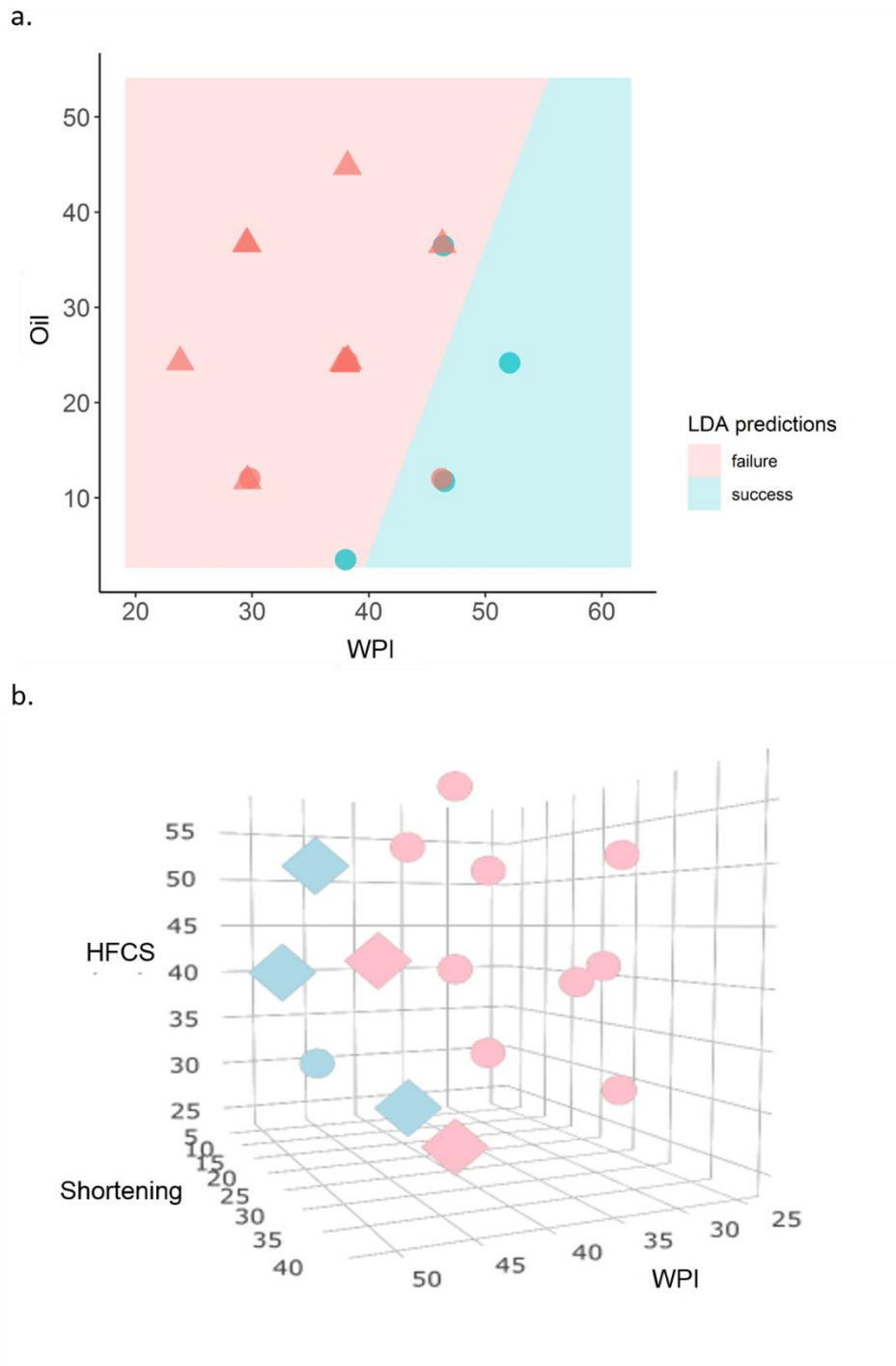

Figure 5.2. Prediction plot based on LDA predictions and expert classifications for processing ability of a) oil formulations and b) shortening formulations. The blue shading denotes predicted good processing and pink denotes predicted poor processing. In a, blue shapes denote good processing and pink shapes denote poor processing, circles denote cold flow and triangles denote no cold flow. In b, blue shapes denote good experimental processing, pink shapes denote poor experimental processing, diamonds denote good predicted processing, and circles denote poor predicted processing.

Table 5.5. Confusion matrix values for ingredients and correlated test responses for oil and shortening formulations.

Formulation type	Confusion Matrix	Correct Predictions	False Positive	False Negative	Accuracy (%)
Oil	Ingredients	17	1	2	85
	Correlated Test Responses	17	3	0	85
Shortening	Ingredients	17	1	2	85
	Correlated Test Responses	18	1	1	90

5.4.2 TEST RESPONSE GRAPHICAL MODELS

Based on the correlated test response data, boxplots were generated to determine cutoff values for each correlated test response. Cold flow for oil was plotted in the ingredient predictive plot instead of a boxplot as the original data was in binary form. For wear in oil formulations (Fig. 5.3), samples that had wear rates between 0.1-0.2 mm/s showed good processing behavior, likely due to their viscoelastic behavior (Chap. 4). There were some discrepancies with wear rate, where several samples with wear rates below 0.2mm/s had poor processing ability (Fig. 5.3). These discrepancies, which may have been caused by other rheological behaviors not conducive to good processing behaviors, were likely the cause for lower accuracy in the confusion matrix for oil test responses (Table 5.5). A similar wear rate cut off point around 0.2mm/s was also seen for shortening formulations (Fig. 5.4 e.), but there was less discrepancy with processing ability. This reduced discrepancy was probably due to the greater precision in the boxplot, which agreed with the greater accuracy of the confusion matrix of shortening versus oil samples. The ability of wear behaviors to be used as a predictor of processing ability for shortening formulations likely related to structural features that contribute to both low wear and processing behavior (Table 5.4). These results suggest that if shortening-based bar formulations have wear rates below 0.2 mm/s, they are likely to process well.

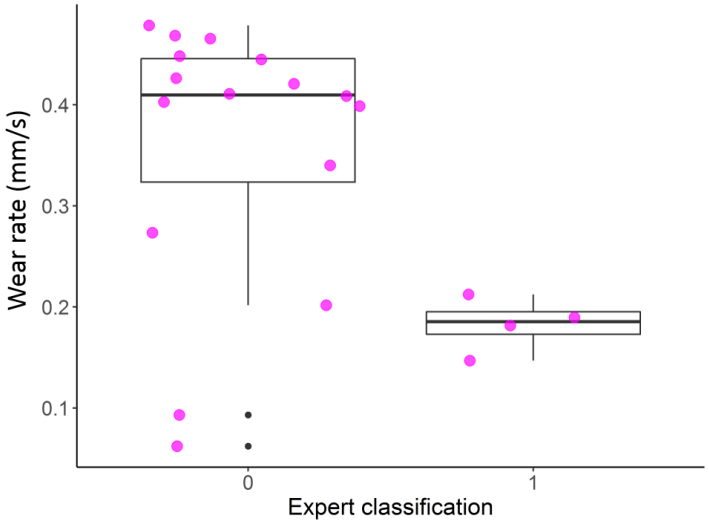

Figure 5.3. Boxplot overlaid scatterplot of oil formulation wear rates and expert classification for processing ability, where 0 is poor processing and 1 is good processing.

Predictions for shortening formulations showed relatively distinct regions of poor and good processing ability. There were several outlying points that reduced prediction accuracy, similar to what was seen in oil formulations (Fig. 5.4 a-d.). For critical stress responses (Fig. 5.4 a.), most formulations with good processing behavior had critical stresses above 30 Pa, suggesting that greater resistance to permanent deformation is important to processing ability. Formulations with good processing ability also had G* values ~ 5 x 10^5 Pa (Fig. 5.4 b.), which indicates that material stiffness is vital to bar processing. Additionally, formulations with increased nonlinear behavior, or higher absolute G_3'/G_1' values, had better processing ability (Fig. 5.4 c.), which suggested that the increased amount of protein interchain interactions interfered with alignment of sugar molecules with the oscillating shear field, affecting both viscoelastic behavior and processing ability (Cifre, Hess, & Kröger, 2004). A crossover strain around 30% also appeared important to processing ability (Fig. 5.6 d.), which suggested that maintaining elastic-dominant behavior is important for good processing ability. In general, these test responses indicated that elastic-dominant behavior and resistance to deformation were key factors in determining processing ability.

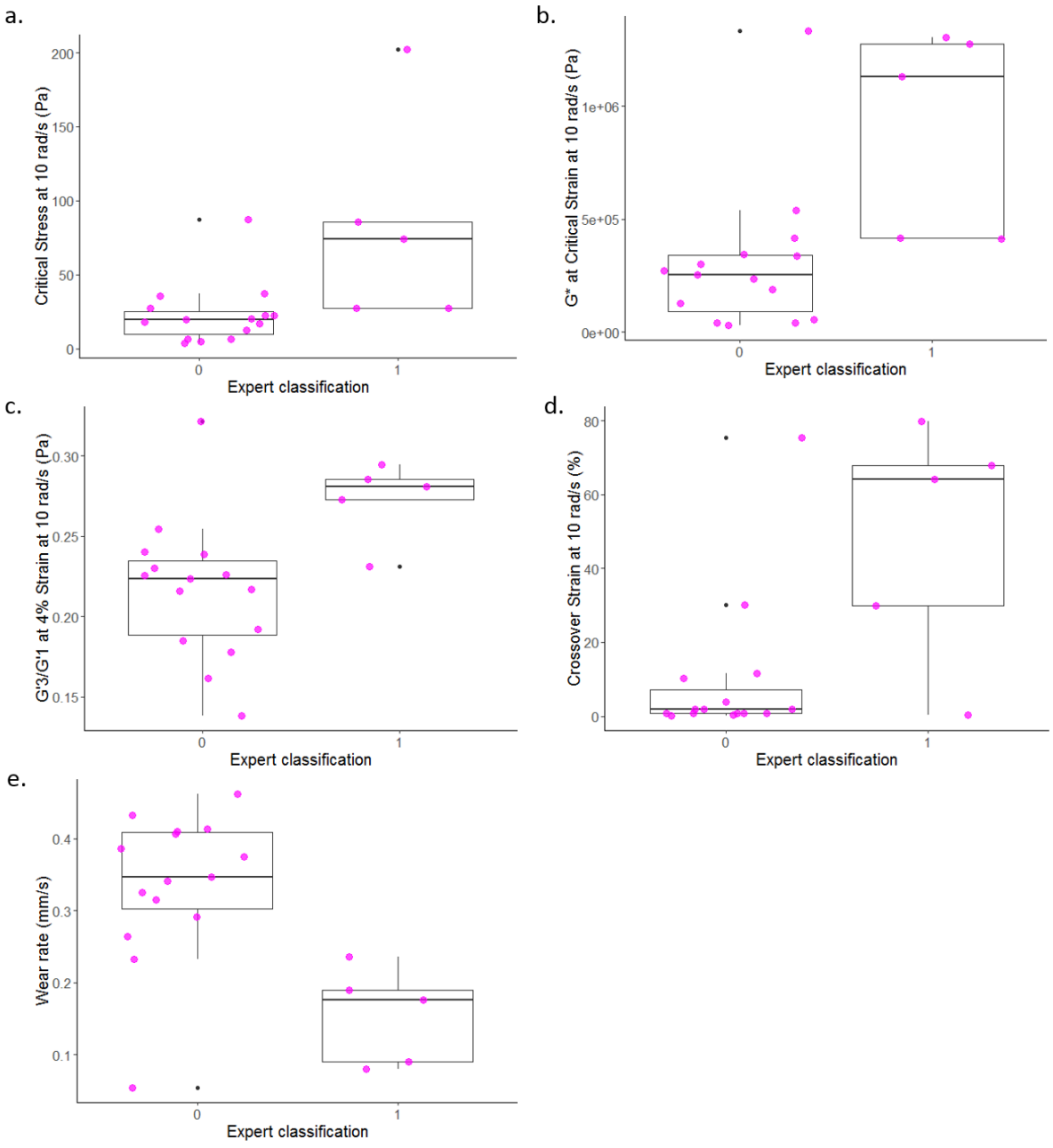

Figure 5.4. Box plots for shortening formulations for expert classifications of processing ability versus a) critical stress at 10 rad/s, b) complex modulus at critical strain at 10 rad/s, c) G_3'/G_1' at 4% strain and 10 rad/s, d) crossover strain at 10 rad/s, and e) wear rate. Here, 0 is poor processing and 1 is good processing ability.

5.4.3 GRAPHICAL MODEL VALIDATION

Further validation of the predictive ingredients and boxplot models was done by testing eight new formulations based on relative ranges in the poor processing and good processing prediction ranges (Table 5.6) given by the LDA prediction plots for both oil and shortening (Fig. 5.2 a. and b.). Cold flow results for W57.F13.C30, W52.F33.C15, and W35.F47.C18 were consistent with predicted cold flow behaviors except for W42.F18.C40, which showed no cold flow, contrary to the prediction (Fig. 5.5). The inconsistent cold flow behavior occurred just outside of the range of formulations which had conflicting responses for cold flow, indicating that the initial range of inconsistent cold flow behavior was larger than originally assumed. W35.F47.C18 also fell into this inconsistent cold flow behavior range, which was concurrent with the previously tested formulations.

Table 5.6. Validation results for oil and shortening formulations.

Oil	Expectation	Formulations	Cold Flow	Wear Rate (mm/s)
	Good	W57.F13.C30	No	0.10
	Good	W52.F33.C15	No	0.12
	Poor	W42.F18.C40	No	0.04
	Poor	W35.F47.C18	Yes	0.23

Shortening	Expectation	Formulations	Critical Stress (Pa)	Complex Modulus at Critical Strain (Pa)	G'3/G'1 at 4% Strain (Pa)[1]	Crossover Strain (%)	Wear Rate (mm/s)
	Good	W48.F35.S17	18.62±5.2	1239±350	0.285±0.0[2]	120.0	0.13
	Good	W45.F47.S10	13.53±4.9	374.0±140	0.271±0.0	0.717	0.19
	Poor	W35.F50.S15	4.072±0.5	14.99±14.3	0.192±0.0	9.942	0.47
	Poor	W27.F35.S23	7.210±1.0	82.30±11.3	0.117±0.0	0.700	0.33

[1]Absolute values were used; the negative values indicated in which quadrant the data were collected during LAOS testing.
[2]Full deviation values were <0.0.

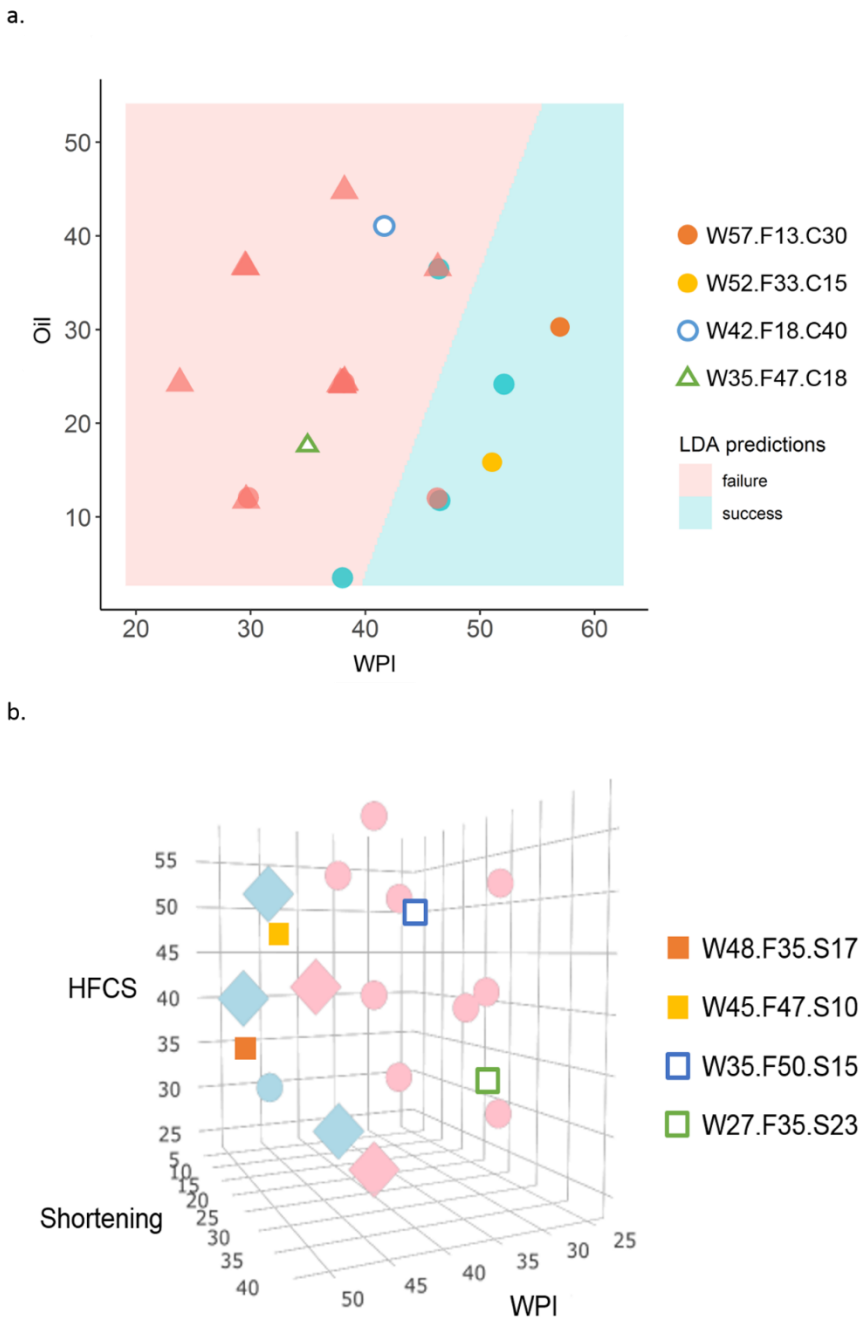

Figure 5.5. Prediction plot for based on LDA predictions and expert classifications for processing ability with validation formulations overlaid to indicate ingredient levels a) oil formulations b) shortening formulations. The blue shading denotes predicted good experimental processing and pink denotes predicted poor experimental processing. In a, circles denote cold flow and triangles denote no cold flow. For both a. and b., blue shapes denote good processing, pink shapes denote poor processing, filled shapes denote predicted good processing, and unfilled shapes indicated poor processing. For b., diamonds denote good predicted processing, and circles denote poor predicted processing.

Wear rate data for the oil validation formulations were overlaid on the wear rate boxplot model (Fig. 5.6). None of the validation formulations had were rates that fell within the previous range for good processing ability, 0.15-0.2 mm/s. W57.F13.C30 and W52.F33.C15 had lower wear rate values than expected based on the formulations. W42.F18.C40 had a wear rate of 0.04 mm/s, which fell in the low range of wear rates for poor processing ability for oil formulations. Based on these results, it is likely that the range of wear rates indicating good processing formulations is smaller than the initial boxplot indicated (Fig. 5.6). The range of wear rates may also be smaller than expected based on the wear rate of W35.F47.C18, which fell close to the predicted good processing range even though the formulation was within the predicted poor processing range. Evaluation of a greater range of formulations would clarify the wear rate range for good processing ability.

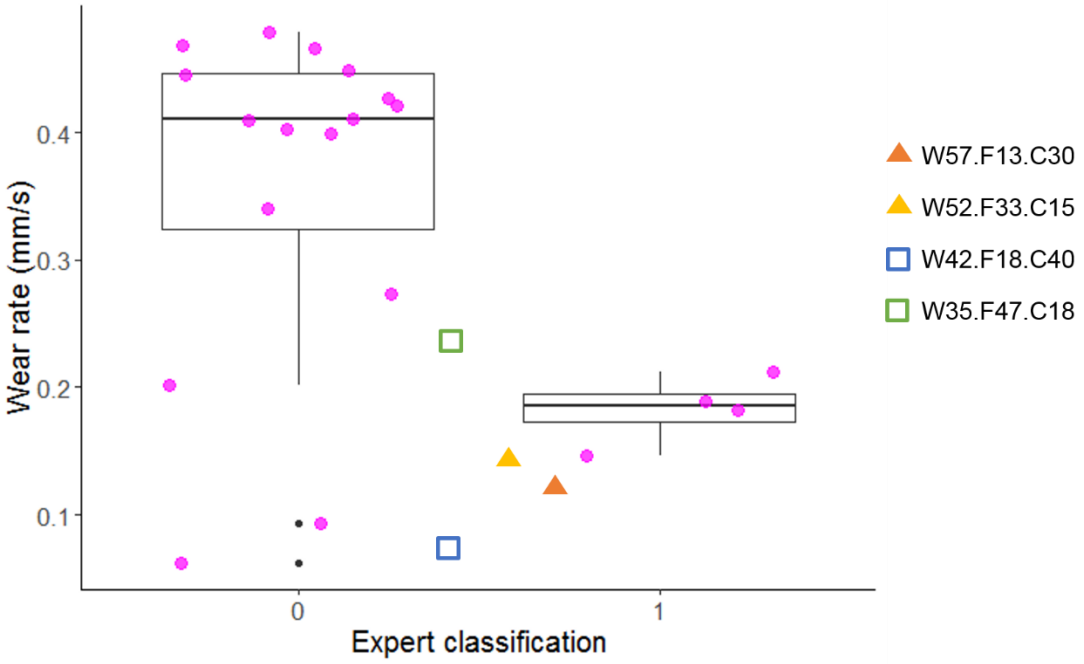

Figure 5.6. Boxplot overlaid with a scatterplot of oil formulation wear rates and overlaid validation formulations wear rated values. Filled shapes denote predicted good processing and unfilled shapes indicated poor processing.

In the shortening validation formulations, critical stress was a poor indicator of predicted formulation processing ability (Fig. 5.7 a. and Table 5.6). All validation

formulations had critical stress values in the range of poor processing ability, indicating that the model and validation data were not in agreement (Fig. 5.7 a.). The G* at critical strain values for W48.F35.S17 and W45.F47.S10 formulations were within the range of G* at critical strain values for good processing behavior based on predicted formulation, indicating agreement between the model and experimental data (Fig. 5.7b.). W35.F50.S15 and W27.F35.S23 were within the range of G* at critical strain for poor processing ability, so were also in agreement with the model predictions (Fig. 5.7 b.). Predicted good formulations W48.F35.S17 and W45.F47.S10 fell within the range of values for G_3'/G_1' at critical strain that indicated good processing ability, and W35.F50.S15 and W27.F35.S23 values that fell within the range of poor processing ability. This indicated agreement of the model and experimental data; hence, G_3'/G_1' at critical strain was a good indicator processing ability (Fig. 5.7 c.). Crossover strain at 10 rad/s was inconsistent as an indicator because all validation formulations were within the range for good processing. This lack of agreement between predicted and experimental values was likely due to the large range of good processing values (Fig. 5.7 d.). Wear rate of shortening validation formulations was a good indicator of processing ability. The wear rate values for W48.F35.S17 and W45.F47.S10 were within the good processing range and the values for W35.F50.S15 and W27.F35.S23 were within the poor processing range, showing agreement between the model and experimental results (Fig. 5.7 e.).

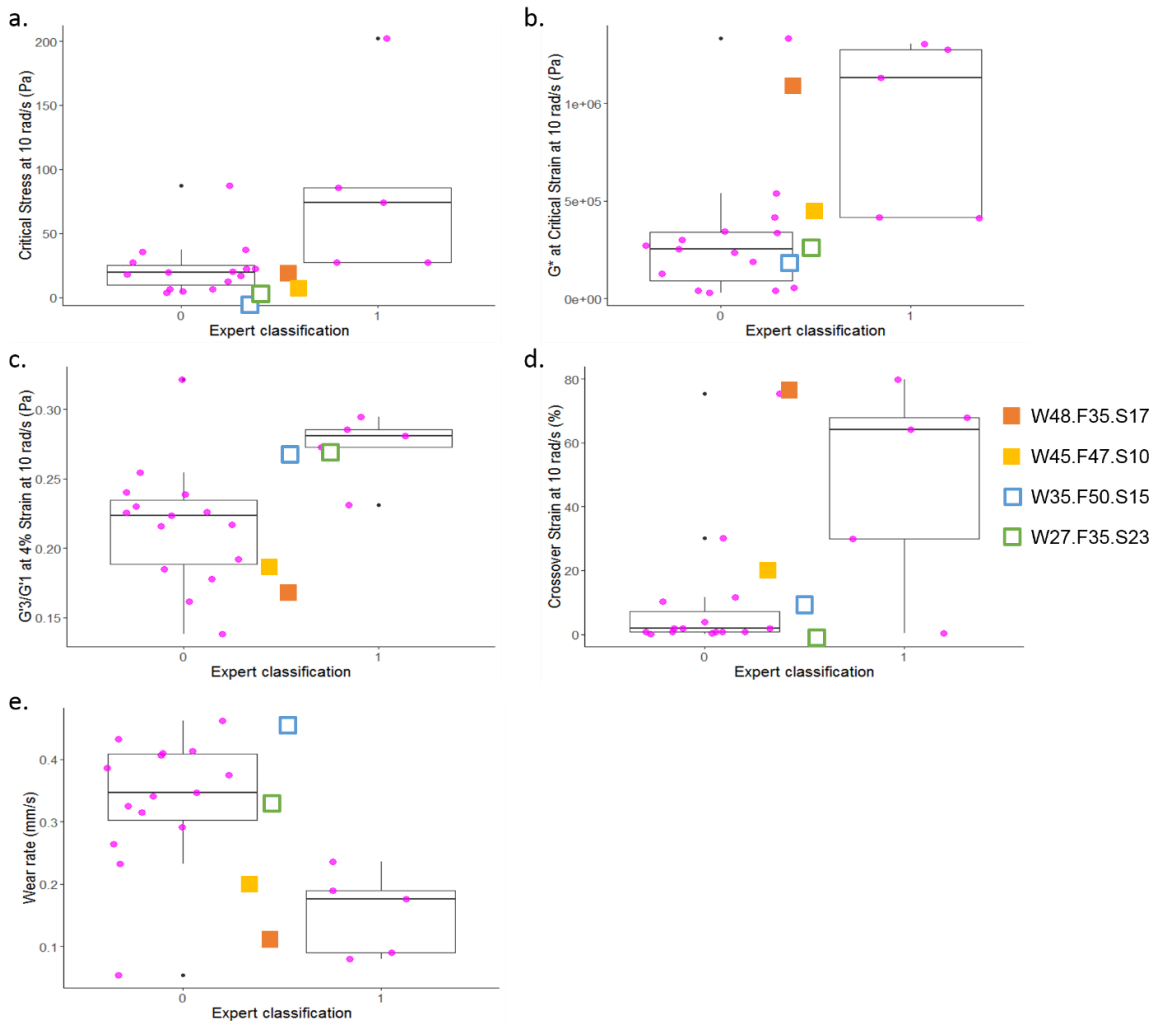

Figure 5.7. Box plots for shortening formulations with validation formulations values overlaid a) critical stress at 10 rad/s, b) G* at critical strain and 10 rad/s, c) G_3'/G_1' at 4% strain and 10 rad/s, d) crossover strain at 10rad/s, and e) wear rate. Filled shapes denote predicted good processing behavior and unfilled shapes indicated poor processing behavior.

From the graphical model validation for oil formulations, cold flow had better prediction accuracy than wear rate; wear rate was not considered accurate for predicting processing ability (Fig. 5.5 and 5.6). For shortening formulations, G_3'/G_1' at 4% strain and 10 rad/s, G* at critical strain and 10 rad/s, and wear rate were the most accurate predictors of processing behavior (Fig. 5.7 c. and e.). The other test response values for shortening formulations did not show good alignment between the predicted processing ability and experimental results (Fig. 5.7 a., b., and d.).

5.5 CONCLUSIONS

The models created for both oil and shortening formulation had accuracy of ≥85% for high protein bar processing ability as predicted by either formulation or test response. However, graphical models for both shortening and oil formulation prediction had ranges that are currently undefined in terms of processing ability, leaving a gray area of prediction. For oil, this grey area was also shown in the cold flow test results. Wear rates for the validation oil formulations did not fall clearly within the predicted good processing values, indicating a smaller good processing range for oil formulation wear rate values than predicted. Shortening formulation models agreed with predicted formulation value ranges for wear rate and G_3'/G_1' at 4% strain and 10 rad/s. Future work is required to create more accurate models, especially within the undefined regions for both oil and shortening. With the current model, new oil formulations based on the predictive model should use cold flow results for prediction of processing ability. For shortening formulations, the test responses that should be used for predicting processing ability are G_3'/G_1' at 4% strain and 10 rad/s, G* at critical stress and 10 rad/s, and wear rate. These results indicated that LAOS, strain sweeps, and wear testing can be used to predict processing behavior of shortening-based formulations. Overall, these models are a good starting point for predictive testing based on formulation for processing ability of high protein bars and can be improved with analysis of additional samples.

5.6 ACKNOWLEDGEMENTS

This study was funded by BUILD Dairy. The authors would like to thank the Consulting Statisticians in the Statistical Programs working in the College of Agricultural and Life Science at the University of Idaho for assistance in creating the code and models for this work. The authors would also like to thank Dr. Lee Deobald the Director of the Mass Spec Core Lab at the University of Idaho, who assisted with proximate ingredient composition analysis.

5.7 REFERENCES

AOAC. (2001). *AOAC Official Method 996.06 Fat (Total, Saturated, and Unsaturated) in Foods*.

https://doi.org/http://down.40777.cn/stardard/8/41.1.28A%20AOAC%20Official%20Method%20996.06%20Fat(Total,Saturated.pdf

Cifre, J. G. H., Hess, S., & Kröger, M. (2004). Linear Viscoelastic Behavior of Unentangled Polymer Melts via Non-Equilibrium Molecular Dynamics. *Macromolecular Theory and Simulations*, *13*(9), 748–753. https://doi.org/10.1002/mats.200400021

Euler, M. J. (2018). Intelligence and Uncertainty: Implications of heirarchial Predictive Processing for the Neuroscience of Cognitive Ability. *Elsevier Science Ltd*, *94*(November), 93–112. Retrieved from https://ida.lib.uidaho.edu:2116/science/article/pii/S0149763418302045

Franco, V. (2015). Market Research Analysis - Market Research Online from MarketResearch.com. Retrieved April 25, 2017, from https://www.marketresearch.com/corporate/aboutus/press.asp?view=3&article=2752&g=1

Freeman, M. E., Furey, M. J., Love, B. J., & Hampton, J. M. (2000). Friction, wear, and lubrication of hydrogels as synthetic articular cartilage. *Wear*, *241*(2), 129–135. https://doi.org/10.1016/S0043-1648(00)00387-2

Kyomoto, M., Moro, T., Takatori, Y., Kawaguchi, H., & Ishihara, K. (2011). Cartilage-mimicking, High-density Brush Structure Improves Wear Resistance of Crosslinked Polyethylene: A Pilot Study. *Clinical Orthopaedics and Related Research®*, *469*(8), 2327–2336. https://doi.org/10.1007/s11999-010-1718-5

Li, F., Wang, A., & Wang, C. (2016). Analysis of friction between articular cartilage and polyvinyl alcohol hydrogel artificial cartilage. *Journal of Materials Science: Materials in Medicine*, *27*. https://doi.org/10.1007/s10856-016-5700-y

Ng, C. M., & Reuter, W. M. (2015). *Application Note: Liquid Chromatography*.

Smith, B. M., Bean, S. R., Schober, T. J., Tilley, M., Herald, T. J., & Aramouni, F. (2010). Composition and Molecular Weight Distribution of Carob Germ Protein Fractions. *Journal of Agricultural and Food Chemistry*, *58*(13), 7794–7800. https://doi.org/10.1021/jf101523p

Steffe, J. F. (1996). *Rheological Methods in Food Process Engineering* (2nd ed.). East Lansing: Freeman Press. Retrieved from https://bblearn.uidaho.edu/bbcswebdav/pid-1105998-dt-content-rid-9580077_1/courses/201610_38230/STEFFE.pdf

Yarimitsu, S., Sasaki, S., Murakami, T., & Suzuki, A. (2016). Evaluation of lubrication properties of hydrogel artificial cartilage materials for joint prosthesis. *Biosurface and Biotribology*, *2*(1), 40–47. https://doi.org/10.1016/j.bsbt.2016.02.005

Zhou, Y., & Roos, Y. H. (2011). Characterization of Carbohydrate-Protein Matrices for Nutrient Delivery. *Journal of Food Science*, *76*(4), E368–E376. https://doi.org/10.1111/j.1750-3841.2011.02126.x

CHAPTER 6: CONCLUSION

This study showed a clear impact of formulation on mechanical and wear behaviors of high protein bars. The impact of WPI ratio to HFCS and either oil or shortening was important for wear rates, elastic-type behaviors, and the extent of nonlinear viscoelastic behavior. Wear tracks were deeper and had greater definition at higher WPI ratio formulations for both oil and shortening. From these results, the relationships of ingredients and processing ability and test responses and processing ability were determined using graphical models. This work revealed that formulations with higher levels of WPI to other ingredients were more likely to process well, which concurred with previous results. The instrumental tests that provided the highest accuracy for predicting processing ability were cold flow testing for oil formulations and wear and LAOS testing for shortening formulations. In general, the instrumental tests in this study showed that increased solid-like behavior was related to good processing ability. Based on these results, bench-scale tests may be used to assist in the high protein bar development process.

Overall, this study indicated clear relationships between formulation, elastic-type behavior and processing ability, and the usefulness of cold flow in the prediction of processing ability for oil-based formulations and wear and LAOS testing in the prediction of processing ability for shortening-based formulations. Additionally, wear testing for shortening formulations appeared to be a viable test for indicating processing ability, suggesting that wear behaviors may be similarly important to processing behaviors of other soft solid foods.

Future work on this project should include testing of formulations with other common proteins and sugar sweeteners. With soy and other legume proteins being popular in high protein bar formulations, further investigation on the impact of these other proteins is needed. Similarly, many low or no caloric sweeteners are used in high protein bars, and their impact on processing ability should also be evaluated. Additionally, while a liquid and solid lipid were investigated in this study, they were just two of the lipids found in commercial high protein bar formulations; different types of lipids could impact processing ability, and this area needs further exploration. With further work on various ingredients, a greater understanding of ingredient impact on processing ability would be developed. Finally, more sample testing within the range of misclassification of ingredients for processing ability. It is likely that a more defined ingredient cut off range for good processing ability for high protein

bars could be gathered from a larger range of ingredient combinations within the misclassification range. This would likely improve the model accuracy. Additional model validation through expert classification of validation formulations would also likely improve the model accuracy.

APPENDIX

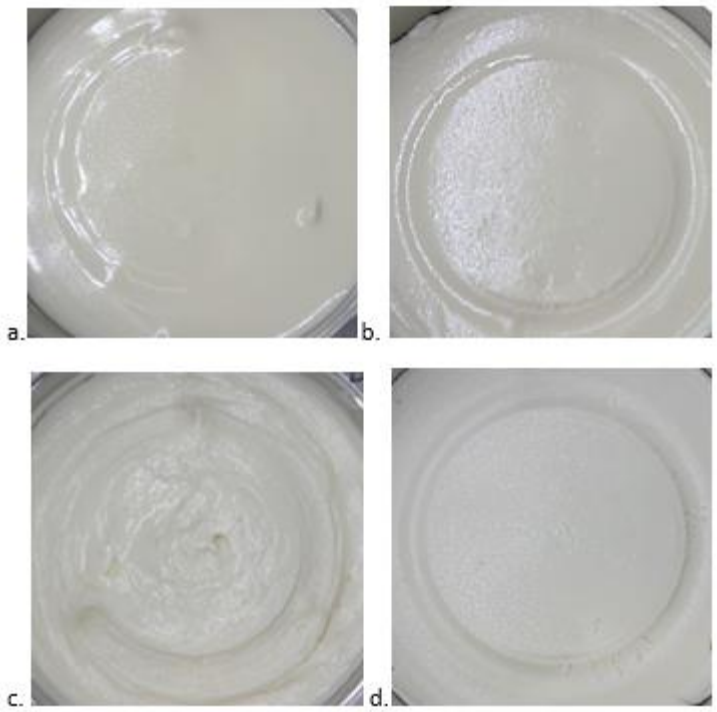

Figure A.1. Examples of where the pin holder interfered with the wear track.

Table A.2. Adhesion data.

Oil			Shortening		
Treatment	**Time of Maximum Force (s)**	**Maximum Normal Force (N)**	**Treatment**	**Time of Maximum Force (s)**	**Maximum Normal Force (N)**
W37.F40.C23	0.22	19.40±1.6	W46.F29.S26	0.12	6.247±1.0
W43.F47.C10	0.24	20.60±1.7	W26.F45.S29	0.16	3.068±0.2
W41.F43.C15	0.22	17.42±2.1	W42.F28.S30	0.16	5.105±0.5
W46.F50.C4	0.24	20.70±0.8	W33.F56.S12	0.24	11.23±0.7
W25.F44.C31	0.22	11.64±1.7	W38.F41.S21	0.18	7.342±0.6
W37.F40.C23	0.22	18.79±0.7	W32.F34.S34	0.16	3.683±0.6
W53.F35.C12	0.1	6.662±1.4	W38.F41.S21	0.18	5.968±2.2
W31.F33.C36	0.2	17.79±1.3	W38.F41.S21	0.18	6.435±1.2
W44.F28.C28	0.12	9.330±0.8	W32.F49.S18	0.20	7.855±1.0
W27.F46.C27	0.22	11.87±1.1	W53.F35.S12	0.10	3.380±0.3
W32.F56.C12	0.24	12.84±0.5	W38.F41.S21	0.20	6.408±2.2
W41.F27.C32	0.12	7.759±0.6	W46.F50.S4	0.22	19.02±4.2
W35.F38.C27	0.20	17.02±0.7	W38.F41.S21	0.18	8.277±1.9
W37.F40.C23	0.22	18.91±0.6	W42.F43.S15	0.16	8.790±1.4
W32.F48.C20	0.24	11.93±1.3	W36.F39.S25	0.22	4.492±2.3
W37.F40.C23	0.24	21.22±0.8	W32.F33.S35	0.16	4.052±0.5
W44.F35.C21	0.18	11.32±0.7	W38.F41.S21	0.18	9.095±1.0
W37.F40.C23	0.24	20.24±0.8	W43.F47.S10	0.18	10.61±3.8
W37.F40.C23	0.24	21.74±0.9	W45.F36.S19	0.14	6.910±0.8
W31.F32.C38	0.18	18.49±2.8	W28.F47.S25	0.18	3.682±0.5

Table A.3. Strain sweep data for oil treatments.

	0.1 rad/s				1 rad/s				10 rad/s			
Treatment	Critical Stress (Pa)	Critical Strain (%)	G* at Critical Strain (kPa)	δ at Critical Strain (degrees)	Critical Stress (Pa)	Critical Strain (%)	G* at Critical Strain (kPa)	δ at Critical Strain (degrees)	Critical Stress (Pa)	Critical Strain (%)	G* at Critical Strain (kPa)	δ at Critical Strain (degrees)
W37.F40.C23	7.15±2.8	0.039±0.0[1]	18.5±5.5	40.0±0.8	4.90±1.0	0.016±0.0	30.5±3.6	40.7±0.7	9.35±2.9	0.016±0.0	62.1±45	41.7±1.4
W43.F47.C10	43.1±10.	0.039±0.0	105±30	37.9±1.2	39.4±6.0	0.016±0.0	246±28	26.1±2.9	5.16±0.6	0.007±0.0	78.4±6.4	40.3±2.2
W41.F43.C15	2.35±0.8	0.016±0.0	14.7±3.8	41.4±1.7	13.9±9.4	0.016±0.0	86.2±44	32.9±2.1	10.3±1.5	0.007±0.0	252±17	23.5±1.0
W46.F50.C4	8.45±3.4	0.039±0.0	21.8±6.7	48.2±1.4	14.0±9.4	0.016±0.0	87.4±44	38.8±3.6	36.5±13	0.016±0.0	321±61	24.8±4.1
W25.F44.C31	6.61±4.9	0.094±0.0	4.59±0.6	38.7±0.1	3.69±1.2	0.039±0.0	9.49±2.4	37.9±0.8	7.35±1.9	0.038±0.0	19.1±3.7	37.1±0.3
W37.F40.C23	6.01±6.9	0.039±0.0	15.5±13	39.9±1.0	2.09±0.5	0.007±0.0	31.5±6.1	38.2±1.5	4.92±2.9	0.007±0.0	74.9±33	34.1±5.2
W53.F35.C12	187±120	0.016±0.0	1470±790	17.2±5.1	244±29	0.016±0.0	1530±140	11.0±0.4	308±120	0.016±0.0	1940±560	11.7±0.5
W31.F33.C36	5.35±1.0	0.094±0.0	5.40±1.0	39.5±1.7	4.87±1.0	0.039±0.0	12.6±1.0	37.6±1.8	4.44±0.4	0.016±0.0	27.9±1.8	39.0±0.4
W44.F28.C28	208±93	0.016±0.0	1280±440	14.2±2.6	97.8±32	0.007±0.0	1490±370	10.5±0.9	285±66	0.016±0.0	1790±310	12.2±1.3
W27.F46.C27	4.11±0.5	0.094±0.0	4.39±0.4	37.4±0.4	7.30±1.5	0.094±0.0	7.77±1.2	37.1±0.8	6.63±2.0	0.038±0.0	17.2±3.9	36.2±0.8
W32.F56.C12	4.07±1.3	0.094±0.0	4.37±1.1	37.9±1.5	7.54±1.0	0.094±0.0	8.03±0.8	37.0±0.5	6.61±2.0	0.038±0.0	19.4±1.6	35.1±0.5
W41.F27.C32	102±39	0.016±0.0	631±170	18.6±2.8	113±31	0.007±0.0	1070±350	12.1±1.6	68.3±35	0.007±0.0	1040±400	12.7±2.4
W35.F38.C27	6.20±0.8	0.094±0.0	6.63±0.7	36.7±0.2	4.49±0.5	0.016±0.0	280±2.1	37.0±0.8	6.19±1.1	0.007±0.0	94.2±12	32.4±0.9
W37.F40.C23	6.13±1.7	0.094±0.0	7.03±1.4	41.7±2.1	4.16±1.0	0.016±0.0	25.9±4.9	37.0±1.0	5.68±0.8	0.007±0.0	86.4±9.4	33.0±0.9
W32.F48.C20	4.82±0.3	0.094±0.0	5.15±0.3	38.4±0.5	3.41±1.2	0.039±0.0	8.78±2.3	36.8±1.7	4.39±0.3	0.016±0.0	27.6±1.4	42.6±1.5
W37.F40.C23	6.34±1.4	0.094±0.0	6.77±1.1	38.2±1.5	4.36±1.3	0.016±0.0	27.2±6.0	34.8±1.3	5.85±0.6	0.016±0.0	36.8±2.8	41.9±1.9
W44.F35.C21	16.5±4.6	0.007±0.0	249±52	32.5±1.8	37.3±9.0	0.007±0.0	562±100	17.8±0.9	84.7±18	0.016±0.0	533±85	24.1±1.7
W37.F40.C23	1.28±0.2	0.039±0.0	3.31±0.4	42.0±1.7	3.35±0.5	0.039±0.0	8.62±0.9	41.7±0.9	4.21±1.0	0.016±0.0	26.5±4.7	43.5±1.1
W37.F40.C23	2.34±0.1	0.039±0.0	6.05±0.2	39.9±0.6	0.65±0.2	0.003±0.0	23.8±4.6	37.1±0.8	3.56±0.2	0.016±0.0	22.4±0.8	44.9±0.4
W31.F32.C38	1.97±0.2	0.039±0.0	5.10±0.4	36.1±1.1	3.33±0.8	0.039±0.0	8.57±1.6	36.2±0.5	4.61±0.1	0.016±0.0	29.0±0.6	44.9±0.4

[1]Full deviation values were < 0.0.

Table A.4. Strain sweep data for shortening treatments.

	0.1 rad/s				1 rad/s				10 rad/s			
Treatment	Critical Stress (Pa)	Critical Strain (%)	G* at Critical Strain (kPa)	δ at Critical Strain (degree)	Critical Stress (Pa)	Critical Strain (%)	G* at Critical Strain (kPa)	δ at Critical Strain (degree)	Critical Stress (Pa)	Critical Strain (%)	G* at Critical Strain (kPa)	δ at Critical Strain (degree)
W46.F29.S26	120±42	0.016±0.0[1]	749±200	17.6±1.9	45.6±23	0.007±0.0	688±36	13.7±1.2	74.3±37	0.007±0.0	1130±420	14.6±2.1
W26.F45.S29	11.4±1.5	0.094±0.0	12.4±1.2	31.4±0.3	11.0±0.3	0.039±0.0	28.2±0.6	23.1±1.0	6.52±0.8	0.016±0.0	41.0±3.9	24.9±1.1
W42.F28.S30	74.8±23	0.016±0.0	467±96	21.2±1.3	88.8±55	0.016±0.0	554±260	14.4±2.2	202±100	0.016±0.0	1270±480	13.4±2.4
W33.F56.S12	1.92±0.4	0.039±0.0	4.96±0.7	39.4±0.3	4.12±1.0	0.016±0.0	2.56±4.6	29.7±0.6	4.86±0.5	0.016±0.0	31.0±2.1	37.3±1.4
W38.F41.S21	4.36±1.9	0.003±0.0	159±52	33.6±4.6	7.92±2.0	0.003±0.0	289±54	17.8±1.6	19.8±2.2	0.007±0.0	301±25	17.1±1.1
W32.F34.S34	16.6±1.0	0.039±0.0	43.0±2.0	31.3±0.6	20.4±1.4	0.016±0.0	817±6.4	20.4±0.1	20.1±5.2	0.016±0.0	127±24	19.3±0.7
W38.F41.S21	4.55±2.3	0.003±0.0	167±64	32.2±4.1	7.77±1.3	0.003±0.0	283±37	20.2±2.3	22.1±3.1	0.007±0.0	337±35	18.8±0.4
W38.F41.S21	4.29±1.2	0.003±0.0	157±56	32.0±3.7	49.7±14	0.016±0.0	310±64	15.8±1.9	37.4±3.5	0.016±0.0	235±16	23.2±0.7
W32.F49.S18	5.33±0.7	0.039±0.0	13.8±1.3	37.0±0.3	2.76±0.6	0.007±0.0	41.5±6.6	26.1±0.3	3.73±0.8	0.007±0.0	56.7±9.1	26.7±2.1
W53.F35.S12	188±33	0.016±0.0	1170±150	16.1±0.5	249±90	0.016±0.0	1560±430	11.9±2.3	87.6±33	0.007±0.0	1330±380	15.2±1.6
W38.F41.S21	7.42±1.4	0.007±0.0	112±16	34.0±1.8	7.81±2.9	0.003±0.0	284±80	17.3±2.7	16.8±7.1	0.007±0.0	255±81	21.3±3.2
W46.F50.S4	30.4±11	0.039±0.0	78.7±22	43.0±1.6	32.4±8.6	0.016±0.0	202±40	28.5±1.9	27.5±7.5	0.007±0.0	418±85	18.0±5.1
W38.F41.S21	10.1±4.1	0.007±0.0	152±46	31.2±3.0	22.0±11	0.007±0.0	330±120	16.2±2.8	22.5±7.4	2.619±0.0	343000±84	18.6±1.7
W42.F43.S15	62.5±10	0.039±0.0	162±20	32.4±2.5	54.7±4.3	0.016±0.0	341±20	19.1±1.1	35.4±1.3	2.619±0.0	538±14	14.2±0.3
W36.F39.S25	3.06±1.1	0.003±0.0	112±30	35.1±0.8	38.4±12	0.016±0.0	239±58	17.8±1.6	17.9±2.5	0.007±0.0	272000±28	17.3±0.9
W32.F33.S35	20.3±0.6	0.039±0.0	52.6±1.2	30.9±0.1	17.6±0.6	0.016±0.0	101±2.9	20.0±0.5	12.4±3.0	0.007±0.0	189±34	16.1±0.3
W38.F41.S21	23.0±6.7	0.016±0.0	144±31	30.3±1.2	38.7±15	0.016±0.0	241±71	18.4±1.5	27.4±3.9	0.007±0.0	416±45	17.2±1.3
W43.F47.S10	8.62±1.9	0.003±0.0	316±52	27.8±2.5	36.8±1.6	0.016±0.0	229±7.6	25.8±0.2	27.1±11	0.007±0.0	412±130	23.1±3.0
W45.F36.S19	90.7±16	0.016±0.0	567±75	21.4±1.4	84.5±19	0.007±0.0	1280±210	11.0±1.3	85.7±38	0.007±0.0	1310±430	12.8±1.8
W28.F47.S25	11.8±0.5	0.094±0.0	12.6±0.4	33.0±0.3	5.08±0.1	0.016±0.0	31.6±0.2	24.1±0.4	6.29±1.0	0.016±0.0	39.6±4.8	27.7±0.7

[1]Full deviation values were < 0.0.

Table A.5. phase angle data at 1 rad/s.

Oil				Shortening			
Treatment	**Phase Angle (degree)**			**Treatment**	**Phase Angle (degree)**		
	0.052	**1.8**	**60**		**0.052**	**1.8**	**60**
W37.F40.C23	41.4±1.02	50.4±0.93	60.2±0.62	W46.F29.S26	18.1±1.65	29.7±1.19	44.5±2.68
W43.F47.C10	27.2±1.45	38.2±1.45	49.3±0.71	W26.F45.S29	23.1±1.05	31.9±1.82	47.8±1.84
W41.F43.C15	34.5±2.34	43.9±2.59	53.7±2.05	W42.F28.S30	17.0±2.50	29.0±1.86	45.4±1.85
W46.F50.C4	39.6±3.31	48.8±2.82	57.9±2.84	W33.F56.S12	30.1±0.66	39.8±2.12	52.2±1.95
W25.F44.C31	37.8±0.78	52.3±1.39	81.9±0.86	W38.F41.S21	21.0±1.40	31.0±0.13	46.0±0.62
W37.F40.C23	39.1±1.16	48.3±1.37	59.0±1.54	W32.F34.S34	21.2±0.14	30.0±0.50	45.4±0.09
W53.F35.C12	13.0±0.36	26.0±0.38	40.3±6.79	W38.F41.S21	21.0±1.40	30.9±0.13	45.9±0.62
W31.F33.C36	25.6±1.78	34.6±2.46	46.6±2.15	W38.F41.S21	18.2±2.13	30.6±2.26	45.3±1.64
W44.F28.C28	13.8±1.11	27.0±2.26	48.2±0.60	W32.F49.S18	26.9±0.54	36.5±1.54	50.3±1.64
W27.F46.C27	35.4±0.51	47.6±2.13	80.5±0.64	W53.F35.S12	13.8±1.98	25.5±0.74	45.9±0.92
W32.F56.C12	35.2±0.51	47.5±1.39	77.9±0.94	W38.F41.S21	20.8±2.30	33.8±1.98	47.8±1.50
W41.F27.C32	16.2±2.87	28.2±1.93	43.3±1.52	W46.F50.S4	30.1±1.75	41.1±2.21	51.5±1.42
W35.F38.C27	37.8±0.80	45.7±1.01	61.1±1.14	W38.F41.S21	20.0±2.46	31.9±3.88	46.6±1.71
W37.F40.C23	37.8±1.05	47.2±1.91	58.3±0.92	W42.F43.S15	21.9±2.06	35.5±1.62	42.3±1.50
W32.F48.C20	36.8±1.69	49.9±2.25	76.3±7.32	W36.F39.S25	19.6±1.86	30.1±1.59	45.0±1.48
W37.F40.C23	35.7±1.06	45.1±1.58	57.2±1.75	W32.F33.S35	20.8±0.35	30.0±0.40	45.7±0.10
W44.F35.C21	23.6±2.08	32.9±1.28	44.8±1.37	W38.F41.S21	20.8±1.40	31.9±1.10	47.7±1.07
W37.F40.C23	41.7±0.86	55.4±1.50	60.6±0.81	W43.F47.S10	28.5±0.40	44.4±1.01	52.8±0.14
W37.F40.C23	37.4±0.23	44.1±1.57	55.0±0.41	W45.F36.S19	15.7±1.28	27.2±1.88	47.6±3.47
W31.F32.C38	36.2±0.45	46.8±0.63	60.8±1.15	W28.F47.S25	24.6±0.60	33.8±1.33	49.1±1.30

Table A.6. LAOS ratios oil formulations.

	0.1 rad/s				1 rad/s				10 rad/s			
Treatment	G'_3/G'_1	G'_L/G'_M	G''_3/G''_1	η'_L/η'_M	G'_3/G'_1	G'_L/G'_M	G''_3/G''_1	η'_L/η'_M	G'_3/G'_1	G'_L/G'_M	G''_3/G''_1	η'_L/η'_M
W37.F40.C23	0.091±0.01	0.622±0.15	0.273±0.01	0.235±0.02	0.064±0.01	0.873±0.03	0.297±0.01	0.223±0.01	0.309±0.02	3.899±0.44	0.189±0.02	0.530±0.04
W43.F47.C10	0.115±0.01	0.598±0.02	0.302±0.11	0.207±0.01	0.060±0.01	0.942±0.02	0.381±0.01	0.196±0.00	0.226±0.04	2.228±0.30	0.250±0.02	0.436±0.04
W41.F43.C15	0.168±0.02	0.477±0.03	0.269±0.02	0.240±0.01	0.136±0.02	0.686±0.06	0.332±0.03	0.194±0.02	0.136±0.00	1.791±0.00	0.325±0.00	0.354±0.01
W46.F50.C4	0.098±0.01	0.766±0.04	0.264±0.03	0.766±0.03	0.143±0.02	0.520±0.02	0.244±0.01	0.274±0.02	0.147±0.02	1.681±0.08	0.272±0.03	0.413±0.03
W25.F44.C31	0.041±0.03	0.661±0.03	0.140±0.00	0.505±0.03	0.173±0.02	1.297±0.19	0.120±0.01	0.583±0.03	0.439±0.05	20.60±13.0	0.096±0.02	0.683±0.06
W37.F40.C23	0.120±0.01	0.565±0.04	0.259±0.02	0.257±0.03	0.100±0.02	0.769±0.05	0.305±0.01	0.216±0.01	0.306±0.07	4.764±2.17	0.162±0.08	0.570±0.16
W53.F35.C12	0.084±0.10	0.923±0.24	0.427±0.06	0.160±0.04	0.303±0.10	3.480±1.62	0.522±0.06	0.159±0.03	0.374±0.08	3.456±1.76	0.285±0.08	0.661±0.16
W31.F33.C36	0.026±0.02	0.637±0.03	0.230±0.01	0.364±0.01	0.069±0.04	1.304±0.16	0.207±0.02	0.335±0.03	0.317±0.02	4.901±0.75	0.156±0.01	0.534±0.02
W44.F28.C28	0.065±0.01	1.098±0.03	0.148±0.00	0.478±0.01	0.006±0.03	0.834±0.08	0.265±0.02	0.310±0.05	0.300±0.06	2.912±0.42	0.299±0.03	0.691±0.14
W27.F46.C27	0.068±0.03	1.287±0.13	0.328±0.04	0.293±0.04	0.027±0.03	0.652±0.05	0.155±0.01	0.431±0.01	0.388±0.04	14.96±9.76	0.114±0.01	0.606±0.02
W32.F56.C12	0.097±0.03	0.502±0.08	0.151±0.01	0.418±0.06	0.082±0.04	0.778±0.08	0.160±0.01	0.434±0.03	0.118±0.05	1.869±0.47	0.188±0.01	0.447±0.03
W41.F27.C32	0.014±0.01	0.864±0.01	0.335±0.03	0.249±0..04	0.017±0.02	1.479±0.09	0.427±0.05	0.253±0.04	0.314±0.04	2.451±0.34	0.300±0.02	0.520±0.04
W35.F38.C27	0.034±0.02	0.682±0.05	0.214±0.01	0.347±0.03	0.062±0.01	0.879±0.04	0.272±0.01	0.247±0.01	0.221±0.01	2.530±0.06	0.226±0.01	0.434±0.01
W37.F40.C23	0.123±0.03	0.517±0.02	0.242±0.02	0.293±0.03	0.129±0.02	0.701±0.06	0.298±0.01	0.218±0.01	0.133±0.02	1.764±0.11	0.294±0.01	0.357±0.01
W32.F48.C20	0.050±0.03	0.615±0.04	0.152±0.01	0.452±0.03	0.151±0.08	1.393±0.31	0.144±0.02	0.482±0.05	0.265±0.03	3.711±0.79	0.035±0.00	0.865±0.02
W37.F40.C23	0.116±0.14	0.541±0.03	0.256±0.00	0.279±0.01	0.127±0.01	0.700±0.02	0.307±0.01	0.214±0.01	0.263±0.02	2.838±0.21	0.217±0.01	0.459±0.02
W44.F35.C21	0.077±0.05	1.382±0.17	0.432±0.03	0.206±0.02	0.048±0.02	0.724±0.10	0.322±0.03	0.209±0.01	0.312±0.03	2.717±0.20	0.280±0.04	0.467±0.03
W37.F40.C23	0.123±0.01	0.490±0.02	0.240±0.02	0.319±0.02	0.118±0.02	0.717±0.06	0.296±0.01	0.225±0.01	0.205±0.01	2.227±0.42	0.250±0.01	0.405±0.02
W37.F40.C23	0.132±0.01	0.490±0.02	0.239±0.02	0.319±0.02	0.116±0.02	0.717±0.06	0.297±0.01	0.225±0.01	0.205±0.01	2.268±0.42	0.250±0.01	0.405±0.02
W31.F32.C38	0.030±0.02	0.694±0.05	0.254±0.03	0.346±0.01	0.133±0.11	1.622±0.42	0.259±0.01	0.321±0.02	0.377±0.04	9.215±5.19	0.114±0.04	0.642±0.10

Table A.7. LAOS ratios for shortening formulations.

	0.1 rad/s				1 rad/s				10 rad/s			
Treatment	G'_3/G'_1	G'_L/G'_M	G''_3/G''_1	η'_L/η'_M	G'_3/G'_1	G'_L/G'_M	G''_3/G''_1	η'_L/η'_M	G'_3/G'_1	G'_L/G'_M	G''_3/G''_1	η'_L/η'_M
W46.F29.S26	0.032±0.02	0.850±0.05	0.335±0.02	0.206±0.01	0.186±0.03	2.114±0.67	0.446±0.04	0.196±0.04	0.263±0.02	2.607±0.18	0.307±0.03	0.595±0.11
W26.F45.S29	0.082±0.00	1.056±0.02	0.247±0.01	0.332±0.01	0.107±0.00	1.436±0.01	0.266±0.00	0.343±0.01	0.203±0.00	2.361±0.11	0.160±0.01	0.512±0.04
W42.F28.S30	0.220±0.01	2.265±0.13	0.561±0.03	0.185±0.01	0.267±0.02	3.111±0.44	0.549±0.09	0.231±0.04	0.127±0.07	1.583±0.49	0.180±0.10	0.794±0.27
W33.F56.S12	0.349±0.02	56.59±20.0	0.384±0.02	0.272±0.03	0.319±0.02	4.030±0.20	0.423±0.02	0.218±0.02	0.354±0.07	2.268±1.53	0.475±0.06	0.531±0.11
W38.F41.S21	0.140±0.01	1.514±0.08	0.539±0.02	0.129±0.01	0.144±0.08	1.976±0.59	0.474±0.08	0.191±0.04	0.285±0.04	2.826±0.48	0.211±0.06	0.552±0.14
W32.F34.S34	0.119±0.04	1.344±0.24	0.329±0.06	0.276±0.08	0.185±0.00	2.065±0.02	0.403±0.00	0.252±0.00	0.242±0.00	2.511±0.19	0.189±0.05	0.562±0.13
W38.F41.S21	0.003±0.01	0.874±0.02	0.381±0.02	0.161±0.01	0.037±0.01	1.242±0.06	0.392±0.02	0.199±0.01	0.245±0.01	2.325±0.11	0.288±0.00	0.392±0.01
W38.F41.S21	0.091±0.07	1.272±0.35	0.442±0.10	0.175±0.06	0.182±0.00	2.249±0.02	0.532±0.01	0.156±0.00	0.342±0.05	3.850±0.70	0.145±0.05	0.652±0.12
W32.F49.S18	0.062±0.06	1.052±0.24	0.328±0.04	0.236±0.01	0.131±0.07	1.717±0.38	0.368±0.05	0.237±0.01	0.244±0.06	2.907±0.83	0.185±0.04	0.482±0.07
W53.F35.S12	0.175±0.05	1.456±0.51	0.547±0.14	0.150±0.01	0.337±0.08	3.609±1.32	0.633±0.18	0.156±0.01	0.402±0.02	3.192±0.73	0.301±0.08	1.767±3.04
W38.F41.S21	0.091±0.06	1.249±0.27	0.446±0.04	0.158±0.00	0.182±0.01	2.039±0.10	0.389±0.03	0.265±0.01	0.298±0.04	3.142±0.93	0.177±0.06	0.591±0.12
W46.F50.S4	0.146±0.02	0.524±0.06	0.269±0.03	0.229±0.01	0.103±0.02	0.731±0.16	0.312±0.06	0.216±0.02	0.238±0.08	2.576±0.78	0.327±0.01	0.360±0.04
W38.F41.S21	0.136±0.01	1.467±0.05	0.517±0.02	0.139±0.00	0.196±0.02	2.278±0.21	0.464±0.06	0.209±0.04	0.314±0.02	3.070±0.26	0.210±0.05	0.540±0.12
W42.F43.S15	0.102±0.01	1.270±0.06	0.342±0.02	0.275±0.01	0.098±0.10	1.563±0.52	0.388±0.03	0.242±0.03	0.277±0.04	2.610±0.32	0.213±0.06	0.657±0.09
W36.F39.S25	0.119±0.05	1.370±0.24	0.450±0.06	0.166±0.01	0.201±0.02	2.395±0.19	0.527±0.04	0.175±0.00	0.312±0.04	3.202±0.51	0.173±0.03	0.621±0.07
W32.F33.S35	0.119±0.05	1.332±0.29	0.355±0.07	0.236±0.02	0.154±0.03	1.800±0.22	0.327±0.01	0.320±0.05	0.267±0.03	2.693±0.23	0.226±0.04	0.514±0.10
W38.F41.S21	0.153±0.01	1.605±0.09	0.437±0.02	0.219±0.01	0.209±0.02	2.442±0.19	0.397±0.09	0.203±0.02	0.303±0.05	2.929±0.53	0.224±0.07	0.570±0.14
W43.F47.S10	0.158±0.06	1.793±0.41	0.585±0.03	0.154±0.03	0.133±0.00	1.762±0.02	0.362±0.01	0.238±0.01	0.325±0.08	3.858±1.53	0.148±0.07	0.687±0.12
W45.F36.S19	0.009±0.04	0.765±0.11	0.310±0.06	0.277±0.07	0.128±0.11	1.121±0.35	0.334±0.08	0.331±0.05	0.333±0.03	2.527±0.13	0.356±0.01	0.547±0.13
W28.F47.S25	0.065±0.01	0.998±0.03	0.269±0.01	0.294±0.01	0.090±0.01	1.353±0.06	0.285±0.00	0.305±0.01	0.219±0.01	2.643±0.11	0.164±0.01	0.492±0.01